THE EFFECTS OF NATIVE AND LIGHT INDUCED DEFECTS IN THE OPTICAL AND ELECTRONIC PROPERTIES OF HYDROGENATED AMORPHOUS SILICON GERMANIUM (a-SiGe:H) ALLOY THIN FILMS

**A Thesis Submitted to
the Graduate School of Engineering and Sciences of
İzmir Institute of Technology
in Partial Fulfillment of the Requirements for the Degree of**

MASTER OF SCIENCE

in Physics

**by
Medine Elif DÖNERTAŞ YAVAŞ**

**November 2005
İZMİR**

We approve the thesis of **Medine Elif DÖNERTAŞ YAVAŞ**

Date of Signature

……………………………………………   **30 November 2005**
Prof. Dr. Mehmet GÜNEŞ
Supervisor
Department of Physics
Muğla University

……………………………………………   **30 November 2005**
Asst. Prof. Dr. Süleyman TARİ
Department of Physics
İzmir Institute of Technology

……………………………………………   **30 November 2005**
Asst. Prof. Dr. Habibe BAYHAN
Department of Physics
Muğla University

……………………………………………   **30 November 2005**
Prof. Dr. Durmuş Ali DEMİR
Head of Physics Department
İzmir Institute of Technology

……………………………………………….
Assoc. Prof. Dr. Semahat ÖZDEMİR
Head of the Graduate School

ACKNOWLEDGEMENTS

ABSTRACT

Hydrogenated amorphous silicon-germanium alloy thin films (a-SiGe:H) of various germanium concentrations, are potential candidates meeting the requirements of high efficiency stacked solar cells and optoelectronic devices where a certain bandgap is necessary. In this thesis to obtain reliable information about the native and light induced defect states present in a-SiGe:H alloy thin films of various germanium concentrations SSPC, DBP, transmission spectroscopy and PDS techniques have been used. A procedure based on Ritter Weiser optical formulation has been applied to calculate fringe free absolute absorption coefficient spectra of a-SiGe:H alloy thin films of various Ge% from the yield DBP and simultaneously measured transmission signals for the first time. The results have been compared with those independently measured by PDS method.

In the annealed state the effects of native defect states in a-SiGe:H alloy thin films of various Ge% have been investigated. For the a-SiGe:H alloy films with Ge concentration in the range of 10% to 30%, $\eta\mu_n\tau_n$-products for the photogenerated free electrons is the highest, therefore they serve as the best photoconductive absorber layer in the multijunction solar cells. The effect of Ge content in amorphous silicon network clearly indicates a systematic decrease in the bandgap with increasing Ge content. The E_{0v} values are almost constant around 55meV for alloying up to 40% Ge. Finally the changes in the defect density present in the bandgap of alloy films are inferred from the $\alpha(1.0eV)$ measured by both PDS and low bias light DBP spectrum. The difference between PDS and low bias DBP spectra is attributed to the underlying physics of these methods. The best film with lowest defect density can be prepared with alloying Ge in the range from 10% to 40% Ge.

In the light soaked state, samples were left under white light illumination (15 suns) for determined time intervals. SSPC measurements indicate that all samples exhibit certain degree of degradation in the magnitude of σ_{ph} and $\eta\mu_n\tau_n$ products. The rate of $\alpha(1.0\ eV)$ decreases as Ge% increases in the light soaked state. Higher Ge content films (50%, 75%) show almost no degradation in sub-bandgap absorption. As the degradation slope of $\alpha(h\nu)$ and $1/\eta\mu_n\tau_n$ product are not same for all samples it can be inferred that subgap absorption and photoconductivity measurements are not controlled by the same set of defects present in the bandgap.

ÖZET

Farklı germanyum konsantrasyonlarına sahip hidrojenlendirilmiş amorf silisyum germanium alaşım ince filmler (a-SiGe: H) yüksek verimli ve katmanlardan oluşan güneş pilleri ve belirli bir bant boşluğunun gerekli olduğu optic ve elektronik uygulamalar için önemli bir potansiyel oluşturur. Bu tezde farklı germanyum konsantrasyonlarına sahip a-SiGe:H alaşım ince filmlerde yerel ve ışık altında bozunuma uğratılmış durumlarda oluşan kusurlar hakkında güvenilir bilgi edinmek amacıyla durağan hal ışıl iletkenlik (SSPC), iki demetli ışıl iletkenlik (DBP), ve ışıl ışın saptırma izgegözlem (PDS) yöntemleri kullanılmıştır. İki demetli ışıl iletkenlik (DBP) methodundan girişim saçaksız mutlak soğurma katsayisi izgesinin elde edilebilmesi için Ritter-Weiser optik denklemleri kullanılan bir prosedür, literatürde ilk kez a-SiGe:H alaşım ince filmlere uygulanmıştır. Elde edilen sonuçlar bağımsız olarak PDS deney düzeneğinden elde edilenlerle karşılaştırılmıştır.

Tavlanmış durumda örneklerdeki doğal kusurlar incelenmiştir. Çok katmanlı güneş pillerinde en iyi ışıl iletken soğurma katmanı olarak $\mu_n\tau_n$-çarpanı en yüksek ölçülen germanyum konsantrasyonu 10% ile 30% aralığındaki örnekler bulunmuştur. Germanyum konsantrasyonu arttıkça bant boşluğunda sistematik bir azalma olduğu gözlenmiştir. 40% germanyum konsantrasyonuna sahip örneğe kadar diğer tüm örneklerin E_{0v} değerleri 55meV civarıda sabit bulunmuştur. Bant boşluğundaki kusur yoğunluğundaki değişim ışıl ışın saptırma izgegözlem (PDS) ve iki demetli ışıl iletkenlik (DBP) metodları ile ölçülen $\alpha(1.0eV)$ değerleri ile gözlemlenmiş ve arada oluşan fark iki metodun farklı fiziksel temellere dayanması ile açıklanmıştır. En düşük kusur yoğunluğuna sahip olan filmlerin 10% ile 40% germanyum konsanstasyonu aralığında hazılanabileği bulunmuştur.

Işık altında bozunuma uğratılmış durumda örnekler belirli zaman aralıkları için 15 güneş şiddetindeki beyaz ışık kaynağı altında bırakılmıştır. Durağan hal ışıl iletkenlik ölçümleri tüm örneklerde fotoiletkenlik ve $\mu_n\tau_n$-çarpanı değerlerinde bir bozunma olduğunu göstermiştir. Işık altında bozunuma uğratılmış durumda germanyum konsantrasyonu arttıkça $\alpha(1.0eV)$ deki değişme oranı azalır. Yüksek germanyum konsantrasyonuna sahip filmler bant içi soğurma değerlerinde bir bozunma göstermemiştir. $\alpha(h\nu)$ daki bozunma ve $1/\mu_n\tau_n$-çarpanı eğimlerinin farklı olması durağan hal ışıl iletkenlik ve iki demetli ışıl iletkenlik ölçümlerinin aynı tür elektronik kusurlar tarafından kontrol edilmediği ile açıklanabilir.

TABLE OF CONTENTS

LIST OF FIGURES

LIST OF TABLES

CHAPTER I

INTRODUCTION

In crystalline materials, atoms are arranged in complete precision so that by knowing the position and species of a few atoms, the position and chemical nature of all the atoms in the sample can be predicted. Such long range order is found only in solids called crystalline. Yet there is another phase of solids in which, atoms are randomly oriented. Neighboring atoms (nearest neighbors or second nearest neighbors) are precisely arranged, but as one moves further out, the arrangement becomes less and less predictable. This kind of order is called short range order. Such materials with short range order and missing long range order are called amorphous materials. Amorphous structure of the same material show different properties then its crystalline structure. Missing long range order results in random variations in the bond lengths, bond angles, strain bonds and broken bonds between the atoms. As a result, a spread of new energy levels into the bandgap between the valence band and conduction band is formed. These "tail" states arise from the distorted bonds and are considered to be localized by the disorder in the potential and they, therefore, cannot take place in conduction. These tail states follow an exponential distribution into the bandgap and the slope of the exponential tail states is characteristic to the disorder present in the structure and called as Urbach energy. The effective mobility of electrons in this region is quiet small due to trapping and detrapping of carriers into these states. Therefore, conduction through energy states between conduction band and valance band becomes negligible. The mobilities in the states above conduction band and below the valence band are significantly higher. A threshold called as the mobility edge in the energy spectrum of mobilities is formed for the conduction mechanism. As a result, the energy gap is replaced by a concept of the mobility gap. The energy gap between the energy of the mobility edge for electrons in the conduction band and that of holes in the valance band is defined to be the mobility gap or the recombination gap (Wagner et al. 1991). The mobility gap is a little bigger than the optical band gap of the material.

Hydrogenated amorphous silicon-germanium alloy thin films prepared by using the Plasma Enhanced Chemical Vapor Deposition (PECVD) and sputtering methods have amorphous structure. It exhibits the characteristics of an amorphous semiconductor

as described above. Hydrogenated amorphous silicon-germanium alloys, (a-Si$_{1-x}$Ge$_x$:H,) are prepared by alloying hydrogenated amorphous silicon (a-Si:H) with various germanium concentrations (x). The deposition technologies of amorphous semiconductors are particularly suited to easily alter the bandgap of these alloys. Consequently, in a-SiGe:H alloy materials, the optical bandgap can be tailored from 1.8 eV to 1.1 eV by changing the germanium concentration, $0< x <0.7$, from purely amorphous silicon to high germanium content a-SiGe:H alloy. By changing the alloy concentration x, several electronic and optical properties of hydrogenated amorphous silicon-germanium alloys (a-Si$_{1-x}$Ge$_x$:H) can be changed to match the electronic and optical device requirements. These are, alloying silicon with germanium and producing a material with a reduced bandgap which better matches the low energy part of the solar spectrum (Finger et al 1987, Street et al. 1987) in stacked solar cells, and allowing production of specific optoelectronic devices with a certain bandgap.

Hydrogenated amorphous silicon-germanium alloy thin films are mostly prepared with Radio Frequency Plasma Enhanced Chemical Vapor Deposition (RF-PECVD) (13.56 MHz) method in a diode type reactor with gas mixtures of SiH$_4$, GeH$_4$ and H$_2$. In addition to using the basic PECVD technique, some alternatives such as hydrogen dilution, fluorinated gases, and some variations in the deposition reactors have also been applied (Matsuda et al 1985). Deposition conditions such as gas sources, conditions in the plasma and at the interface have been varied to have a fine control and enhancement on material properties. A considerable development of chosen properties and associated device applications is accomplished by some deposition techniques but an overall degradation of the optoelectronic properties as a function of germanium content is a continual problem in all cases. It appears that this weakening might be an intrinsic alloying effect rather than a matter of non improved efficiency on preparation conditions.. Although deposition techniques like photo-CVD, sputtering, thermal CVD, catalytic CVD and evaporation have also been used for the preparation of a-SiGe:H alloys, for which details are reported in literature, until today the most successful and most used approaches include hydrogen dilution of the process gases and the use of disilane-germane mixtures. (Finger and Beyer 1997a, Finger and Beyer 1997b and the references therein).

One of the main applications of hydrogenated amorphous silicon-germanium alloys of various Ge concentrations (a-SiGe:H) is to use it as an intrinsic layer of the bottom cell of a multi-junction cell structure (stacked cells) as shown in Figure 1.1.
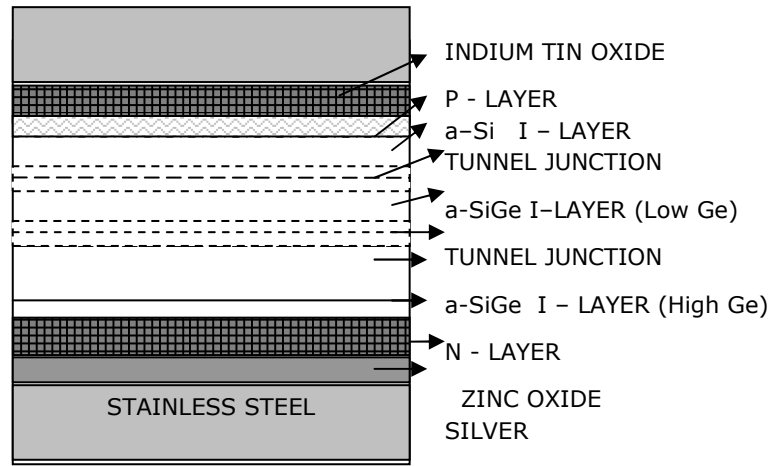
Figure 1.1   A schematic of the USSC /Canon a-Si triple junction structure with which Stabilized Conversion Efficiency of 13% is reached. (Jang et al. 1997)

To enhance the efficiency of silicon solar cells, multi-junction solar cells are manufactured. They are made up of several layers and optimized cell designs aiming to absorb the whole solar spectrum efficiently. Multi-junction solar cells are solutions to two important problems in solar cell design. First one is to improve higher efficiency, and the second one is to improve the stability after light soaking. For the first case, the bandgaps of the layers of the single cells in the stack have to be different. While the top layers of this structure intend to absorb the high energy part of the spectrum, the purpose of the bottom layer is to absorb the low energy region. For the second objective, absorber materials such as intrinsic a-SiGe:H with different bandgaps and good optoelectronic properties are necessary. As these lower bandgap materials act to extend the infra red response of the cell, an increase in the photo-generation of free charge carriers result in. Improvement in photo generation means an increase in photocurrent generation and collection in solar cell characteristics (Jang et al. 1997). An example of amorphous silicon-germanium alloy thin films as an intrinsic absorber layer of the bottom cell in a multijunction solar cells for the state of the art low bandgap thin film material for silicon based thin film multijunction solar cells are shown in Figure 1.1 with a reported recorded stabilized efficiency of 13% on a 0.25cm^2 device area (Jang et al. 1997). In this figure beginning from the highest level down to the substrate, materials with different bandgaps are used. a-Si with its highest bandgap absorbs the high energy region of the solar spectrum, but as Ge% increases as the bandgap of the material decreases, these layers absorb the low energy region of the solar spectrum. However there are several unanswered questions in understanding of degradation of multijunction solar cells with a-SiGe:H layers of different germanium concentrations. A detailed study

of degradation under light for each intrinsic a-SiGe:H absorber layer with different germanium concentrations will provide valuable information for the long term stability of these devices.

The effects of alloying process in a-SiGe:H thin film production are observed as a deterioration in the optoelectronic properties. The slope of the valence band tail states which is also called Urbach energy, changes when the material is alloyed with various germanium concentrations. Urbach energy is a representation of disorder in the material. The defect density of the material increases when Urbach energy increases. Mackenzie et al. states that as a result of alloying process, the slope of the exponential edge decreases with increasing germanium content by about 30%. This is also assumed to be an indication that alloying leads to an increase in the width of the valence band tail (Mackenzie et al. 1984).

An increase in localized defect states in the bandgap and a corresponding degradation in mobility lifetime product of electrons and holes have been detected experimentally. There have been numerous studies on the characterization of the defect states in the gap of a-SiGe:H alloys using various techniques such as subgap optical absorption spectroscopy (Carius et al. 1998) and Electron Spin Resonance (ESR) (Stutzmann et al. 1989, Fuhs and Finger 1989).

In a study by Carius et al. (Carius et al. 1998), gap states in a-SiGe:H alloys were examined by numerical simulations of sub-bandgap absorption spectra measured by the constant photocurrent method (CPM) and PDS to see the changes of the density of states with increasing Ge concentration. The simulations yielded information on the energy distribution and the charge state of the defects. The results showed the coexistence of charged and neutral defects. The defect distributions were similar to those found in hydrogenated amorphous silicon. In the a-Si_xGe_{1-x}:H samples with Ge content higher than 0.5, charged states were found to dominate the defect density. If the position of the defect states were taken as a reference level, both band edges shifted towards the defect states with decreasing bandgap. In contrast to ESR, no evidence was found for a distinction between Si-related or Ge-related defect states.

It is well known from a variety of ESR studies that both Si and Ge dangling bonds exist in the a-Si,Ge:H alloys (Stutzmann et al. 1984). Since germanium bonds are, in general, less strong than silicon bonds, one expects that Ge dangling bonds will dominate in alloys with significant fractions of Ge. This has definitely observed to be the case. Figure 1.2 summarizes ESR results from three such studies (Stutzmann et al.

1989, Fuhs and Finger 1989) of the a-Si,Ge:H alloys. The ratio of Ge to Si dangling bonds against the Ge fraction in the film is plotted. For alloys with Ge fractions above 30 at%, the Ge dangling bonds seem to dominate by at least an order of magnitude. On the other hand for Ge fractions below about 10 at%, density of Si and Ge dangling bonds appear to be comparable.
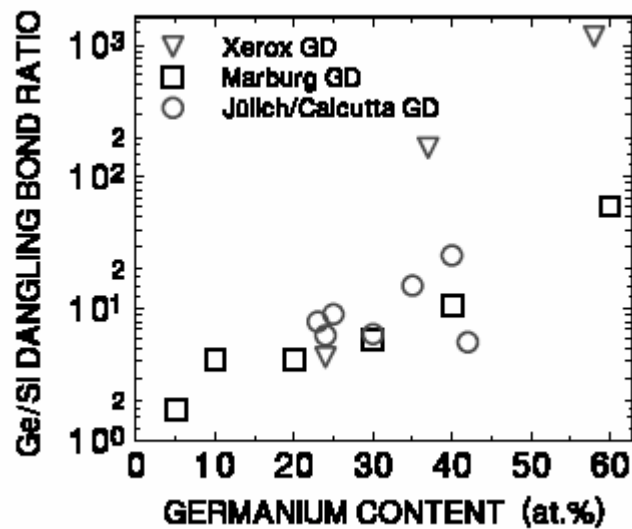
Figure 1.2 Ratios of germanium to silicon dangling bonds determined from ESR studies of a-Si,Ge:H samples (Cohen et al. 2003).

Both dark and photoconductivity decreases after light soaking as discovered by Staebler and Wronski in 1977. This effect is known as the Staebler-Wronski effect (SWE). It is an intrinsic and reversible effect in a-Si:H based thin films. Both dark and photoconductivity are restored back to original values measured in the annealed state after annealing in dark at temperatures above 150°C. This effect is also observed in solar cells with absorber layers of intrinsic amorphous silicon and amorphous silicon-germanium alloy as a degradation in solar cell conversion efficiencies. The reason for the effect in thin films and solar cells is due to creation of new defect states by the light, which are located in energies in the bandgap of a-SiGe:H based thin film material.

The creation of defect states by light illumination can be clearly seen through several other important investigations. Reversible changes in field effect experiments (Goodman 1982), (Grunewald et al. 1981), deep revel transient spectroscopy (Lang et al. 1982), defect luminescence (Pankove and Berkeyheiser 1980), subgap absorption studies (Amer et al. 1983) and an increase of silicon dangling bond signal in electron

spin resonance (Hirabayashi et al. 1980), (Dersch et al. 1981). Even tough an extensive research have been carried out on understanding of the origin of the SWE in a-Si:H thin films for more than two decades, an improved understanding on the defect creation mechanism have been established and the role of hydrogen is strongly pointed out. However a complete picture of the understanding and a well developed theory on the SWE in a-Si:H has not been established yet.

On the other hand, studies to understand the effects of light soaking on a-SiGe:H alloy thin films are very few when compared to the studies on a-Si:H. Studies on light induced changes in a-SiGe:H alloys are very important not only because of their crucial applications but also insights of such kind of studies can provide information to the issue of degradation in unalloyed a-Si:H.

When light induced degradation in a-SiGe:H alloys are considered, first studies were performed during 1980's. In this first group of studies, the initial material quality of a-SiGe:H alloys was poor. The slope of the valence band tail (Urbach tail), E_{0v}, which is the measure of the disorder in the amorphous network, was above 60meV. Since device quality a-Si:H thin films can be prepared with an Urbach energy below 50meV, it was thought that light-induced changes in these alloys were quite negligible (Bullot et al. 1983, Nakamara et al. 1983). However in the second half of 1980s, more detailed research programs were undertaken to develop and understand the properties of the a-Si,Ge:H alloys (Aljishi et al. 1989, Guha et al. 1987, Stutzmann et al. 1989, Nebel et al. 1988). Several of these studies analyzed the issue of light-induced degradation.

One of these studies is carried out by Aljishi et al. In their very extensive research, they found that the photoconductivity typically decreased by an order of magnitude after light soaking for films with optical gaps that exceeded about 1.4 eV (Aljishi et al. 1989). They also tested the effects of light soaking on the deep defects by measuring the sub-band-gap optical spectra. They found considerable increases in the magnitude of the deep defect band upon light soaking as derived from the increase in the sub-bandgap absorption coefficients at low energies. Quiet unexpectedly, they observed that the photoconductivity was unchanged in spite of the increase in midgap absorption for alloys with optical gaps below 1.4 eV.

 In another study carried out by Stutzmann and collaborators at Xerox PARC, an increase of dangling bonds in light soaked a-SiGe:H alloys were determined by means of ESR spectroscopy (Stutzmann et al. 1989). It was found that the silicon dangling bonds with characteristic g-number increased with light soaking for alloys with Ge

concentration less than about 20 at %. On the other hand, for the alloys with Ge fractions x>0.4, no light-induced changes in dangling bond densities could be detected at all. It should be noted, however, that for these higher Ge alloy samples, the Ge dangling bond density with its characteristic g-number was found to exceed 10^{17} cm^{-3} and the Urbach energies were greater than 60 meV.

In contrast to the a-SiGe:H alloys studied during the 1980s, a-SiGe:H materials studied in 1990s gained a much greater degree of improvement of efficiency (Paula et al. 1993, Guha et al. 1992, Unold et al. 1994). This is acknowledged by the fact that the Urbach energies for alloys covering nearly the whole range of Ge fractions could now be sustained at or below 50 meV, which is essentially identical to those found in the best quality a-Si:H thin films (Cohen and Searle 1998). Likewise, the deep defect densities in such optimized material were found to lie at or below the mid 10^{16} cm^{-3} level in the as deposited state for Ge levels up to 50 at%. It is after this point that the first deliberate efforts to examine the degradation kinetics in the a-SiGe:H alloys were published in two studies during 1992. (Schumm et al. 1992, Morin et al. 1992, Wang et al. 1992)

One of these important investigations was performed by Schumm et al. (Schumm et al. 1992). The degradation of photoconductivity was examined for four a-SiGe:H films with varying Ge concentration from x = 0 to x = 42, correspondingly optical gaps change between 1.66 to 1.45 eV. To guarantee spatially uniform optical exposure for the samples of varying gaps, a second piece of each sample was used as an optical filter to cut off photon energies above the optical gap. The intensities following the filtering were also adjusted to be the same for all films. In this manner, the carrier generation rates were reasonably well matched around 2x10^{22} cm^{-3} s^{-1} for the complete set of samples. The results of this study pointed out that the photoconductivity degraded roughly as the cube root of exposure time. This is in a good agreement with the degradation kinetics in pure amorphous silicon and thus indicating a similar defect creation process. It was also found that a smaller absolute degradation rate was found for the alloys with higher Ge concentration and decreased optical gaps which agreed with previous findings of some earlier work (Kolodzey et al. 1986).

In the second study, Wang, Morin and Wagner reported an extensive study of metastable deep defect creation in the a-SiGe:H alloys by measuring the changes in the sub-band-gap absorption coefficient spectrum using the constant photocurrent (CPM) method (Morin et al. 1992, Wang et al. 1992). The procedure to estimate the density of

midgap states in CPM method is the integration of the excess sub-bandgap absorption. It is due to the contribution of deep defects to the absorption up to the Urbach energy. The excess absorption ($\Delta\alpha$) due to sub-bandgap states can be found by deducing the exponential absorption tail from the measured absorption spectrum. $\Delta\alpha(E) = \alpha - \alpha_{exp}$. The density of states in terms of excess absorption can be estimated as in Equation 1.1

$$N = C \int_{E1}^{E2} \Delta\alpha(E)dE \qquad (1.1)$$

In this equation, C is a constant determined by the index of refraction of the material, electron mass and charge and speed of light etc. Wronski et al (Wronski et al. 1987) found the constant $C=7.9e^{15}$ $cm^{-2}eV^{-1}$ using Electron Spin Resonance experiments, which only measures neutral dangling bond density for a-Si:H. In the study by Morin et al. 1992, and Wang et al. 1992, the effect of this constant has been underestimated and as the exact constant cannot be calculated quantitatively for a-SiGe:H thin films of various Ge%, the constant for a-Si:H has been used. It was found that the saturated defect densities at room temperature were nearly constant at 7×10^{16}-9×10^{16} cm^3 even tough the initial defect densities changed between mid 10^{15} to mid 10^{16} cm^{-3} in the annealed state. In addition, similar defect creation kinetics and temperature dependence of saturated defect density have been found for both pure a-Si:H and a-SiGe:H alloy thin films with different optical gaps from 1.62eV to 1.51eV, as agreed with previous investigators.(Aljishi et al. 1989, Schumm et al. 1992)

The above studies clearly established that degradation occurs in the a-SiGe:H alloys in a manner similar to pure a-Si:H. (Schumm et al. 1992, Morin et al. 1992, Wang et al. 1992). They suggest that the kinetics of deep defect creation and thermal annealing are also similar and that the systematic variation with increasing Ge content seems to be a result of varying optical gap, not the Ge content directly. (Schumm et al. 1992, Kolodzey et al. 1986).

Another important question regarding deep defect creation is whether it actually persists to alloys with higher Ge fractions. To illustrate this, data from a couple of studies (Cohen 1998 and Cohen 2002) employing optimized United Solar a-SiGe:H films showing the deep defect densities before and after light-induced degradation as determined by the drive-level capacitance profiling method was compiled (Michelson et

al. 1985). These data, also shown in Figure 1.3, clearly indicate that there is an increase in both the annealed and degraded state deep defect densities as the germanium concentration increases but the factor of deep defect density increase becomes smaller as the Ge fraction increases (Cohen et al. 2003).
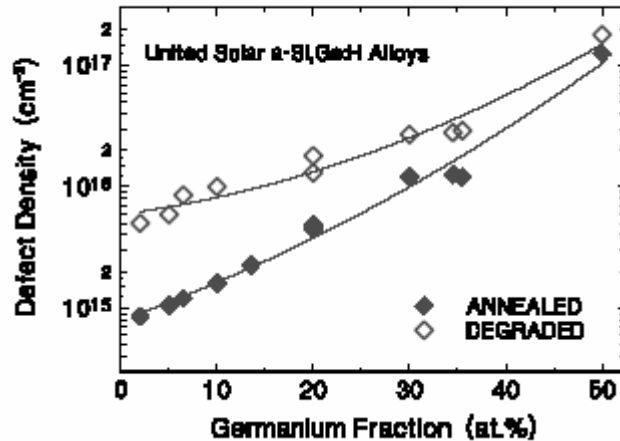
Figure 1.3   Initial and degraded deep defect densities of 11 United Solar glow discharge a-Si,Ge:H films as determined by the drive-level capacitance profiling method, although both the annealed and degraded state deep defect densities increase with increasing Ge fraction, the relative increase decreases with Ge fraction (Cohen et al. 2003).

Fritzsche et al. and Unold, have suggested that the production of metastable deep defects under light exposure might actually cease for optical gaps below a certain value. Fritzsche has pointed out that one has not observed light-induced deep defect creation in pure a-Ge:H even for cases of very low initial defect densities (Fritzsche et al. 1996). Unold proposed in 1994 that, a-SiGe:H with Ge fractions above about 65 at% Ge (optical gaps below 1.3 eV) would be stable (Unold 1994). If this turns out to be true it would suggest that there exists a certain energy threshold below which the recombination of electrons and holes does not lead to the creation of metastable deep defects.

Recently, in 2003, Cohen made a research to identify the types of dangling bonds present in the a-Si,Ge:H alloys with an alternative method to ESR, called modulated photocurrent (MPC) method (Cohen et al. 2003). The difficulty in interpreting ESR to deduce types of dangling bonds led Cohen to use MPC method. In this study it appears that there may be three distinct regimes depending on the Ge fraction of the material. The first regime that was found seems to be a low Ge fraction

regime, below 20 at%, where Ge dangling bonds dominate the annealed state deep defect population but where Si dangling bonds dominate the metastable deep defect population. Second, there appears to be an intermediate Ge fraction regime, extending from about 30 to 60 at%, where the Ge dangling bonds seem to dominate in both the annealed as well as the light-degraded states. Third regime was for samples with Ge fractions exceeding 60 or 70 at% and no light induced degradation was observed. As has been suggested by several researchers, this would reflect the fact that carrier recombination for alloys with lower gaps no longer have sufficient energy to generate metastable defects.

The summary of the studies on a-SiGe:H alloy thin films and degradation mechanism have improved the understanding of defect structure in the annealed state as a function of germanium concentration and also its effect on the SWE in a-SiGe:H alloy thin films. However, much detailed studies using the different methods are necessary to improve the understanding of the effect of Ge content on defect creation mechanism due to light induced degradation.

1.1 Thesis Objectives

Hydrogenated amorphous silicon-germanium alloy thin films of various germanium concentrations, are potential candidates meeting the requirements of high efficiency stacked solar cells and optoelectronic devices where a certain bandgap is necessary. The aim of this thesis is to obtain reliable information about the native and light induced defect states present in a-SiGe:H alloy thin films of various germanium concentrations.

To study the effects of native defects in the opto-electronic properties of a-SiGe:H alloy thin films, samples with varying Ge concentration have been studied experimentally. SSPC, DBP and optical transmission measurements have been performed to see the effects of Ge concentration on the majority carrier $\mu_n\tau_n$-products, absolute absorption coefficient at low energies, changes in the optical gap, and the Urbach tail slope, E_{0v}. Absolute absorption coefficient spectrum has been calculated for the first time for a-SiGe:H alloy thin films from the dual beam photoconductivity yield, Y_{DBP} and optical transmission, T, spectra using the Ritter Weiser optical equations. The calculated absolute optical absolute absorption coefficient spectrum of each sample was

compared with that of independently measured by another absolute absorption coefficient measurement technique called PDS. PDS measurements in the annealed state were measured at Research Center Juelich in Germany.

Another aspect of this study has been to investigate the kinetics of Staebler Wronski Effect (SWE) on various a-SiGe:H alloys with different Ge content. The effects of different intervals of white light illumination, on the SWE has been investigated by looking at degradation in SSPC and increase in the sub-band gap absorption coefficient obtained from DBP measurements. Kinetics of defect creation for different germanium contents has also been compared with those present in unalloyed hydrogenated amorphous silicon films (a-Si: H). The results in a-Si:H and a-SiGe:H alloy thin films were compared with those previously reported data in the literature.

CHAPTER II

EXPERIMENTAL TECHNIQUES

2.1 Material Fabrication

Hydrogenated amorphous silicon germanium alloy thin films (a-SiGe:H) used in this study with consisting of different germanium concentrations were deposited by using PECVD technique as shown in Figure 2.1. PECVD process is based on a glow discharge of hydrogen containing gases (like silane (SiH_4), germane (GeH_4), and H_2), which are decomposed in an alternating electrical field with a frequency of usually 13.56 MHz (rf- PECVD). It is a technique in which one or more gaseous reactors are used to form a solid insulating or conducting layer on the surface of a substrate, enhanced by the use of a vapor containing electrically charged particles or plasma at lower temperatures. The main mechanism for the dissociation of the molecules is the impact of electrons, which take up sufficient kinetic energy from the electrical field. As a result, film precursors, like SiH_3, that contribute to the growth of the solid film onto the substrate, which is usually placed on one of the electrodes, are produced.

The properties of the deposited films are mostly under the effect of gas flow in the medium. In this study, a-SiGe:H alloy thin films of various Ge concentrations were prepared at Research Center Juelich in Germany. The parameter determining the Ge concentration in the resulting film can be given as the ratio of germane gas flow to the total gas flow in the system:

$$\gamma = \frac{\left[GeH_4\right]}{\left[GeH_4\right] + \left[SiH_4, Si_2H_6\right]}$$

One important aspect of PECVD method is that the dissociation energy of the process gas molecules and part of the energy required for the formation of crystallites need not be supplied thermally. Consequently, low substrate temperatures (T_s) may be used in PECVD method. Other parameters altering the properties of the prepared films are gas pressure, discharge power (P), and plasma excitation frequency (ν_{ex}).

The a-SiGe:H alloy thin films of various Ge% which are used in this study are prepared by PECVD method at standard 13.56MHz frequency. The process temperature was 200°C and pressure was 700mTorr. The Ge% of the samples vary between 0% (a-Si:H reference sample) and 75%. The thicknesses of the films were calculated from the corresponding transmission spectra. The properties of the samples used in this study are summarized in table 2.1

Table 2.1 A list of a-SiGe:H alloy thin films used in this thesis.

Sample Name	Ge %	t (cm)	Deposition Method
DL 146	10%	6.9E-05	PECVD, 13.56 MHz, 200C. 700mTorr
DL 147	20%	6.7E-05	PECVD, 13.56 MHz, 200C. 700mTorr
DL 148	30%	6.1E-05	PECVD, 13.56 MHz, 200C. 700mTorr
DL 149	40%	4.4E-05	PECVD, 13.56 MHz, 200C. 700mTorr
DL 156	50%	9.9E-05	PECVD, 13.56 MHz, 200C. 700mTorr
DL 154	75%	8.8E-05	PECVD, 13.56 MHz, 200C. 700mTorr
02B393	0%	6.6E-05	PECVD, 13.56 MHz, 200C. 700mTorr
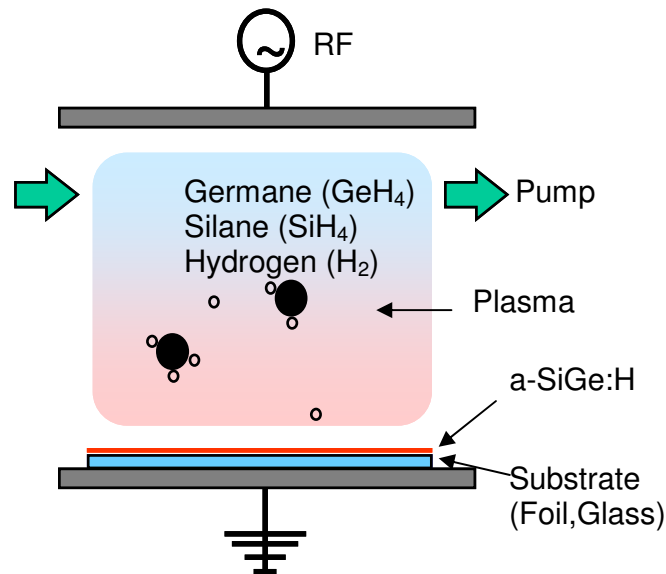
Figure 2.1 Schematic diagram showing the PECVD System (Juelich Research Center)

2.2 Characterization Techniques

In this section the experimental techniques used to characterize the optoelectronic properties of a-SiGe:H thin films of different germanium concentrations will be explained in detail. These techniques are steady state photoconductivity (SSPC), DBP, and PDS. Finally, the procedure that is used to calculate the absolute absorption coefficient spectrum from DBP method will be discussed.

2.2.1 Steady State Photoconductivity Method

Steady state photoconductivity measurements were carried out using a homemade steel box and Osram 250W ENH white light source which is cooled by a fan. The configuration of the system is illustrated by figure 2.2. The incident light flux was determined with a calibrated pin photodiode which has 14.5 mm^2 active area. The monochromatic, uniformly absorbed light was achieved by using interference bandpass filters with energy hν=E>E$_{opt}$ of the sample studied. To get a higher generation rate, volume absorbed RG610 long bandpass filter which transmits wavelengths greater than 610nm was used. Light intensity was adjusted to lower flux values by using neutral density filters which transmit 0.1%, 1%, 10%, and 50% of incident light. Constant voltage was applied and the photocurrents were measured using a Keithley 6517 A Electrometer in the ohmic regime of current-voltage curve.
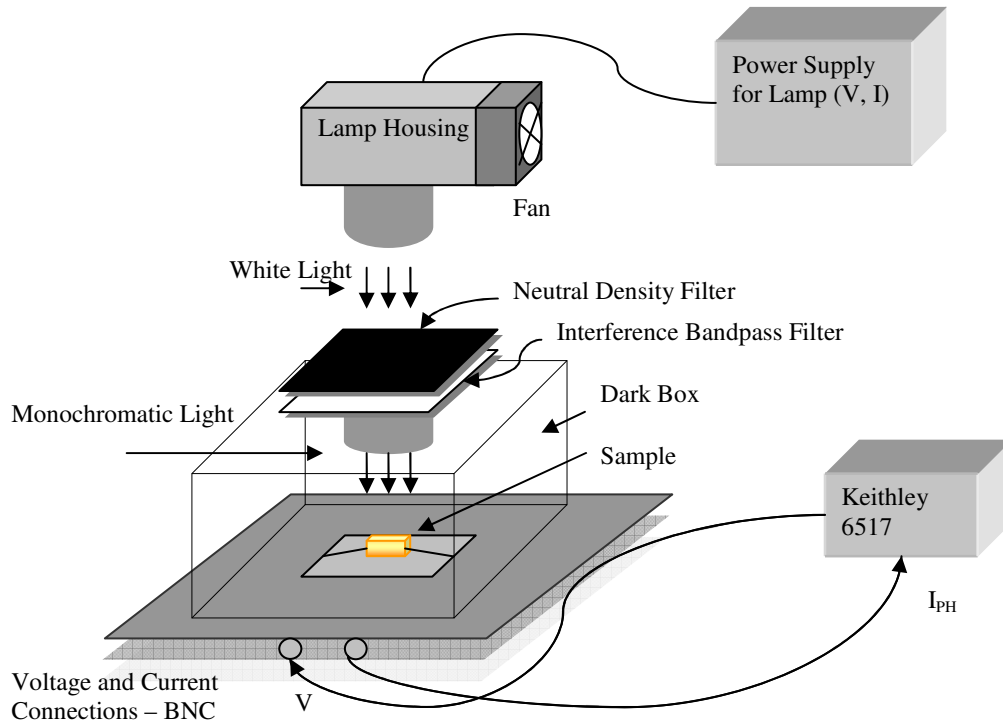
Figure 2.2 Schematic diagram of SSPC System.

For samples in coplanar geometry, photoconductivity is calculated from measured photocurrent (I_{ph}) and sample geometry as seen in figure 2.3.
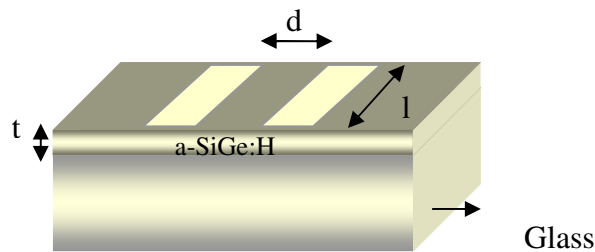
Figure 2.3 Schematic diagram showing sample geometry.

Ohm's Law is used to correlate the measured photocurrent:

$$R = \frac{V}{I_{ph}} \qquad (\Omega) \qquad\qquad (2.1)$$

where V is the applied voltage, I_{ph} is the measured photocurrent and R is the resistance of the material. The resistance of a material is dependent on its resistivity ρ and its geometry. Here d is the distance between the contacts, A is the area which is equal to

15

the length of the contacts (l) times the thickness (t) of the film. The units are taken to be centimeters. Thus, the coplanar photoconductivity becomes dependent on I_{ph}, the measured current in amperes, V the applied voltage in volts, and the geometry.

$$\sigma_{ph} = \frac{1}{\rho} = \frac{I_{ph}d}{Vlt} \qquad (\Omega\text{-cm})^{-1} \qquad (2.2)$$

On the other hand, photoconductivity can also be written as a function of photogenerated free carriers:

$$\sigma_{ph} = q\mu_n n + q\mu_p p \qquad (\Omega\text{-cm})^{-1} \qquad (2.3)$$

In this formula μ_n and μ_p are extended state mobility of free electrons and holes, n and p are the number of free electrons and holes per cm^3 in their respective extended states. Hydrogenated amorphous silicon germanium alloy thin films show slightly n-type conduction. Therefore, only electron dominated conduction is measured in the samples. Using measured photoconductivity, σ_{ph} becomes:

$$\sigma_{ph} \cong q\mu_n n \qquad (\Omega\text{-cm})^{-1} \qquad (2.4)$$

Free majority carrier density n is created by the generation rate of monochromic light and can be stated as:

$$n = G\tau_n \qquad (cm^{-3}) \qquad (2.5)$$

where G is generation rate and τ_n is lifetime of free electrons. From this point, a very important parameter about the photo generated carriers, $\mu_n\tau_n$-product also known as photosensitivity can be calculated as follows:

$$\mu_n\tau_n = \frac{\sigma_{ph}}{qG} \qquad (cm^2V^{-1}) \qquad (2.6)$$

The generation rate of electrons is expressed as follows:

$$G = \frac{F(h\nu)\eta(h\nu)[1-R(h\nu)][1-e^{-\alpha(h\nu)t}]}{t} \qquad (cm^{-3}s^{-1}) \qquad (2.7)$$

where R is reflection from film surface, α is the absorption coefficient at given wavelength of monochromatic light, t is the thickness of the film and F is the incident flux calibrated using a pin photodiode. The flux of monochromatic light is calibrated by measuring the characteristics of pin photodiode and expressed as:

$$F(h\nu) = \frac{I_{ph}(h\nu)}{AQE(h\nu)q} \qquad (\text{cm}^{-2}\text{s}^{-1}) \qquad (2.8)$$

where $I_{ph}(h\nu)$ is corresponding photocurrent measured by pin photodiode at photon energy $h\nu$, A is the area of the detector, $QE(h\nu)$ is the quantum efficiency of pin photodiode at energy $h\nu$, and q is the electron charge.

SSPC exhibits a non-integer power low dependence on light intensity $F(h\nu)$ or on generation rate G.

$$\sigma_{ph} \propto G^{\gamma} \qquad (\Omega\text{-cm})^{-1} \qquad (2.9)$$

And correspondingly, mobility lifetime product also proportional to the generation rate as:

$$\mu\tau \propto G^{(\gamma-1)} \qquad (\text{cm}^2\text{V}^{-1}) \qquad (2.10)$$

where γ, the constant in the exponential term, is related to recombination kinetics of light generated electron-hole pairs in the material. γ has a value between 0.5 and unity. If, $\gamma = 0.5$, it represents bimolecular recombination kinetics, where electrons in the conduction band directly recombine with the holes in the valence band as in crystalline silicon. If, γ has a value between 0.5 and unity, it represents monomolecular recombination, where electrons in the conduction band recombine with holes in the valence band through the recombination centers localized in the bandgap. In other words, it is an indication of continuous distribution of defect states in the bandgap of a semiconductor.

SSPC measurements give information about the nature of defects through the mobility-lifetime products which is directly correlated with transport and recombination kinetics of photogenerated carriers as described above. The non-integer power law dependence on light intensity is a consequence of the continuous distribution of gap

states. Since the states between quasi-Fermi levels act predominately as recombination centers, SSPC is sensitive to both density and nature of these states. In this thesis, samples were characterized in the annealed and light soaked states. SSPC measurements in both states give rise to understanding effects of native and light induced defect states on $\mu_n\tau_n$-products. In more detail, in the annealed state, SSPC measurements result in understanding the effects of various Ge% the native defect states present in the bandgap of thin film created during the deposition. In the light soaked state, the effect of Ge concentration on the degradation of $\mu_n\tau_n$-products and correspondingly on the evolution of the Staebler-Wronski defects have been investigated through the changes in the SSPC results.

2.2.2 Dual Beam Photoconductivity

The DBP technique is dependent upon measuring a.c. photoconductivity of a sample as a function of energy of monochromatic light (Wronski et. al 1982, Lee et. al 1998, Gunes and Wronski 1992a, Gunes et. al 2003b). It uses two light beams to measure photoconductivity spectrum. These are high generation dc bias light beam and an a.c. monochromatic light beam modulated with a frequency of 13Hz. The generation rate of the modulated monochromatic ac light is much lower than the generation rate of the dc light beam. In DBP method, the aim of using high generation rate dc bias light is to maintain the free carrier lifetime constant by keeping the electron and hole quasi-Fermi levels constant during the measurement.
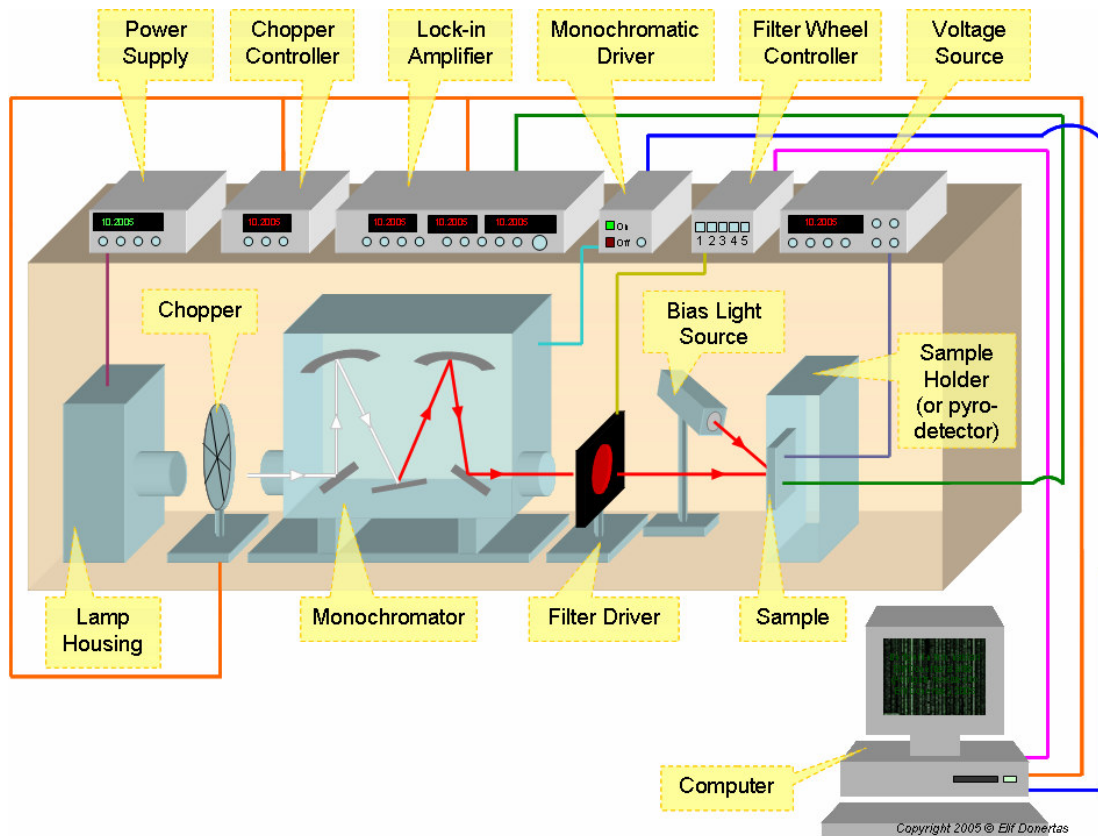
Figure 2.4 DBP System used to measure the sub-bandgap absorption and transmission in a-SiGe:H thin films.

Therefore, the distribution of the occupied defect states in the mobility gap remains unchanged during the measurement. On the other hand, modulated light beam has a very low generation rate (g(hν)) than the dc bias light so that the quasi-Fermi levels are not altered by the ac light beam. As a consequence, a.c. photoconductivity linearly depends on monochromatic a.c. light intensity. Hence, no changes are observed in the mobility lifetime product of dc light due to additional a.c. monochromatic light incident on the sample. This indicates that, the statistics of occupied defect states will be unchanged during the measurements. Then, the monochromatic a.c. light excites the electrons from the occupied localized defects to the conduction band. Those electrons in the conduction band are detected as a.c. photocurrent when energy of the monochromatic light is changed. As a result, the effects of occupied localized defect states will be measured as a.c. photoconductivity.

Photoconductivity for a sample in coplanar geometry was derived previously in equation 2.4. This formula was simplified as the contribution of hole transport is negligible due to its low mobility lifetime-product compared to that of electrons.

19

$$\sigma_{ph}(a.c.) = q\mu_n n \tag{2.11}$$

This equation can be written for ac photoconductivity, $\sigma_{ph}(a.c)$, by using the equivalent relation for the number of electrons which is the product of free electron lifetime and generation rate of ac light: $(n_{ac}=\tau_n g(h\nu))$. Finally, the sub-bandgap photoconductivity arising from the monochromatic beam as a function of generation rate can be written as:

$$\sigma_{ph}(a.c.) = q\mu_n \tau_n g(h\nu) \tag{2.12}$$

When generation rate given in Eq. 2.8 is used in Eq 2.12 and for the condition $\alpha t<<1$ is applied; $\sigma_{ph}(a.c)$ is simplified as:

$$\sigma_{ph}(ac) = q\mu_n \tau_n \eta(h\nu) F_{ac}(h\nu)(1-R(h\nu))\alpha(h\nu) \tag{2.13}$$

Photoconductivity divided by incident flux gives normalized photoconductivity, which is called DBP yield spectrum, $Y_{DBP}(h\nu)$:

$$Y_{DBP}(h\nu) = \frac{\sigma_{ph}(ac)}{F_{ac}(h\nu)} = [q\mu\tau\eta(h\nu)(1-R)]\alpha(h\nu) = c\alpha(h\nu) \tag{2.14}$$

where c is a constant as:

$$c = [q\mu_n \tau_n \eta(h\nu)(1-R)] \tag{2.15}$$

Absolute absorption coefficient, $\alpha(h\nu)$, is proportional to the DBP yield spectrum only by a constant c, by making these necessary assumptions, such as: In DBP technique, $\mu\tau$ product is fixed to be constant using the high intensity bias light and it is not altered by the monochromatic beam. The multiple reflections in the air-film-substrate structure are neglected. $R(t,E)$ and $\eta(E)$ are assumed to be constants of energy and $\alpha(h\nu)t$ product is much smaller than unity.

$$\alpha(h\nu) \propto Y_{DBP} \tag{2.16}$$

These assumptions are essential principles of the DBP method and must be fulfilled to obtain reliable absorption coefficient spectrum. It is extremely important to state that DBP is a relative measurement, and it doesn't give the absolute absorption coefficient spectra. As a result of DBP measurements we have the DBP yield spectrum (Y_{DBP}), which is proportional to absolute absorption spectra. Generally, to reach to absolute absorption coefficient spectra at low energies, Y_{DBP} spectra is normalized to absolute absorption coefficient spectrum obtained from transmission and reflection measurements (T&R) (Cody et. al 1980) or from PDS (Gunes et. al 2003b)

The main feature of the Y_{DBP} spectrum is that in the low photon energy region it shows fringes rather than a smooth curve due to multiple reflections at the film-substrate interface. On the other hand, there are no fringes in the absolute absorption spectra. These fringes depend on film thickness, for thicker films, the fringes are smaller and closer together. These interference fringes are generally removed by using fast Fourier transform (FFT) procedure (Wiedeman et. al 1987). In this thesis, a procedure based on Ritter-Weiser formula for calculating fringe free absorption spectra from DBP yield spectrum will be applied. The method has already been applied by Goktas. The procedure applied to obtain absolute absorption coefficient by using Ritter-Weiser formula is given in detail in the next section.

The DBP system is shown in Figure 2.4. All optical elements were aligned on an Oriel optical table and a box completely concealing the system from outside effects is used to cover the system. A Quartz Tungsten Halogen (QTH) lamp is used as a white light source. The QTH is located in an Oriel 66182 model lamp housing controlled by a 300 W Radiometric power supply. A chopper blade was mounted in front of the white light source just before the entrance slit of the monochromator to chop the white light off to have an ac signal and it is regulated by a chopper controller at 13 Hz. While using DBP method the appropriate frequency for the response time of the material is low frequencies. 13 Hz has been used in this study, as it is an optimum frequency for this material and DBP method. The chopper controller has 1Hz sensitivity. The chopper controller is connected to lock-in amplifier to determine the reference frequency of the measurements. An Oriel monochromator having 0.2 nm sensitivity was used with a 600-lines/mm grating. Monochromator crank was controlled by Oriel monochromator driver. A filter driver is placed at the exit slit of the monochromator in order to cut-off unwanted second and high order wavelength refraction peaks. An Oriel filter wheel

controller was used to change filters. There are three long pass filters with wavelengths of 500 nm, 700 nm, 900 nm, and single crystalline silicon with wavelength of 1100 nm.

The two beams, white light which is adjusted to the desired wavelength and frequency and dc bias light from a set of red light emitting diodes (LED) are focused to fall on the sample mounted on a sample holder. The sample is connected to the lock-in amplifier and the voltage source by BNC connections. To apply external d.c. voltage to the sample and to measure both dark current and photocurrent due to bias light, a Keithley 6517A Electrometer was used. a.c. signals coming from the sample and detectors were detected by SR830 lock-in amplifier.

For flux and transmission measurements, a pyroelectric detector has been used. The detector is placed behind the sample for transmission measurements and it faces the monochromatic light directly for flux calibrations. The detector is connected to a 9V battery.

DBP system is computer controlled. A Keithley IEEE 488 card was used to provide General Purpose Interface Bus (GPIB) protocol. SR830 lock-in amplifier, monochromator driver and filter driver are connected to IEEE 488 card. A computer program written by Objectbench software is used to control the experimental system and for data acquisition. Having placed the sample on the sample holder, the computer program was called to start measurements. After initializing the lock-in amplifier and monochromator, program requires adjusting initial energy, energy step value, and number of measurements for each energy. The program also controls the changing of bandpass at certain energies. In DBP measurement, raw current, phase, and averaged current divided by flux were measured for each energy value and recorded to data file. After the measurements, absolute absorption coefficient values were calculated by a computer program based on Ritter–Weiser formula. Finally, the data files are processed using a graphics program to plot true $\alpha(h\nu)$ spectra. The computer program used for DBP measurements, flux measurements and transmission measurements is given in appendix.

2.2.3 Flux Calibration

The Quartz Tungsten Halogen (QTH) lamp used as a white light source in DBP system does not have a flat flux spectrum but a spectrum depending on the photon

energy and time. Therefore, before each DBP measurement, it is essential to have flux calibration to eliminate possible flux change of the lamp with time. Flux calibration was carried out using a pyroelectric detector in energy range from 0.6eV to 2.5eV. An example of the flux spectrum of monochromatic white light source of a Quartz Tungsten Halogen lamp is shown in Figure 2.5. A pyroelectric material has electric polarization even in the absence of an applied voltage. They are thermal type infrared detectors that
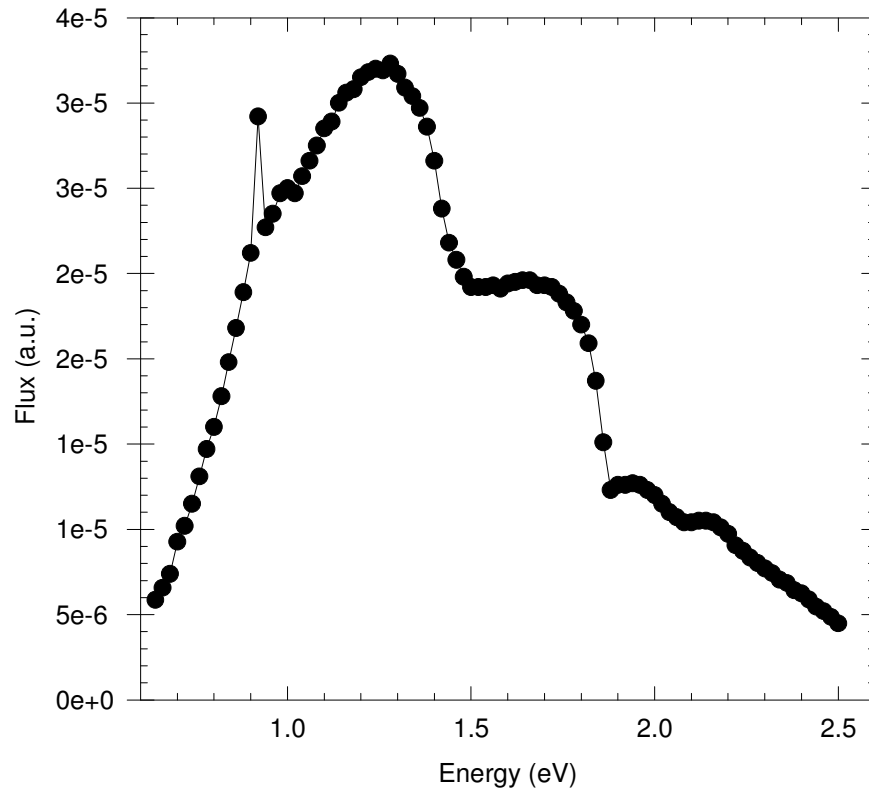
Figure 2.5 Flux spectrum of Quartz Tungsten Halogen (QTH) lamp obtained using pyroelectric detector.

feature stable operation at room temperature and show a responsivity independent of wavelength. When light enters the element and is absorbed, the element's temperature increases resulting in a change in the state of spontaneous polarization. These changes are detected as a voltage change. Since the pyroelectric detector detects light only when a temperature change in the element occurs, it is necessary to use an optical chopper and lock-in amplifier to receive data. The advantage of the pyroelectric detectors is that it is sensitive to a wide range (0.1μm-100 μm) of the optical spectrum and has a flat photoresponse. Then, the flux data were used for normalization of DBP spectrum and transmission spectrum.

2.2.4 Transmission Spectrum

The pyroelectric detector was mounted in to the sample holder at the backside of the sample to obtain the transmission by measuring the voltage changes by means of lock-in amplifier. A 9V standard battery was used to operate the pyroelectric detector. A typical transmission spectrum of a hydrogenated amorphous silicon germanium alloy thin film is presented in Figure 2.6.
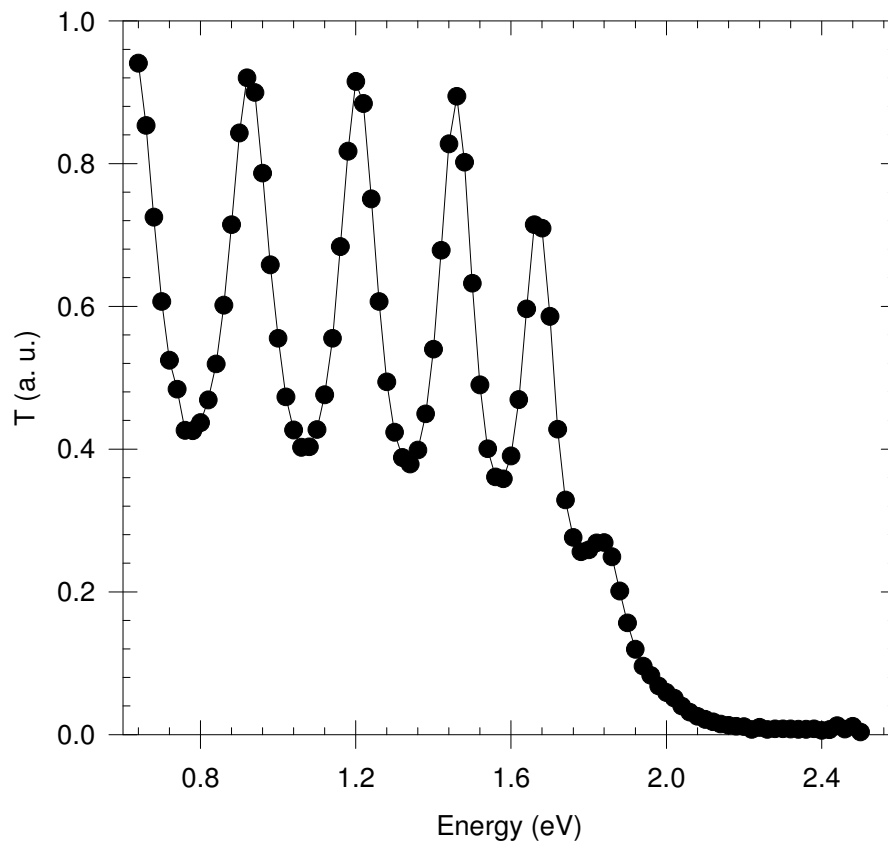
Figure 2.6. Transmission spectrum of a a-SiGe:H thin film.

At higher energies, most portion of the light is absorbed by the film and transmission decreases with increasing absorption. Therefore, transmission goes to zero. Then, it gradually increases with decreasing energy since absorption of investigated films decrease sharply in this energy region. It was found in the literature that reflection is observed not to be changed significantly in this energy region. The appearing fringes are due to interference of light in the film resulting from reflection of light in the film-substrate interface. The first interference peak is observed when the wavelength of

incident light is comparable to the film thickness. For thicker films, interference fringes appear in the lower energy values. The normalized spectra were obtained by dividing the voltage-photon energy ratio to flux. Transmission data were also used to calculate the film thickness using two energy values corresponding to two peaks in the transmission spectrum in the low energy region and refraction index of silicon germanium alloys. In addition, the transmission spectrum was used to calculate fringe free absolute absorption coefficient spectrum of these films using the Ritter-Weiser optical equations (Ritter and Weiser 1986).

2.2.5 DBP Spectrum

The experimental setup and theory of DBP spectrum was presented at the beginning of this chapter. DBP is based on relative measurement of the ac photoconductivity and does not give rise to absolute absorption coefficient spectrum. Energy dependence of the raw current spectrum is attained by altering the energy of the incident light on the sample. Since the incident light does not give a flat flux curve, the raw photocurrent is divided by the relative flux data. The resulting spectrum is called normalized photocurrent spectrum.

A characteristic raw and normalized photocurrent spectra for the a-SiGe:H alloy thin films measured by DBP are shown in the Figure 2.7. The relative flux data is used to normalize raw photocurrent spectrum. The normalized photocurrent spectrum, DBP yield spectrum, $Y_{DBP}(ac)=\sigma_{ph}(ac)/Flux$, is proportional to the absorption spectrum when certain assumptions of DBP are satisfied. First, constant $\mu\tau$ product of majority carrier electrons must be satisfied. This condition is controlled by calculating I_{dc} / I_{ac} ratio where I_{dc} is dc photocurrent arising from applied dc bias light and I_{ac} ac photocurrent is measured by the Lock-in amplifier. For high generation rate of dc bias light, I_{dc} / I_{ac} is much higher than unity which implies that quasi-Fermi levels of free carriers are fixed by dc bias light and are not altered by a.c. light. However, this condition is not satisfied for low generation rate of dc bias light especially in the high-energy region of the spectrum. In this case, the section of the photocurrent spectrum that satisfy $I_{dc}/I_{ac}>=10$ were taken as the reliable photocurrent spectrum. The second condition is uniform absorption of light. Since absorption coefficient of a-SiGe:H alloy thin films is typically
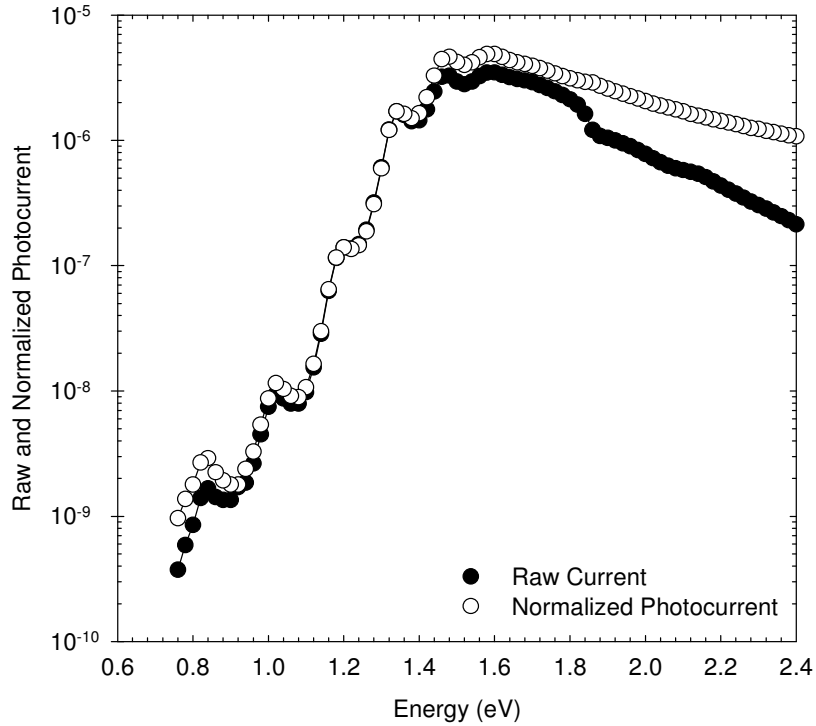
Figure 2.7. A typical row and normalized photocurrent spectra of a a-SiGe:H thin film measured by DBP method.

in the order of 10^3 cm^{-1} in the high-energy region of the spectrum and thickness of the investigated films are in the order of 0.4-0.9 μm, αt is smaller than unity even at higher energy part of spectrum. As energy decreases, $\alpha(h\nu)$ decreases exponentially and at $\alpha(h\nu)t \ll 1$ in all low energies.

One of the major benefits of DBP technique is that it uses two light beams. The monochromatic a.c. light is used to examine band-gap defects in particular. Bias light is used to investigate sub-bandgap absorption for different generation rate values. A red light emitting diode (LED) arrangement was used as a bias light to perform the experiments. The LED's were held close to each other and a diffuser glass was used to obtain a uniform illumination. Physically, bias light controls the quasi-Fermi levels in the bandgap. For all a-SiGe:H alloy thin films, sub-bandgap absorption was measured for a few generation rate values of bias light. Since the intensity of the modulated light is much smaller than the bias light, the generation rate of the modulated light is insignificant. An example of DBP yield spectrum including interference fringes measured at high and low bias light intensities is shown in Figure 2.8. It is clearly seen that DBP yield spectrum exhibits a dependence on dc bias light intensity in the low energy region.

Since the use of bias light is to control the quasi-Fermi levels and the $\mu_n\tau_n$ product of electrons, the occupation of defect states can be altered by changing bias light intensity. For that reason, by increasing bias light intensity more defect states above the Fermi level are occupied and transition from these occupied states to conduction band can be observed as an increase in DBP spectrum. This is called as the intensity dependence of DBP. As it can be seen from the Figure 2.8, the deviation of spectra for different bias light intensities begins at the end of exponential edge, which characterizes the exponential valance band tail states. Therefore, intensity of bias light has no effect on the Y_{DBP} above this energy. However, at lower energies, the Y_{DBP} spectrum is not unique and depends on bias light intensity.
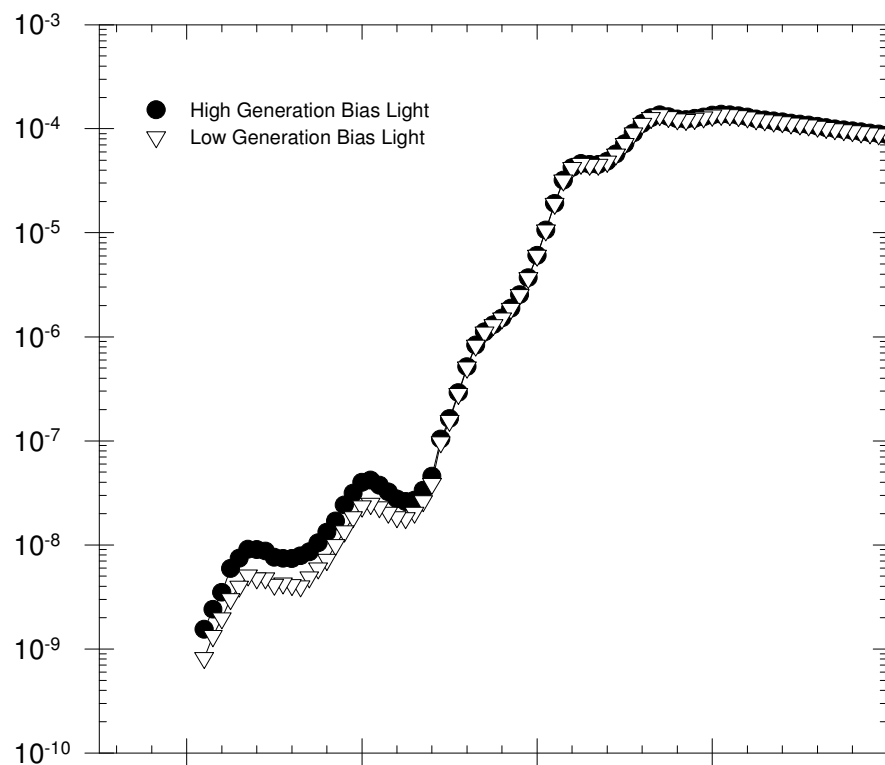
Figure 2.8. DBP spectra for different intensities of bias light.

The deviation in the spectrum at lower energy part is correlated to the occupation of defect states in the midgap. Thus, Y_{DBP} spectrum does not result in absolute absorption coefficient below the bandgap. It rather reveals the effect of electron occupied defect states present in the bandgap of the material. For low bias light intensity, occupation of defect states is very close to that in the dark condition. Thus DBP spectrum at low energies is due only to the transitions from the occupied defect

27

states below the dark Fermi level and α(hν) spectrum can be correlated to the defect states present in the bandgap below the dark Fermi level. For most of samples, DBP spectrum at possible lowest bias light intensity and high bias light intensity were measured together. Only the DBP spectrum measured at low bias light was used to compare different samples and to see defect evolution under light soaking.

2.2.6 Fringe Free Optical Absorption Coefficients Spectrum from DBP Yield Spectrum

The optical absorption coefficient, α (hν), of hydrogenated amorphous silicon germanium alloy (a-SiGe:H) thin films is important because it determines the spectral response of solar cells and other opto-electric devices. With the purpose of obtaining correct absorption coefficient of the film, several studies were made. In the previous studies, mainly interference fringes in the absorption and transmission spectrum were averaged to obtain the real spectrum (Cody 1984b). Ritter and Weiser (Ritter and Weiser 1986) was the first to report that the interference fringes could be eliminated using the normalization of the absorbance (A) and transmission (T) spectrum, A/T, of the films.

For homogenous films the maxima and minima of transmission and the absorbance take place approximately at the same energy of the spectrum. Therefore the obtained spectrum is free of fringes. A/T is also used for "absolute" CPM method to calculate the absorption coefficient spectrum of samples (Vanecek et. al 1995b) and it gives more exact and suitable results than that of averaging procedure.

As indicated earlier, DBP is a relative ac photoconductivity measurement and therefore obtained absorbance and transmission spectra are both in relative scale. To acquire absolute absorption coefficient, absorbance and transmission spectra must be in absolute scale. To be able to set A/T in absolute scale, initial step is setting the transmission spectrum in absolute scale. The maximum of transmittance is written as a function of the optical refraction index, n_s, (Swanepoel 1983).

$$T_{\max} = \frac{2n_s}{n_s{}^2 + 1} \qquad (2.20)$$

For the Corning glass 7059, T_{max} is approximately 0.92. When T_{max} in the transmission spectrum is set to this value, the absolute transmission spectrum is obtained. The following step is setting A/T in absolute scale. In order to attain absolute A/T, one reference energy point E_x is chosen in high energy region of the transmission spectrum where T is free from the interference fringes. In general $T_x=0.05$ is a fine choice since transmission spectra of the films are free of interference fringes. At this point the reflectance value, R_x, is taken to be 0.35 (Kroesen et al. 1992). The sum of the absorbance, reflectance, and transmittance is unity (A+R+T=1). Using the reflectance and transmittance value in relation A+R+T=1, the absorbance value, A_x, can be calculated at this reference energy point. After finding A_x, the relative absorbance values set to this value at the reference energy, therefore whole absorbance spectrum is obtained in absolute scale.

In more detail, the absorbance, A, is given by 1-R-T, where, T is transmittance, R is reflectance. Transmission is given in formula 2.21 and reflectance is given in formula 2.22 where n is refractive index, t is film thickness, α is absorption coefficient, λ is the wavelength of light, $k=\lambda\alpha/4\pi$, $\beta=2\pi nt/\lambda$ and δ is phase of complex Fresnel coefficient. Interference effect is due to the phase angle β.

$$T = \frac{(1-R_1)(1-R_2)(1+k^2/n^2)}{\exp(\alpha t)+R_1 R_2 \exp(-\alpha t)-2\sqrt{R_1 R_2}\cos(2\beta-\delta_1-\delta_2)} \quad (2.21)$$

$$R = \frac{R_1 \exp(\alpha t)+R_2 \exp(-\alpha t)-2\sqrt{R_1 R_2}\cos(2\beta+\delta_1-\delta_2)}{\exp(\alpha t)+R_1 R_2 \exp(-\alpha t)-2\sqrt{R_1 R_2}\cos(2\beta-\delta_1-\delta_2)} \quad (2.22)$$

A/T can be seen in equation 2.23 after doing the required calculations:

$$\frac{A}{T} = \frac{\exp(\alpha t)-R_2\exp(-\alpha t)-(1-R_2)(1+\frac{k^2}{n^2})}{(1-R_2)\left(1+\frac{k^2}{n^2}\right)} - \frac{4\sqrt{R_1 R_2}\sin(\delta_1)}{(1-R_1)(1-R_2)\left(1+\frac{k^2}{n^2}\right)}\sin(2\beta-\delta_2) \quad (2.23)$$

The first term is free of interference fringes since it is not dependent of β. The interference fringes are due to only the second term. However, for thin films of interest,

the second term can be neglected since it is much smaller than first term. The ratio of first term to the second one, as calculated in the original paper of Ritter and Weiser, is 66 for λ=t=1 μm, n=3.5, n_s=1.5 (glass) and αt«1. Since t and R_2 are constant in equation 2.23, equation 2.24 is found by omitting the second term and neglecting k^2/n^2 in the first term.

$$\alpha t = \ln 0.5 \left\{ \left(1 - R_2\right)\left(1 + \frac{A}{T}\right) + \left[\left(1 - R_2\right)^2\left(1 + \frac{A}{T}\right)^2 + 4R_2\right]^{\frac{1}{2}} \right\}$$

(2.24)

Then to have T and Y_{DBP} in absolute scale as described above is necessary. Absolute T and Y_{DBP} in absolute scale which is proportional to absolute absorption coefficient spectrum, absolute Y_{DBP}/T, is substituted in equation 2.24 instead of A/T to find equation 2.25.

$$\alpha t = \ln 0.5 \left\{ \left(1 - R_2\right)\left(1 + Y_{DBP}(abs)/T(abs)\left(hv\right)\right) + \left[\left(1 - R_2\right)\left(1 + Y_{DBP}/T\left(hv\right)\right)^2 + 4R_2\right]^{1/2} \right\}$$

(2.25)

The optical absolute absorption coefficient, α (hv), spectrum in absolute scale calculated from the absolute A/T spectrum using the Ritter and Weiser formula is given by formula 2.25.

In this thesis, the procedure to obtain fringe free absolute absorption coefficient spectrum using A/T for a-SiGe:H alloy thin films for DBP is applied for the first time. In Figure 2.9 Y_{DBP} and transmission spectra, and in Figure 2.10, calculated absolute absorption spectrum in absolute scale can be seen. The absolute absorption coefficient spectra obtained for a-SiGe:H alloy thin films of various Ge% is also compared with the absolute absorption coefficient spectra obtained by PDS method on the same samples.
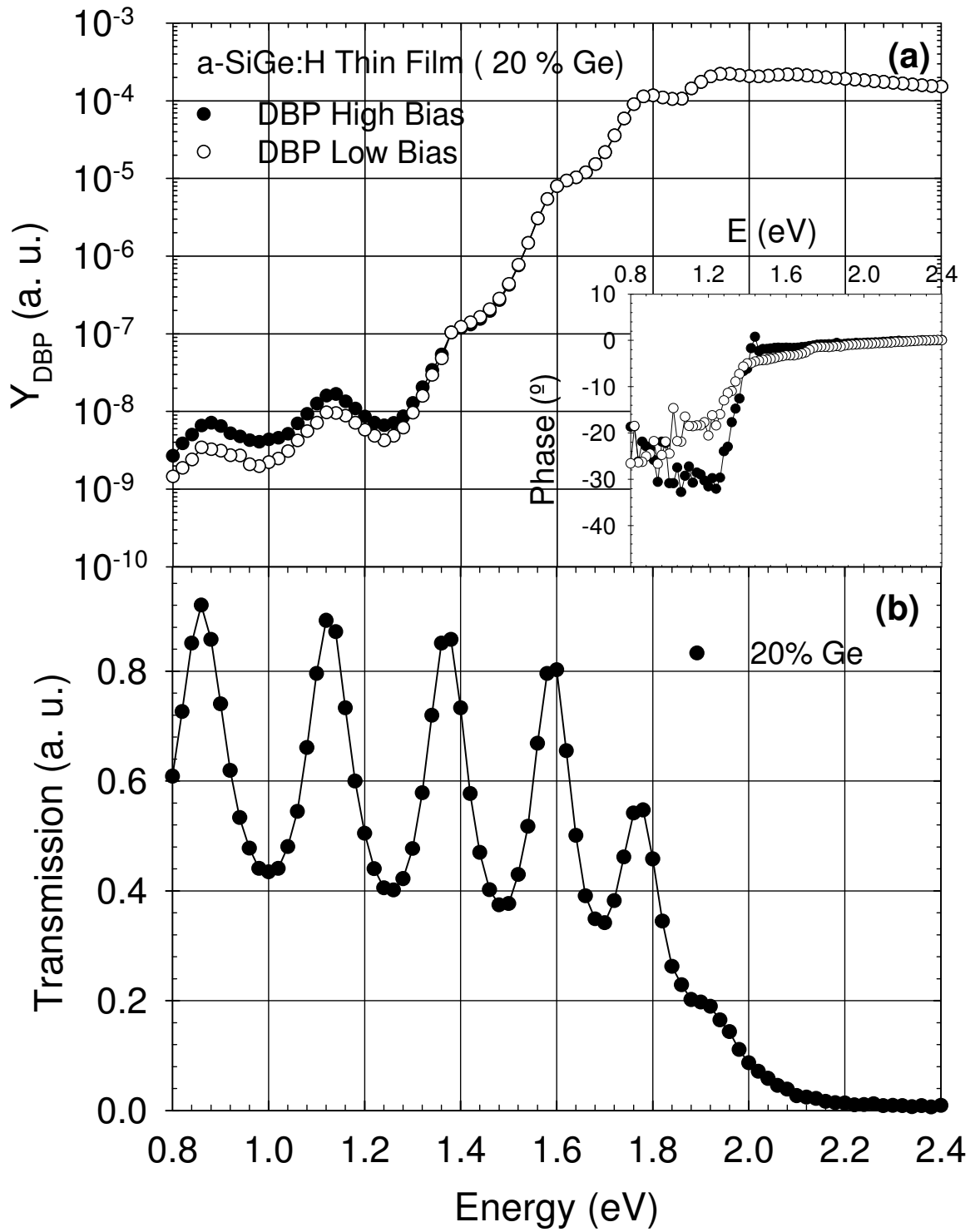
Figure 2.9 a) Y_{DBP} spectrum. b) The transmission spectrum of the film is shown.
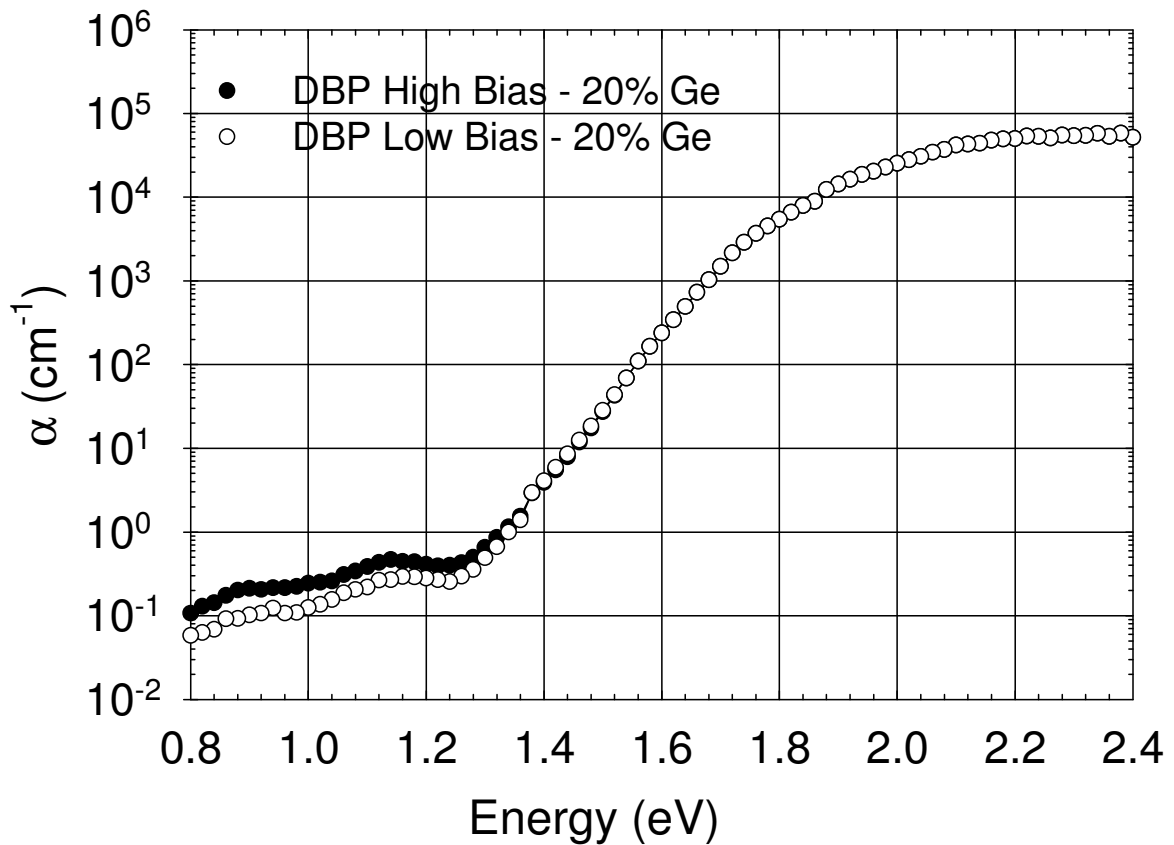
Figure 2.10 Fringe free absolute $\alpha(h\nu)$ spectrum Calculated from Y_{DBP} spectrum.

2.2.7 Photothermal Deflection Spectroscopy

Photothermal Deflection Spectroscopy (PDS) method developed by Jackson et al. (Jackson et al. 1981) is established upon measuring thermal energy deposited in the material when photons are absorbed. Just as it could be observed from the Figure 2.11, sample is illuminated with an alternating monochromatic light. The temperature of the film changes as the photons are absorbed. As the heat is transferred to the CCl_4 medium it causes a corresponding modulation in the index of refraction near the film surface. CCl_4 medium has a temperature-sensitive refraction index. The laser beam grazing sample surface experiences a periodic deflection synchronous with modulated light. The amplitude and phase of the deflected laser beam is measured using a position sensitive detector. Thus as the wavelength of the pump beam is varied, the deflection of the probe beam becomes a measure of optical absorption spectrum of the thin film. $\alpha(h\nu)$. Experimental setup of PDS is shown in Figure 2.11.
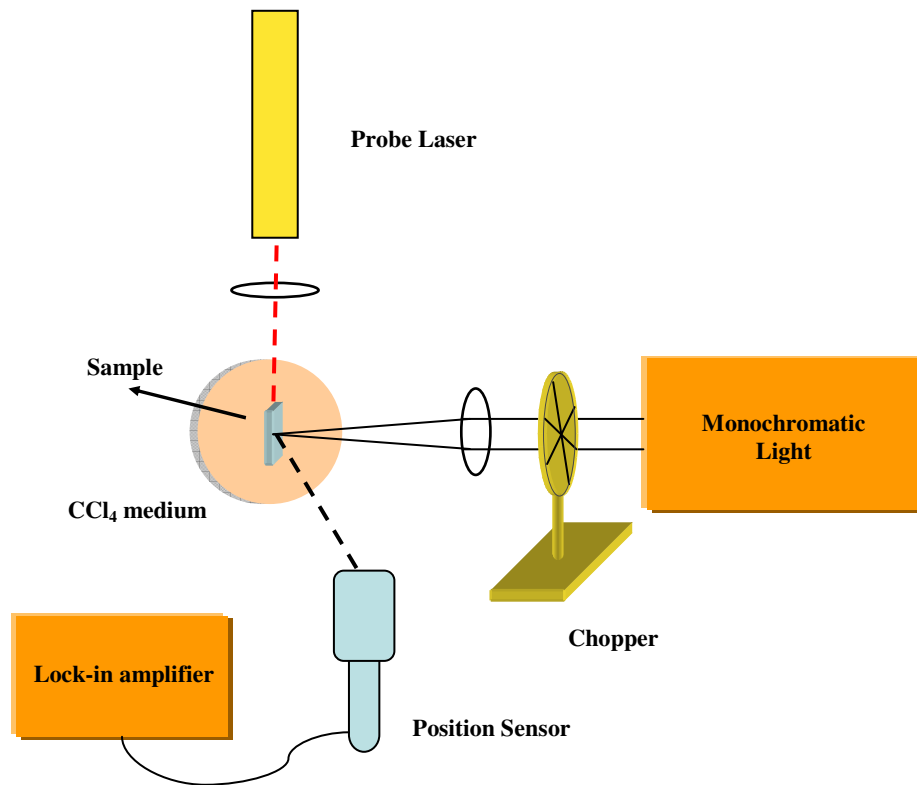
Figure 2.11. Schemetic representation of PDS System.

Generally CCl_4 is used as a deflection medium because it has extremely low absorption in the photon energy range of 0.4-2.3 µm (Jackson and Amer 1982) and does not modify the properties of silicon based thin films. PDS is a difficult measurement and very sensitive to small modulations of probe beam. Therefore, very low vibration and fine adjustments are required to obtain reliable data. The experimental setup must be well aligned and placed on a optical table in order to avoid effect of vibrations. The probe beam should be as close to the film surface as possible. The deflecting medium should be as clean as possible since particulates in the deflecting medium can results in a significant noise. The optical paths should be enclosed to eliminate effect of air currents. The probe beam should be well focused on the sample.
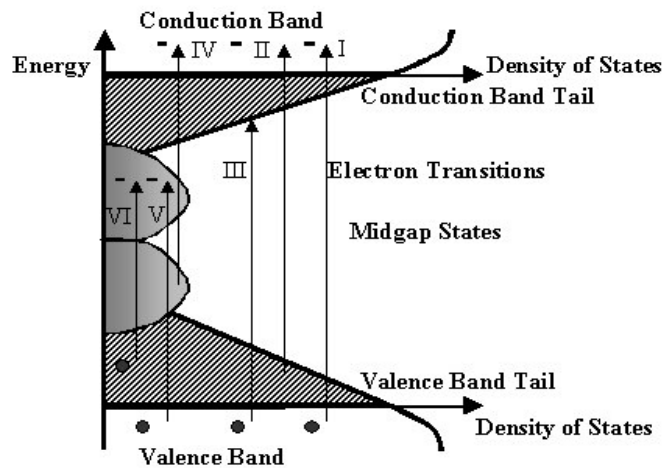
Figure 2.12 Possible optical transitions in undoped a-Si:H where (-) denotes electrons and (•) denotes holes.

Since PDS process is not a photoconductivity measurement, it does not depend on the Fermi level position. It is commonly believed that this technique is sensitive to both surface, interface and bulk states. In other words, it measures all possible optical transitions from and into empty localized defect states in the mobility gap as illustrated in Figure 2.12. In addition to transitions into the conduction band (I, II, IV), PDS detects also the other transitions (III, V, VI), which are not observed in any photoconductivity measurement. The contribution of the other transitions appears as high sub-bandgap absorption in the optical absorption spectrum of PDS. Since surface and interface defects affect the absorption spectra, for accurate measurements, a series of high quality films with different thicknesses must be investigated to interpret sub-bandgap absorption correctly.

The PDS measurements given in this thesis are done in Juelich Research Center, Germany. These measurements are only used to compare the absolute absorption coefficient spectra of two independent techniques, PDS and DBP. Absolute absorption coefficient spectra calculated for a-SiGe:H alloy thin films of several Ge% by using a computer program with the inputs of the low generation rate DBP measurements together with the simultaneously measured transmission spectra is used for DBP.

2.2.8 Light Induced Degradation Procedure

The aim of this research has been to investigate the evolution of the light induced defect states for the long term stability of a-SiGe:H based thin films of various Ge concentrations. Since it is not feasible to expose the films to AM1 light up to a few years to determine their long term stability, accelerated high intensity of 15 suns of degradation was applied to a-SiGe:H thin films.

Annealing station is made up of an annealing box, a vacuum pump connected to the box, a heater which is fixed on the copper sample holder, and Omega Temperature controller. The schematic representation of the annealing station is seen in figure 2.13. During annealing the sample is treated with vacuum under high temperatures ($3.3*10^{-1}$ torr). Temperature measurement was carried out using Omega Multimeter with a K-type thermocouple. The thermocouple is mounted on a Corning glass substrate which is similar to the substrate of SiGe:H alloy thin films. All samples were annealed in vacuum at 180 °C for 2 ½ hours before annealed state characterization.
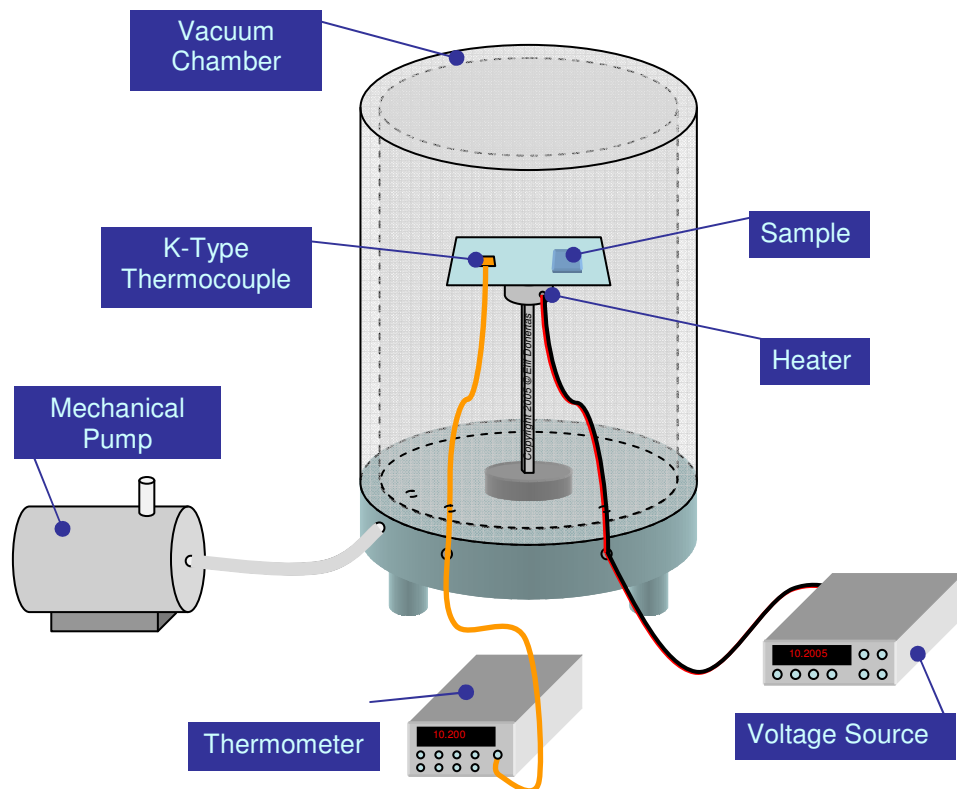
Figure 2.13 Schematic representation of annealing station

Schematic representation of the light soaking station used in this study can be seen in the Figure 2.14. An ELH lamp is used as a white light source. Light is focused to have a uniform beam by using a combination of two lenses. Both the lamp and the sample are cooled by fans during experiment. The sample temperature was measured using a thermocouple which was glued on to a glass substrate, one similar to the substrate of the film. The temperature was kept constant at about 40 °C during high intensity light soaking. Light intensity was calibrated using a pin photodiode and neutral density filters. Same product of ELH lamps were used each time to eliminate any effects from the light input. The samples were kept under high intensity light soaking for several periods and at the end of each period characterization measurements were performed.
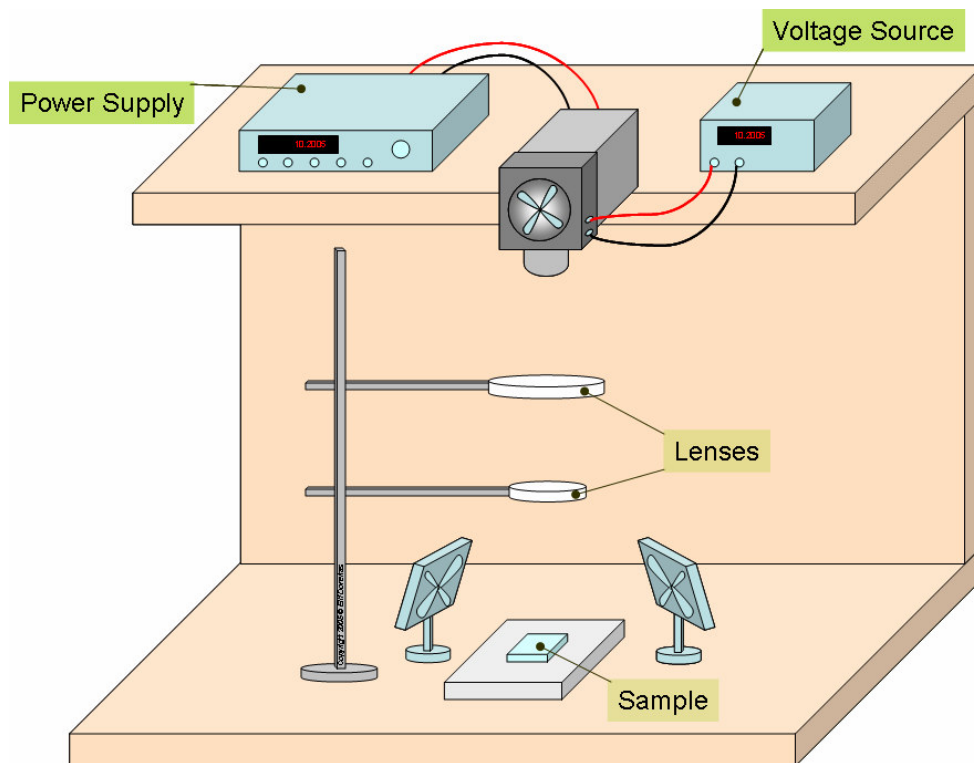
Figure 2.14 Schematic representation of Light Soaking Station

In Figure 2.15, the measurement cycle is given. The cycle begins with annealing the sample. Then for a predetermined time interval sample is left under high intensity white light illumination. After light soaking photoconductivity and DBP measurements are carried out.

36
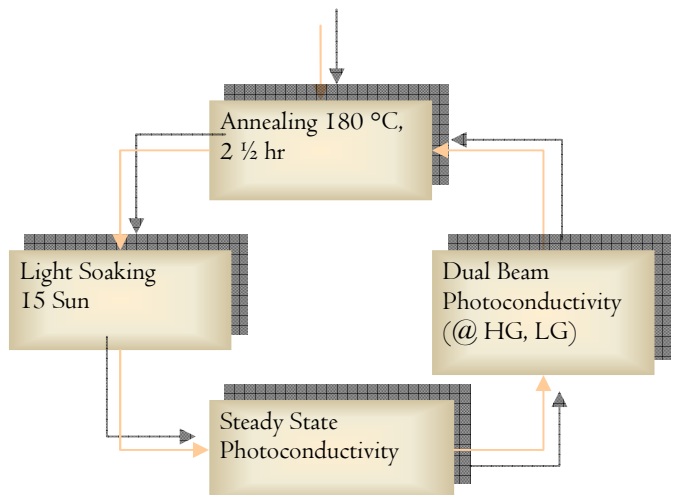
Figure 2.15 Schematic representation of Light Soaking cycle.

CHAPTER 3

EXPERIMENTAL RESULTS IN HYDROGENATED AMORPHOUS SILICON GERMANIUM ALLOY THIN FILMS (a-SiGe:H) IN THE ANNEALED STATE

3.1 Introduction

Hydrogenated amorphous silicon germanium alloy thin films of various germanium concentrations are subjected to much interest in the development of high efficiency multi-junction photovoltaic solar cells and other optoelectronic devices. By changing the alloy concentration, the electronic and optical properties of hydrogenated amorphous silicon germanium alloys can be turned to match the electronic and optical device requirements. In the annealed state, transport properties of a-SiGe:H alloy thin films are controlled by the native defects present in amorphous network. In this part of the thesis, the aim is to see the effect of germanium concentration (Ge%) on the photoconductivity, mobility lifetime product ($\mu_n\tau_n$-product) and absolute absorption coefficient spectrum of the samples. For this purpose, SSPC, DBP and optical transmission measurements were carried out to investigate the effects of germanium concentration on the defect density of hydrogenated amorphous silicon germanium alloy thin films. In SSPC, majority carrier electron mobility-lifetime product ($\mu_n\tau_n$) is obtained quantitatively. Absolute absorption coefficient spectrum is obtained from the relative DBP and optical transmission spectra. In addition, PDS measurements resulting in absolute $\alpha(h\nu)$ spectra are used to compare the absolute absorption coefficient spectra obtained by DBP method. The effect of germanium concentration on low energy absorption coefficient is taken as comparison criteria among the films.

3.2. Steady State Photoconductivity Results

SSPC is a complex mechanism made up of three main parts: generation of free electron-hole pairs across the bandgap, recombination of excess free carriers through the defect states, and transport of mobile carriers at the conduction band mobility edges. Therefore, it involves the absorption coefficient of material α (hν), density and nature of recombination centers and mobility of free carriers at the extended states. As a consequence, SSPC method can be used to obtain direct quantitative information about the material. Photoconductivity exhibits a non integer power-law dependence on light intensity ($\sigma_{ph} \propto G^{\gamma}$), which is important physical feature to obtain information about recombination kinetics between photogenerated electrons and holes. Using SSPC measurements, information about the mobility-lifetime product, $\mu_n\tau_n$–product, of majority carriers is obtained. This is called "photosensitivity" and it is an important parameter for photoactive semiconductor thin films.

Experimental SSPC results for a-SiGe:H alloy thin films in annealed state with different germanium concentrations are shown in Fig 3.1a as a function of generation rate. The photoconductivity versus generation rate obeys the well-known non-integer power-law dependence rule, $\sigma_{ph} \propto G^{\gamma}$, for all the samples. However, a difference occurs in the slope as a major change in the germanium concentration exists. The exponent γ has values between 0.70 – 0.90, indicating a continuous distribution of recombination centers present in films of various germanium concentrations.

Majority carrier $\mu_n\tau_{n-}$ products calculated from the results in Figure 3.1a are presented in Figure 3.1b as a function of generation rate. The SSPC is dominated by the majority carrier electrons, and since the $\mu_n\tau_{n-}$ product of electrons is much higher than that of holes ($\mu_n\tau_n \gg \mu_p\tau_p$), the transport for these hydrogenated amorphous silicon germanium alloy thin films show slightly n type behavior. The $\mu_n\tau_n$ - products decrease as generation rate increase, with its characteristic power law $\mu_n\tau_n \propto G^{\gamma-1}$, implying that more defect states act as recombination centers with increasing generation rate.

Figure 3.1 a) σ_{ph} versus generation rate for a-SiGe:H alloy thin films of various Ge concentrations in the annealed state. b) $\mu_n\tau_n$ -product versus generation rate of the same a-SiGe:H alloy thin films in the annealed state.

For investigated a-SiGe:H alloy thin films of various germanium concentrations, the functional dependence on germanium concentration can be seen through Figure 3.2a and Figure 3.2b for the photoconductivity and $\mu_n\tau_n$-product values, respectively, measured at generation rate of 10^{20} cm^{-3}s^{-1}.

Both σ_{ph} and $\eta\mu_n\tau_n$-products exhibit the similar functional dependence on the germanium concentration. $\eta\mu_n\tau_n$-product has a value around 1×10^{-7} cm^{2}V^{-1} for the reference sample with 0% Ge, which is pure a-Si:H. As Ge% increases, $\eta\mu_n\tau_n$-product increases and peaks at 5×10^{-7} cm^{2}V^{-1} for 20% Ge a-SiGe:H alloy thin film. It then starts decreasing back to the value of a-Si:H thin film for 40% Ge a-SiGe:H alloy thin film. The decrease in the $\eta\mu_n\tau_n$-product indicates that the density of defect states present in the bandgap of the alloy increases with increasing germanium concentration up to 40%. A further increase of Ge concentration to 50% cause a sharp decrease in the $\eta\mu_n\tau_n$-products indicating a substantial increase in the defect states acting as recombination centers. Finally, for the highest Ge concentration film of 75%, no significant change is detected in the $\eta\mu_n\tau_n$-products.

As a conclusion, these results indicate that alloy films with Ge concentration in the range of 10% to 30% have the highest $\eta\mu_n\tau_n$-products for the photogenerated free electrons, which serve as the best photoconductive absorber layer in the multijunction solar cells. For the a-SiGe:H alloys prepared with Ge% above 40% Ge indicate the high level of the recombination centers causing degradation of $\eta\mu_n\tau_n$-products more than an order of magnitude. These results are consistent with those previously reported results in the literature (Finger et al. 1987).
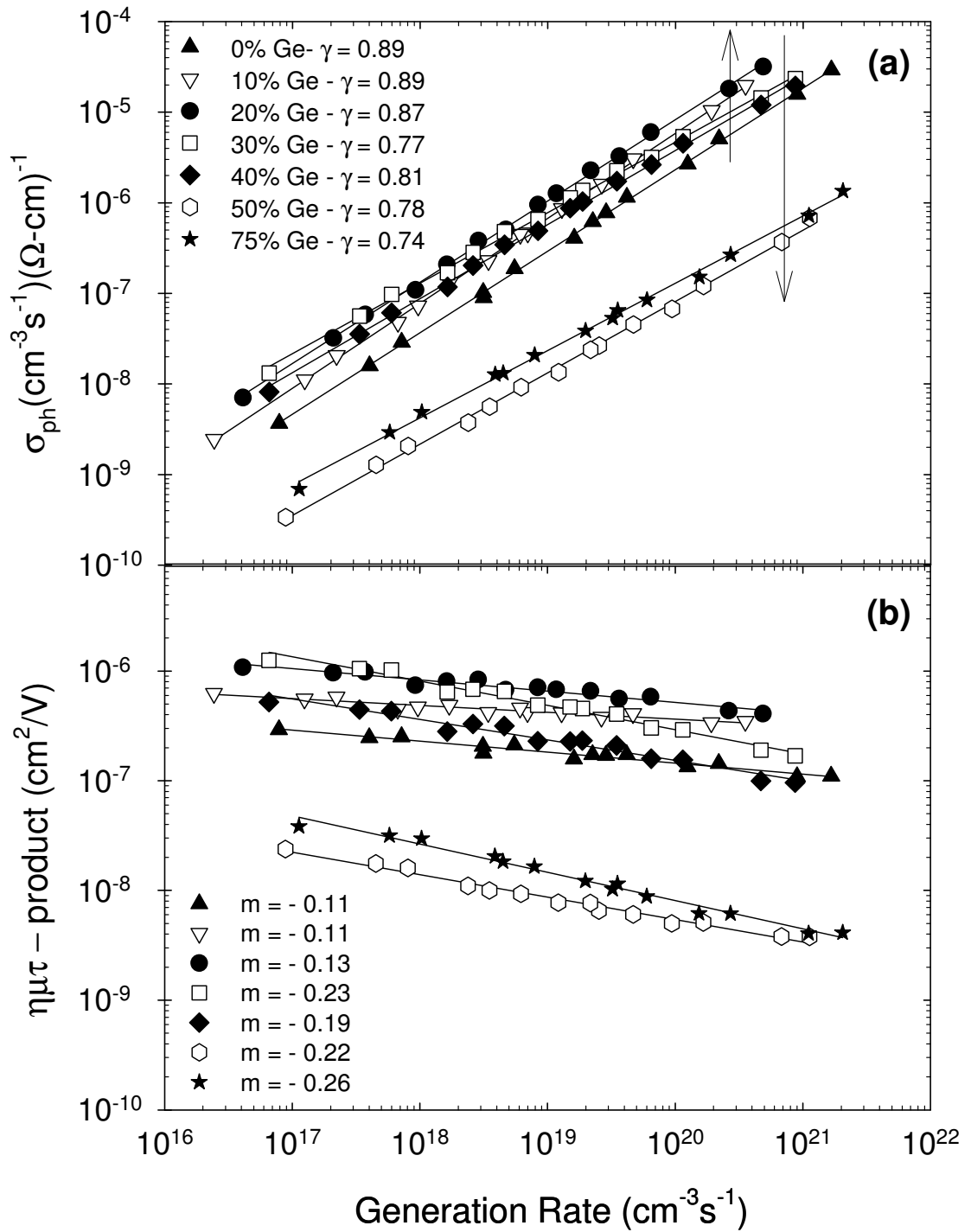
Figure 3.2 a) σ_{ph} versus Ge concentration for a-SiGe:H alloy thin films of various Ge concentrations in the annealed state. b) $\mu\tau$ - product versus Ge concentration for a-SiGe:H alloy thin films of various Ge concentrations in the annealed state. Dashed lines are guide to eye.

3.3 Sub-bandgap Absorption Results

Optical absorption spectrum of thin films is an important parameter to characterize optical and electronic properties of absorber materials. Sub-bandgap absorption spectrum is due to absorption of photons with energies lower than the optical gap of semiconductor. For a-SiGe:H alloy thin films, there are continuous distribution of defect states below the bandgap energies. This was confirmed by the exponent γ value of σ_{ph} in the previous section. These defect states consists of exponential valence band tail states originating from the disorder in amorphous network and midgap defect states due to dangling bonds and broken bonds originating from both silicon and germanium atoms. Therefore, electrons excited from these defect states into the conduction band edge by absorption of low energy photons can be detected by measuring sub-bandgap photoconductivities. The measurements of optical absorption, α (hν), especially in the sub-bandgap region, are very important since absorption in that region is related to defect states present in the materials. As the germanium concentration changes, the microstructure and defect distribution of the a-SiGe:H alloy thin films changes substantially. This affects the resulting optical and electronic properties of deposited thin films. To obtain reliable α(hν) spectrum of a-SiGe:H alloy thin films of different Ge concentrations, especially in the sub-bandgap region, is one of the essential goals of this thesis. In this section, optical absorption spectra of a-SiGe:H alloy thin films of various Ge concentrations will be presented. Absolute α (hν) spectrum was calculated from the relative DBP and optical transmission spectra and finally compared with those independently measured by PDS method. PDS measurements were performed in Jülich Research Center, Germany.

An example of DBP yield spectrum for high and low bias light intensities together with transmission spectrum are presented in Figure 3.3a and Figure 3.3b, respectively for a-Si:H thin film, reference sample with 0 % Ge concentration. As seen in Figure 3.3a, at sub-bandgap energies DBP yield spectrum shows a dependence on the bias light that is used. The divergence between high bias and low bias light spectra is related to change in the occupation of defect states in the bandgap. At the low bias light condition, the distribution of defect states which DBP probes is very close to the occupied defect states in the dark, below the Fermi level. When intensity of bias light is increased, more defect states above the Fermi level are occupied. This will result in an
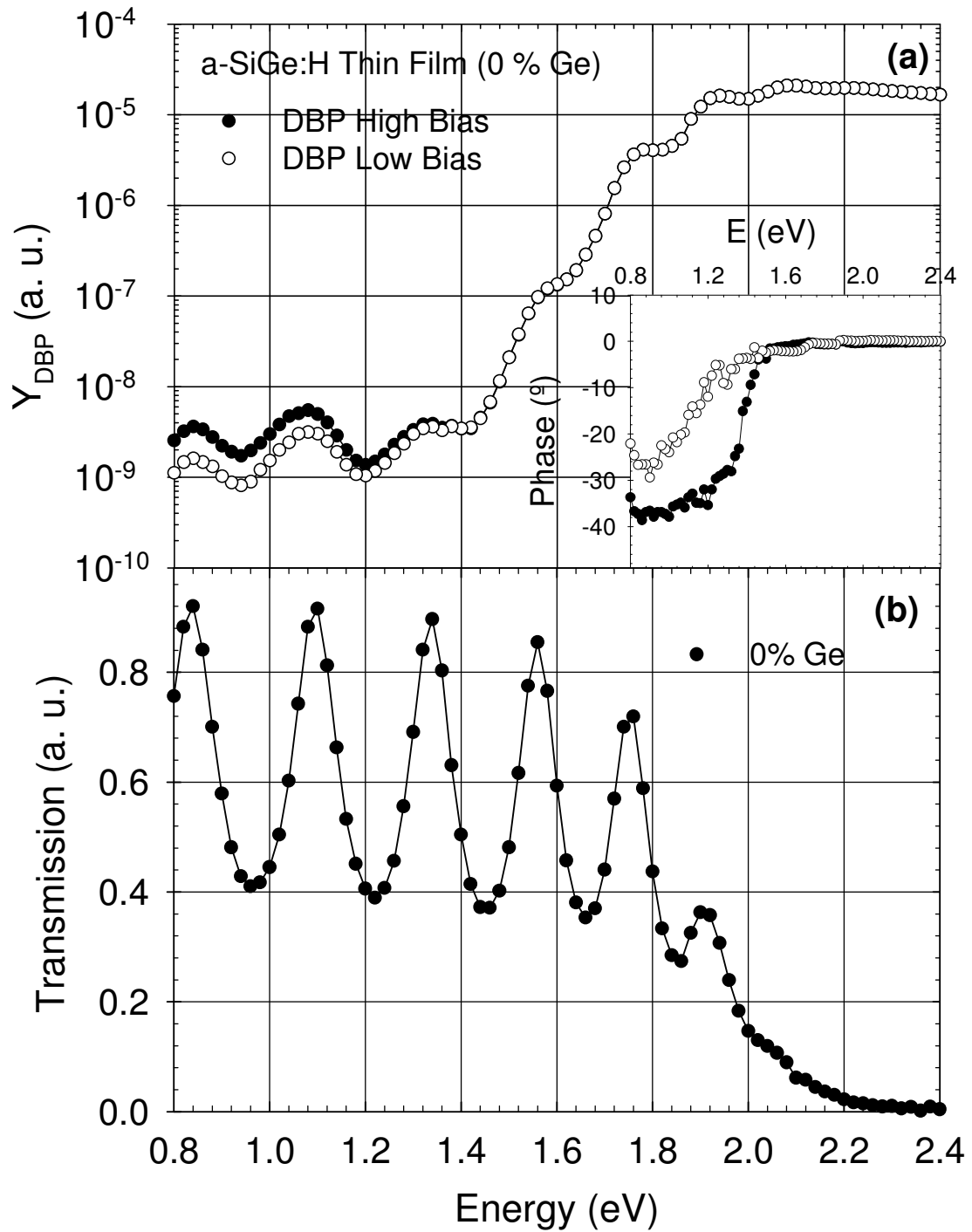
Figure 3.3 a) DBP Yield spectrum of a-Si:H thin film (0% Ge) at high and low bias light intensities in the annealed state. In the inset phase of both measurements are shown. b) Transmission spectrum of the same sample.

44

increase in the number of transitions of electrons from these occupied defect states into the conduction band. Therefore, an increase in Y_{DBP} values in the lower energy region of the spectrum is observed. This intensity dependence is one of the major advantages of DBP method as sub-bandgap absorption for different generation rate values can be investigated.

For both high and low bias light cases, DBP yield spectrum is directly proportional to the absorbance and thus absorption coefficient. In figure 3.3a, there are also interference fringes on the spectrum due to multiple reflections of the incoming light on the film and substrate interface. However, there are no interference fringes on the absolute absorption coefficient spectra, thus the aim is to obtain absorption coefficient spectrum from the Y_{DBP} spectrum without interference fringes. Usually, the fringes have been removed using fast Fourier transform method (Wiedeman et al. 1987) and resulting fringe free Y_{DBP} spectrum is normalized to absolute $\alpha(h\nu)$ values obtained from T&R or from PDS measurements. (Wronski et al. 1982, Gunes and Wronski 1992a). In most cases, Fourier transform process introduces artificial errors in the spectrum for films less than 1 μm and absolute $\alpha(h\nu)$ obtained from T&R measurement is not reliable for such thin films at normalization energies. Therefore fringe free normalization of Y_{DBP} always introduces a significant degree of errors and accuracy in this process is questioned (Chen et al. 1996). For this reason in this thesis, the fringe free absolute $\alpha(h\nu)$ spectrum is directly calculated from DBP yield spectrum and transmission spectrum shown in Figure 3.3b measured on the same sample, using a procedure based on the Ritter-Weiser formula as explained in Chapter 2.

In Figure 3.3b, optical transmission spectrum for the same sample is shown. The maxima and minima of the transmission and DBP yield spectra take place at the same energies indicating a uniform absorption of light throughout the material. Using the transmission fringes at lower energies, the exact thickness of the sample is calculated using the interference fringe equation (Web_1, 2003). This thickness value was used for correct calculation of the SSPC and $\eta\mu_n\tau_n$-products of majority carriers presented in preceding section.

Fringe free absolute α ($h\nu$) spectrum acquired for high and low bias light DBP measurements are shown in Figure 3.3c. The spectrum represents a typical $\alpha(h\nu)$ spectrum of an amorphous silicon thin film. It is made up of three different regions. The

Figure 3.3 c) The calculated absolute α (hν) spectra of DBP for high and low bias light measurements of a-Si:H (0% Ge) thin film.

first one is the high energy region due to absorption from the parabolic extended states similar to that of crystalline silicon. The second part is the exponential valence band tail state absorption region. It begins generally at the optical band energy and extends down to 1.4 eV. It is a characteristic absorption region for amorphous semiconductors. It originates from the disorder in the amorphous network. Its characteristic slope called as the Urbach energy, E_{0v}. It shows the degree of disorder. The E_{0v} slope calculated for the a-Si:H film with 0% Ge is 55 meV, which indicates an electronic quality film. The third region in the α(hν) spectrum is called sub-bandgap absorption region due to localized defect states in the bandgap of the amorphous sample. The magnitude of α(hν) in the low energy part is an integration of all optical transitions from the defect states into the conduction band edge. Therefore, a qualitative comparison with α(hν) at one energy can be made. For this purpose, the α(hν) at 1.0 eV is taken to see the level of defect absorption. For hydrogenated amorphous silicon sample, α(hν) spectrum of low bias light DBP is around 1.0 cm^{-1}. This value is taken to compare the sub-bandgap absorption coefficient of other alloy films as Ge concentration changes. This will let us

infer how defect states changes as alloying with Ge changes. There is a fine overlap in the absolute α (hν) spectrum obtained for both bias light DBP measurements at higher energies, down to the exponential valance band tail state. In low energy region, high bias light α (hν) spectrum gives higher values than low bias light α (hν) spectrum. The reason for the increase is that high bias light intensity increases the separation of quasi Fermi levels in the bandgap, the electron quasi Fermi level moves closer to the conduction band edge and hole quasi Fermi level moves closer to the valance band edge. Therefore, the density of electron occupied defect states above the dark Fermi level increases and a.c. monochromatic light of DBP excites more electrons from the occupied states into conduction band at lower energies. This results in an increase only in the α(hν) spectrum at lower energies since there is no change in the occupation of states at higher energies.

As the Ge% increases to 10%, $\eta\mu_n\tau_n$-products were found to increase in the previous section. It was inferred that 10% Ge a-SiGe:H alloy thin film has lower defect density than pure a-Si:H film. In order to see the direct effect of defect states, subgap absorption spectrum of 10% Ge a-SiGe:H alloy thin film is compared with that of a-Si:H. in Figure 3.4a and Figure 3.4b, raw DBP yield spectra and optical transmission spectrum are shown. Absolute α(hν) spectra for low and high bias light DBP results are calculated similarly using the Ritter-Weiser optical equations. In Figure 3.4c absolute α(hν) spectra of both DBP measurements are presented. Both spectra without any interference fringes overlap well at energies above the exponential region. High bias light spectrum shifts to higher values consistently. For low bias light DBP spectra, the α(hν) values at 1.0 eV has a value around 0.3 cm^{-1}, which is a factor of 3 lower than that of a-Si:H film shown in Figure 3.3c. It indicates that 10% Ge a-SiGe:H alloy thin film has lower defect density than pure a-Si:H film. For this reason, $\eta\mu_n\tau_n$-products for 10% Ge a-SiGe:H alloy are higher than that of a-Si:H film. However, the slope of exponential valence band tail absorption and energy at $\alpha=10^4$ cm^{-1} are almost the same for a-Si:H and 10% Ge a-SiGe:H alloy thin films.

Figure 3.4 a) DBP Yield spectrum of a-SiGe:H alloy thin film of %10 Ge concentration at high and low bias light intensities in the annealed state. In the inset phase of both measurements are shown. b) Transmission spectrum of the same sample.
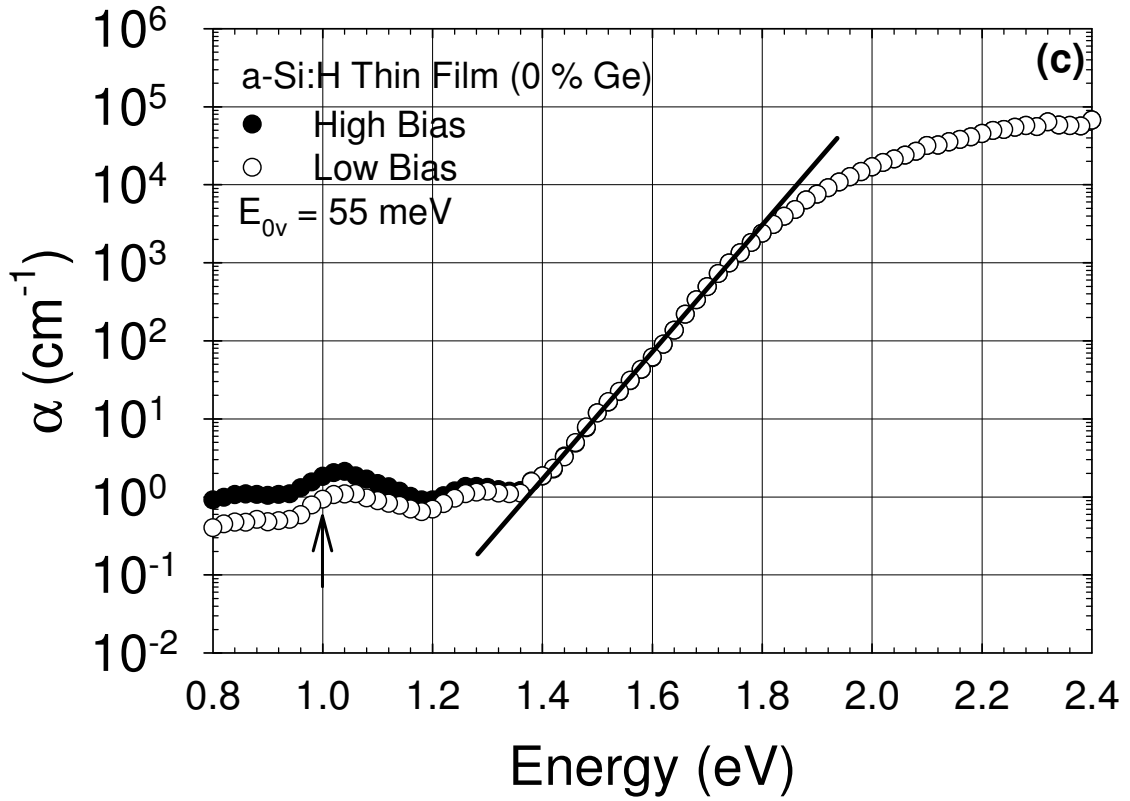
Figure 3.4 c) The calculated absolute α (hν) spectra of DBP for high and low bias light measurements of a-SiGe:H thin film with 10 % Ge concentration.
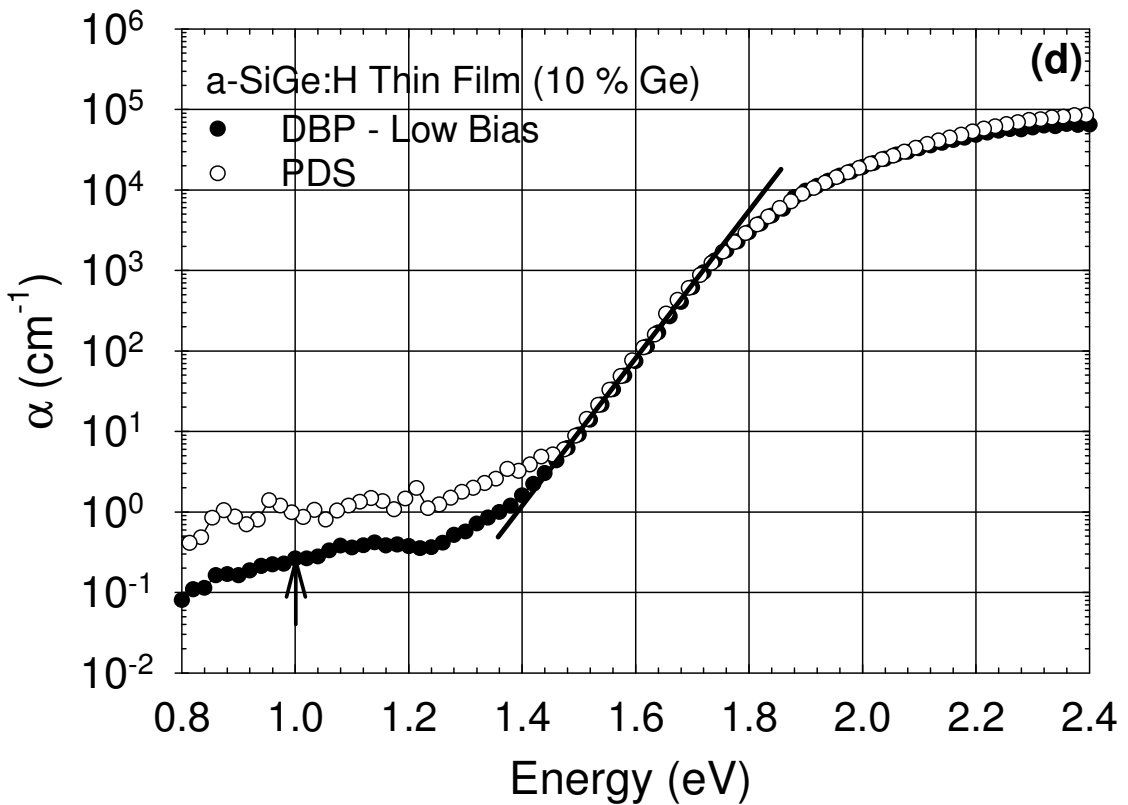
Figure 3.4 d) The calculated absolute α (hν) spectra of PDS and DBP for low bias light measurements of a-SiGe:H thin film with 10% Ge concentration.

Furthermore, the reliability of absolute $\alpha(h\nu)$ spectrum calculated from the DBP spectra are compared with that independently measured by PDS on the same piece of the sample. These results are represented in Figure 3.4d for both PDS and low bias light DBP measurements. It is clearly seen that both spectra overlap very well at higher energies above 1.4 eV. However, a difference exists only in the sub-bandgap energies. In this region, PDS spectrum has higher $\alpha(h\nu)$ values by almost a factor of 3. In the PDS spectrum, a correction for the substrate absorption has been taken into account. The difference here is related to the detection of optical transitions from occupied defect states into empty states. In DBP, only transitions shown in Figure 2.12, to the conduction band are detected. However, PDS detects all transitions to empty states; conduction band, conduction band tail states, and defect states above the bandgap. For this reason PDS spectrum results in higher $\alpha(h\nu)$ values in subgap region. DBP spectrum is more representation of the occupied defect states below the dark Fermi level. As a conclusion, both techniques probe the same distribution of defect states at higher energies and absolute $\alpha(h\nu)$ spectrum of DBP can be reliably used to compare films with different Ge concentrations.

As Ge concentration increases to 20%, $\eta\mu_n\tau_n$-products show the highest values as discussed in the previous section. Raw DBP results and optical transmission of 20% Ge a-SiGe:H alloy thin film are shown in Figure 3.5a and Figure 3.5b respectively. Calculated absolute $\alpha(h\nu)$ spectra of two DBP spectra are presented in Figure 3.5c. The slope of the exponential valence band tail absorption is 53 meV indicating good quality film and energy at $\alpha=10^4$cm^{-1} decrease from 1.90 to 1.86 eV. Absolute $\alpha(h\nu)$ at 1.0 eV for the low bias light DBP spectrum is around 0.2 cm-1, lower than that of 10% Ge a-SiGe:H alloy. It means that 20% Ge alloy has lower defect density than 10% Ge alloy film. This results in a higher $\eta\mu_n\tau_n$-products for 20% Ge a-SiGe:H alloy thin film as presented in figure 3.2b. The $\alpha(h\nu)$ spectra calculated from DBP results are similarly compared with that obtained from the PDS measurements. A perfect overlap of two spectra at higher energies can be seen in Figure 3.5c at higher energy part of spectrum similar to that found in 10% Ge sample. A similar difference is found in the low energy part of spectrum. In this case, PDS is a factor of 10 higher than 10% Ge film. This could be due to higher surface defects that PDS is very sensitive to in 20% Ge film.

Figure 3.5 a) DBP Yield spectrum of a-SiGe:H alloy thin film of %20 Ge concentration at high and low bias light intensities in the annealed state. In the inset phase of both measurements are shown. b) Transmission spectrum of the same sample.

Figure 3.5 c) The calculated absolute α (hν) spectra of DBP for high and low bias light measurements of a-SiGe:H thin film with 20 % Ge concentration.
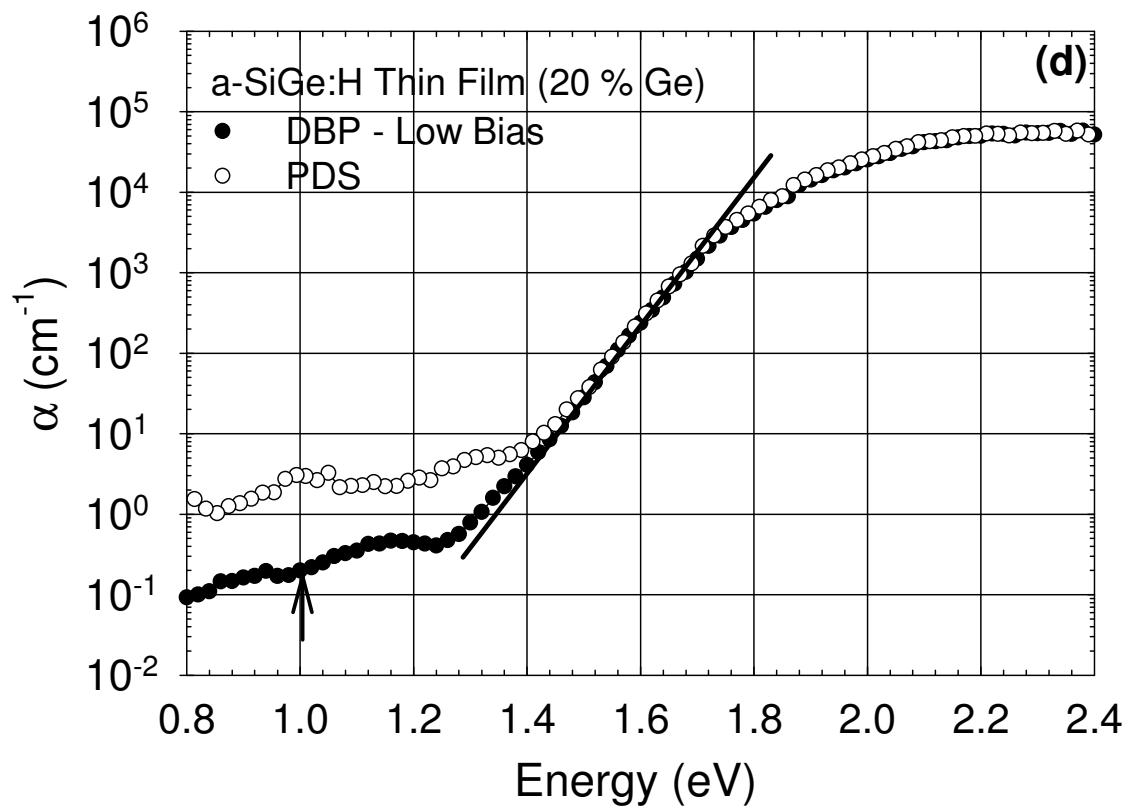
Figure 3.5 d) The calculated absolute α (hν) spectra of PDS and DBP for low bias light measurements of a-SiGe:H thin film with 20% Ge concentration.

A further decrease in Ge% starts to degrade $\eta\mu_n\tau_n$-products. In raw DBP and optical transmission spectra of 30% Ge and 40% Ge samples are presented in Figure 3.6 and Figure 3.7, respectively. Absolute $\alpha(h\nu)$ spectra were calculated from these raw spectra and presented in Figure 3.6c and Figure 3.7c, respectively. The slope of exponential tail absorption are 55meV and 53meV for 30% Ge and 40% Ge alloy film, which are similar to previous samples. The energy at $\alpha=10^4\text{cm}^{-1}$ decreases to 1.80eV for 30% Ge and to 1.75eV for 40% Ge, showing the effect of Ge, which decrease the bandgap of the alloy. Corresponding effect on defect states is monitored on the $\alpha(h\nu)$ at 1.0 eV. It increases from 0.2 cm^{-1} to 0.5cm^{-1} as Ge increase from 20% to 30% and it is around 0.6 cm^{-1} for 40% Ge alloy. This slight increase in the $\alpha(1.0\text{eV})$ indicate an increase in defect density as Ge concentration increases from 20% to 40% and these results are consistent with slight decrease found in $\eta\mu_n\tau_n$-products of same samples in Figure 3.2b. In addition, for both samples PDS measurements show a perfect agreement with that of DBP as previous samples. They can be seen in Figure 3.6d and Figure 3.7d, respectively. Increasing Ge concentration above 40%, cause a decrease in $\eta\mu_n\tau_n$-products drastically. The alloys prepared at 50% Ge and 75% Ge have been characterized in a similar way using the same measurements. Raw DBP results and optical transmission spectra of these two samples are shown in Figure 3.8 and Figure 3.9, respectively. Calculated absolute $\alpha(h\nu)$ spectra of these high Ge content films are presented in Figure 3.8c and Figure 3.9c, respectively. The energy gap at $\alpha=10^4\text{cm}^{-1}$ decrease to 1.64eV for 50% Ge and to 1.46eV for 75% Ge sample. The characteristic Urbach energy, E_{0v}, also increases to 60meV for both samples, indicating higher disorder in these highly Ge content samples. The defect absorption at 1.0 eV increases substantially to 2 cm^{-1} for 50% Ge film. For 75% Ge film, the $\alpha(h\nu)$ at 0.9 eV is taken to be away from the exponential absorption edge since bandgap decreased substantially for 75% Ge film. The $\alpha(0.9\text{eV})$ is around 6 cm^{-1}, which is the highest among other films. It indicates that high Ge content films have higher defect states in the bandgap, which cause a sharp degradation in electron lifetime τ_n, as measured from photoconductivity measurements.
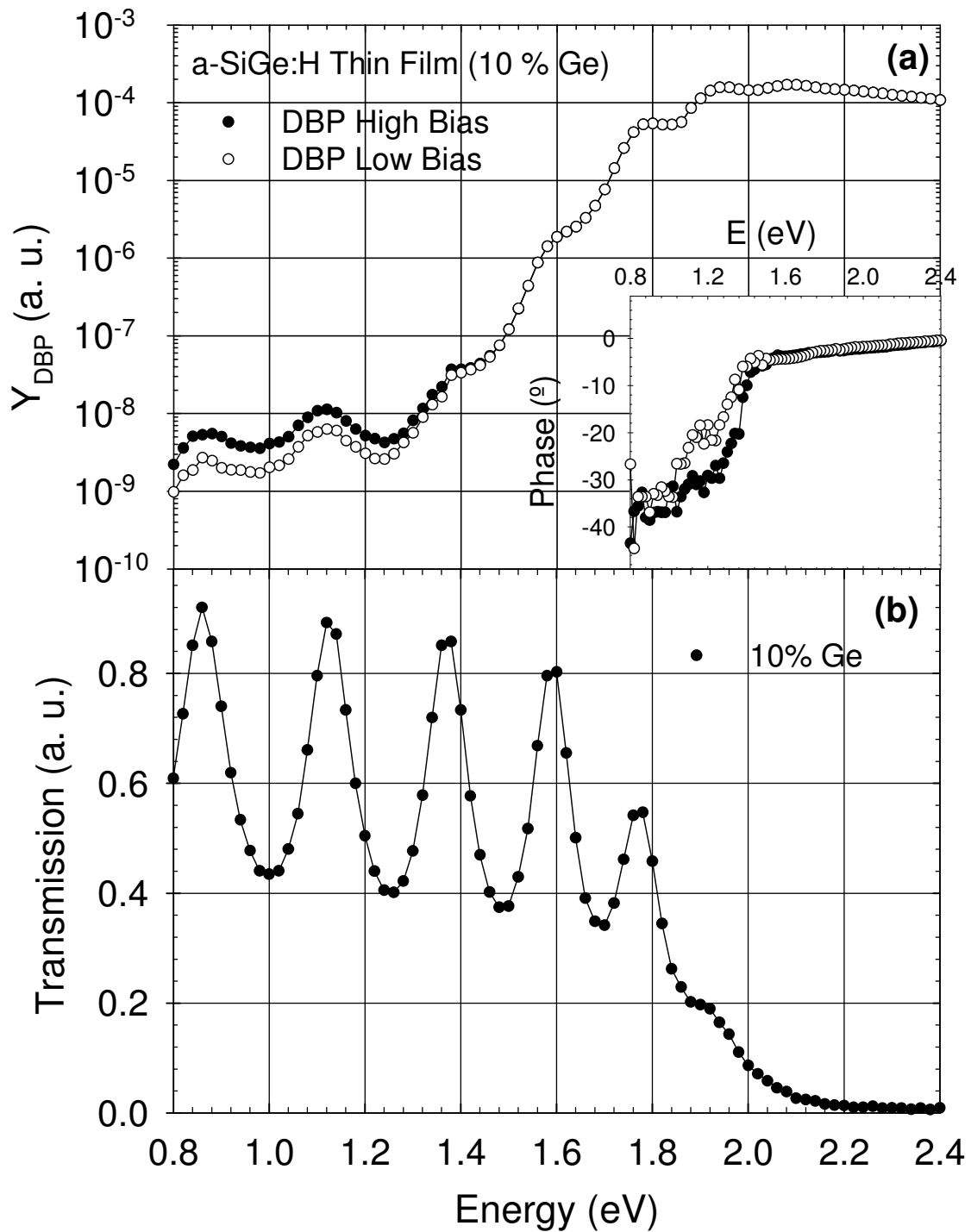
Figure 3.6 a) DBP Yield spectrum of a-SiGe:H alloy thin film of %30 Ge concentration at high and low

bias light intensities in the annealed state. In the inset phase of both measurements are shown.
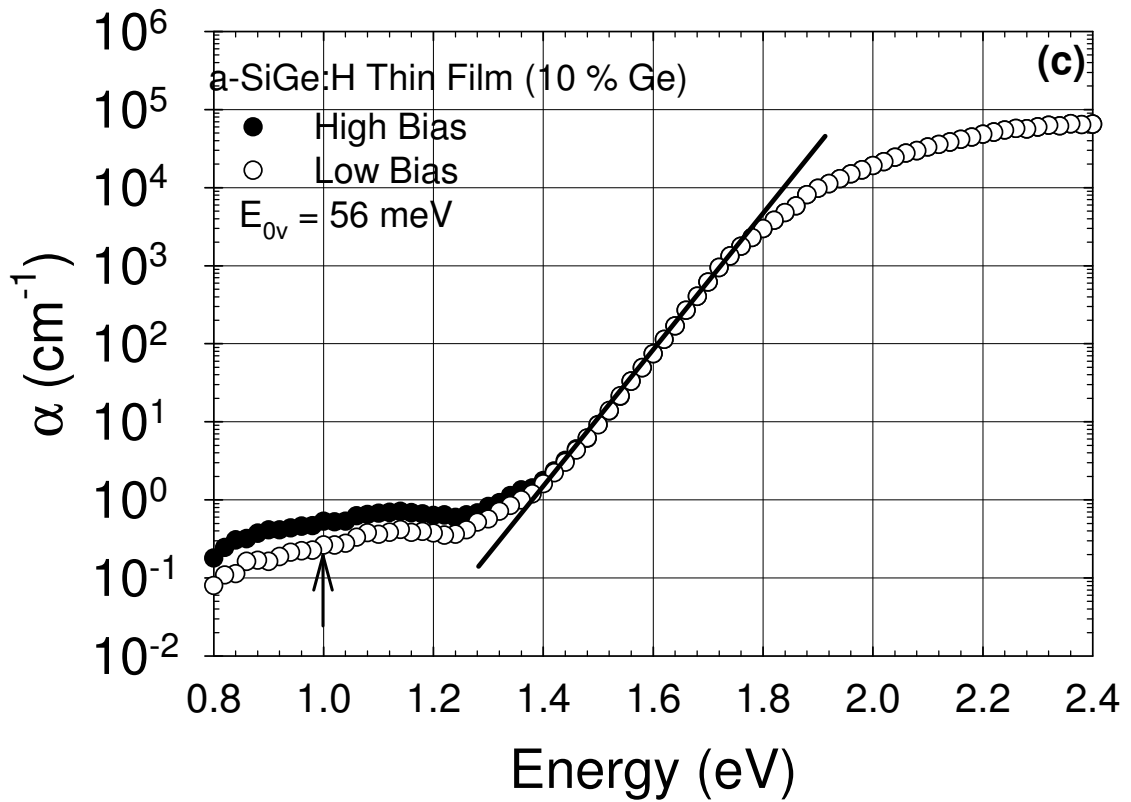
b) Transmission spectrum of the same sample.
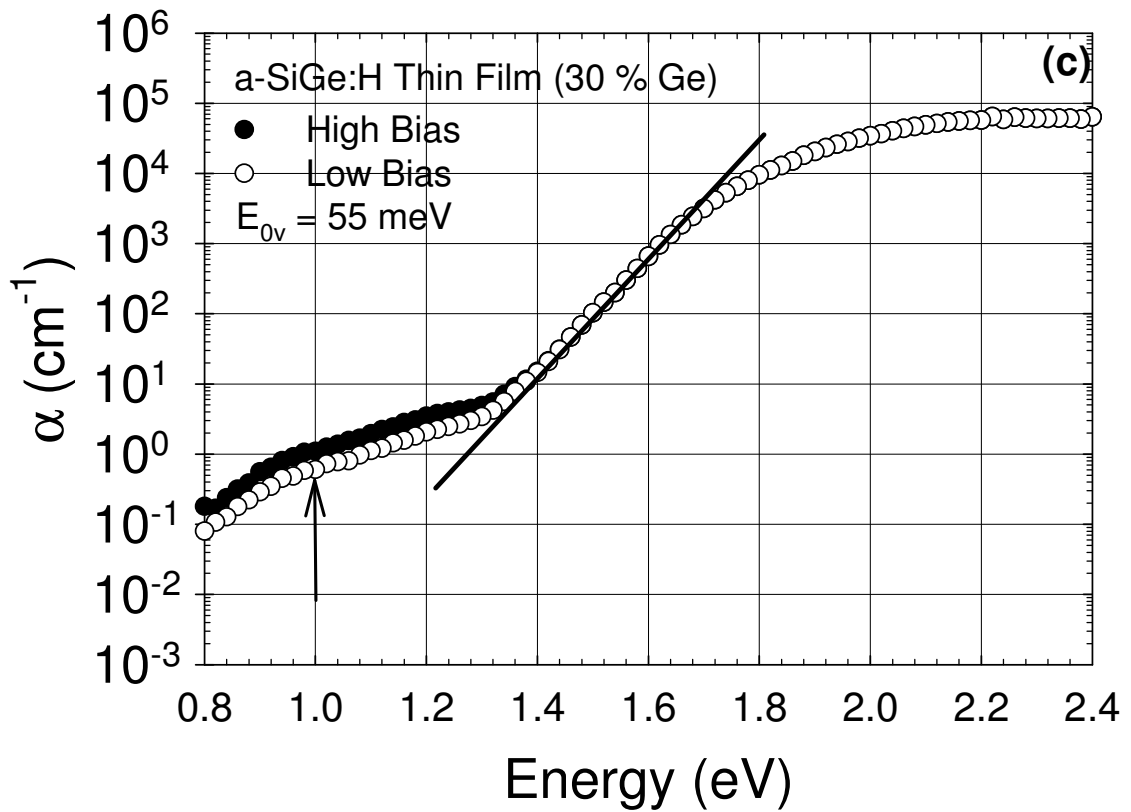
Figure 3.6 c) The calculated absolute α (hν) spectra of DBP for high and low bias light measurements of a-SiGe:H thin film with 30 % Ge concentration.
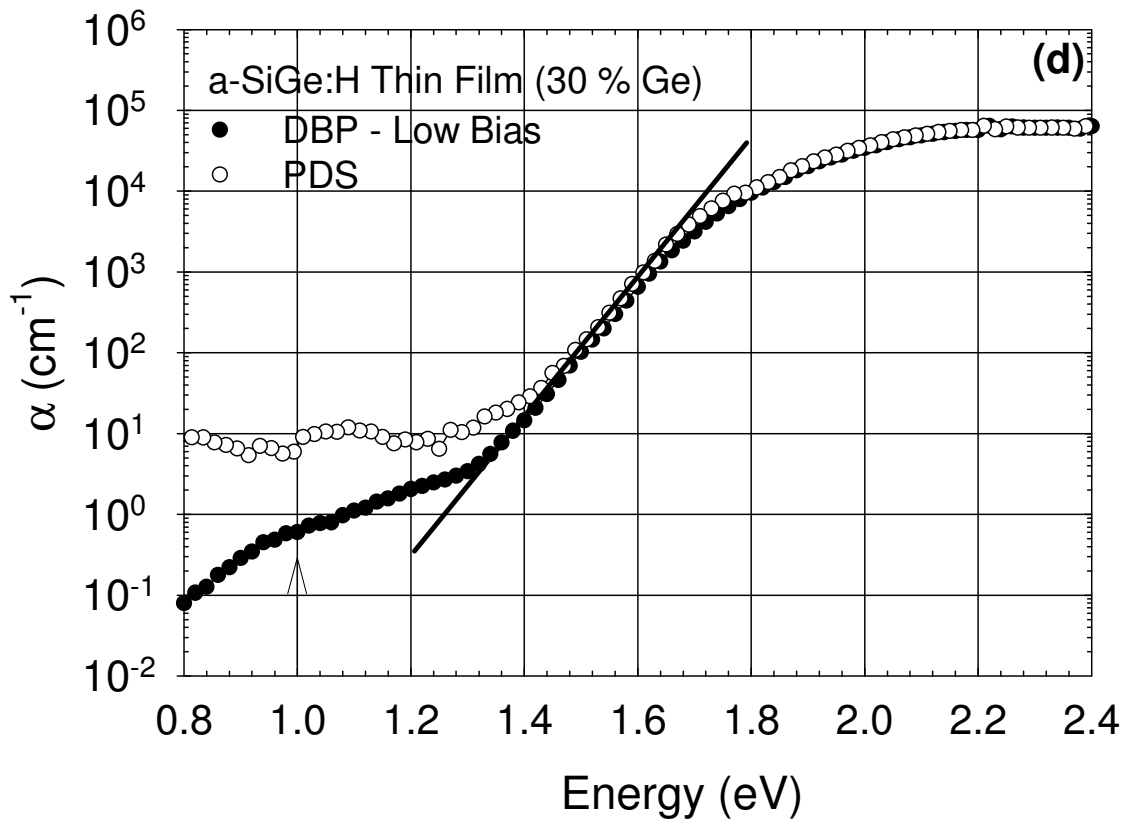
Figure 3.6 d) The calculated absolute α (hν) spectra of PDS and DBP for low bias light measurements of a-SiGe:H thin film with 30% Ge concentration.
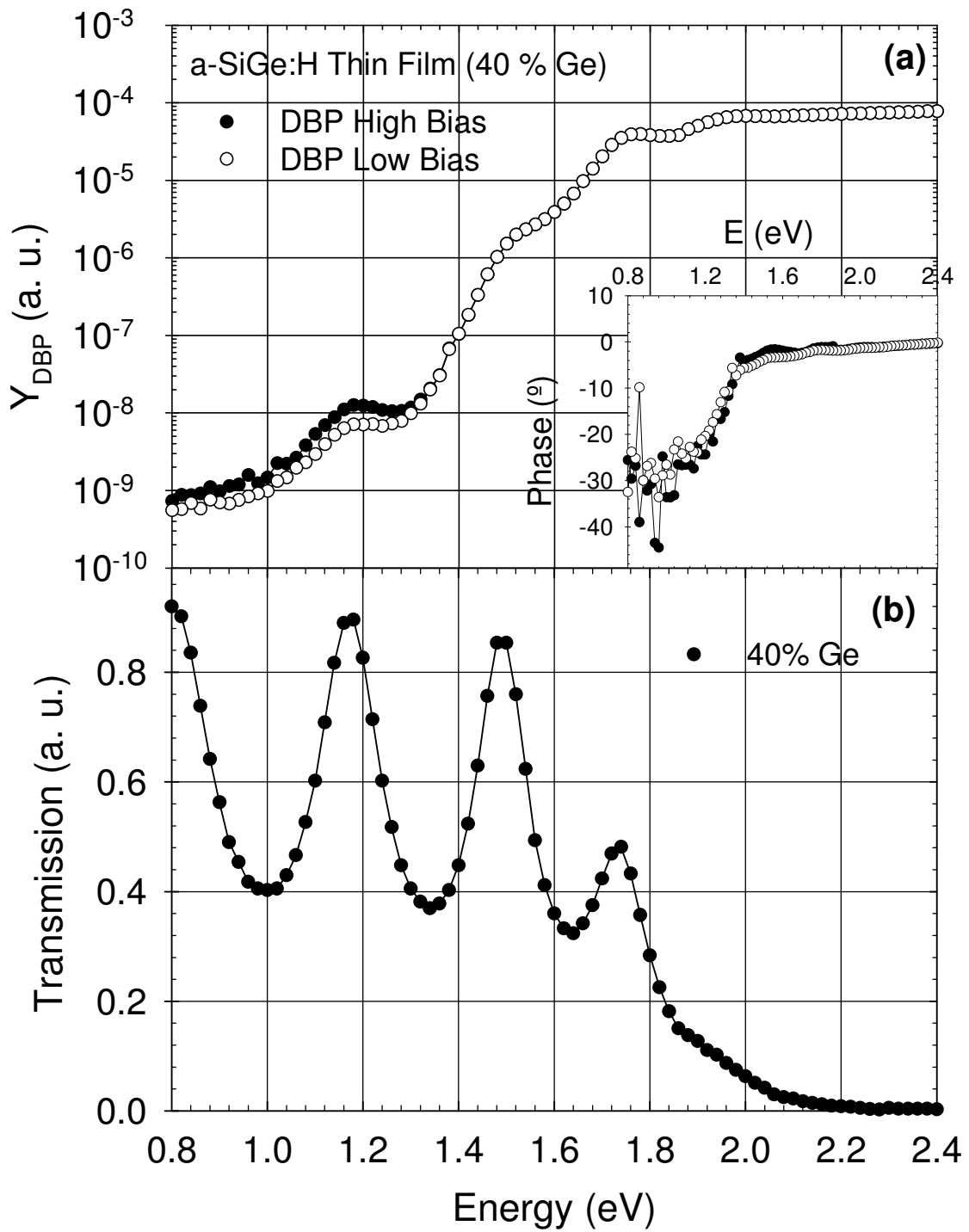
Figure 3.7 a) DBP Yield spectrum of a-SiGe:H alloy thin film of %40 Ge concentration at high and low bias light intensities in the annealed state. In the inset phase of both measurements are shown. b) Transmission spectrum of the same sample.
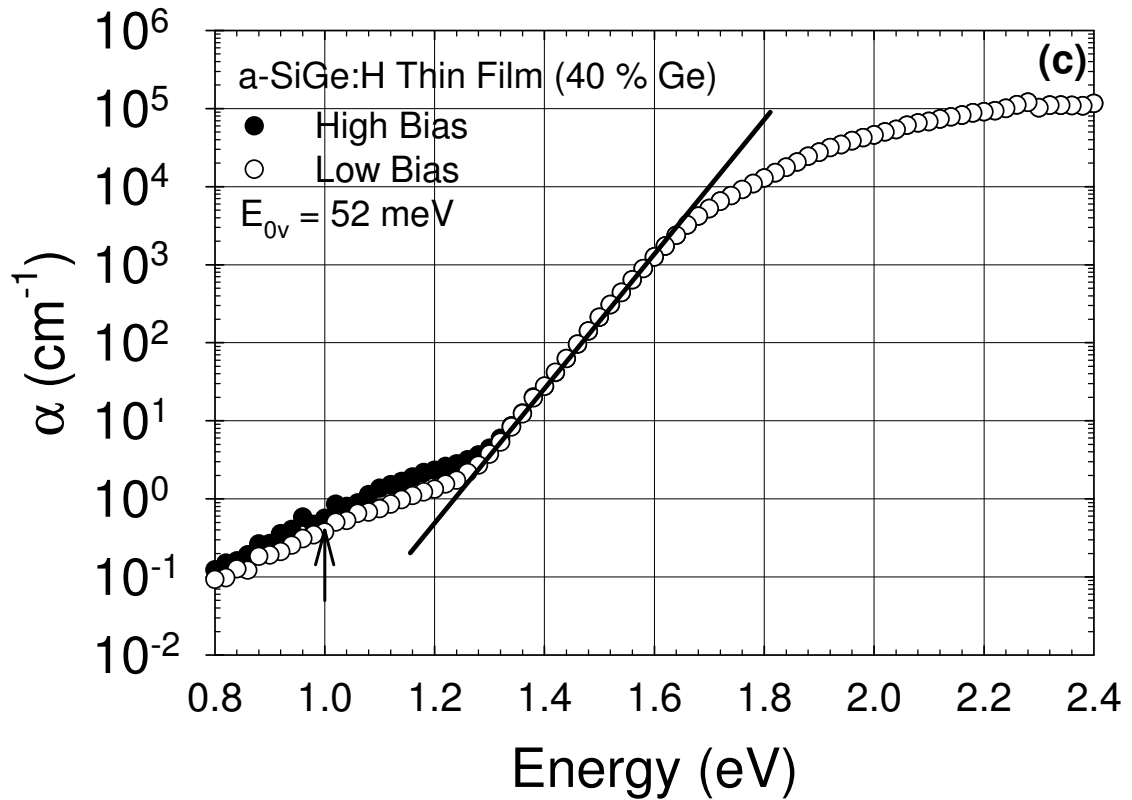
Figure 3.7 c) The calculated absolute α (hν) spectra of DBP for high and low bias light measurements of a-SiGe:H thin film with 40 % Ge concentration.
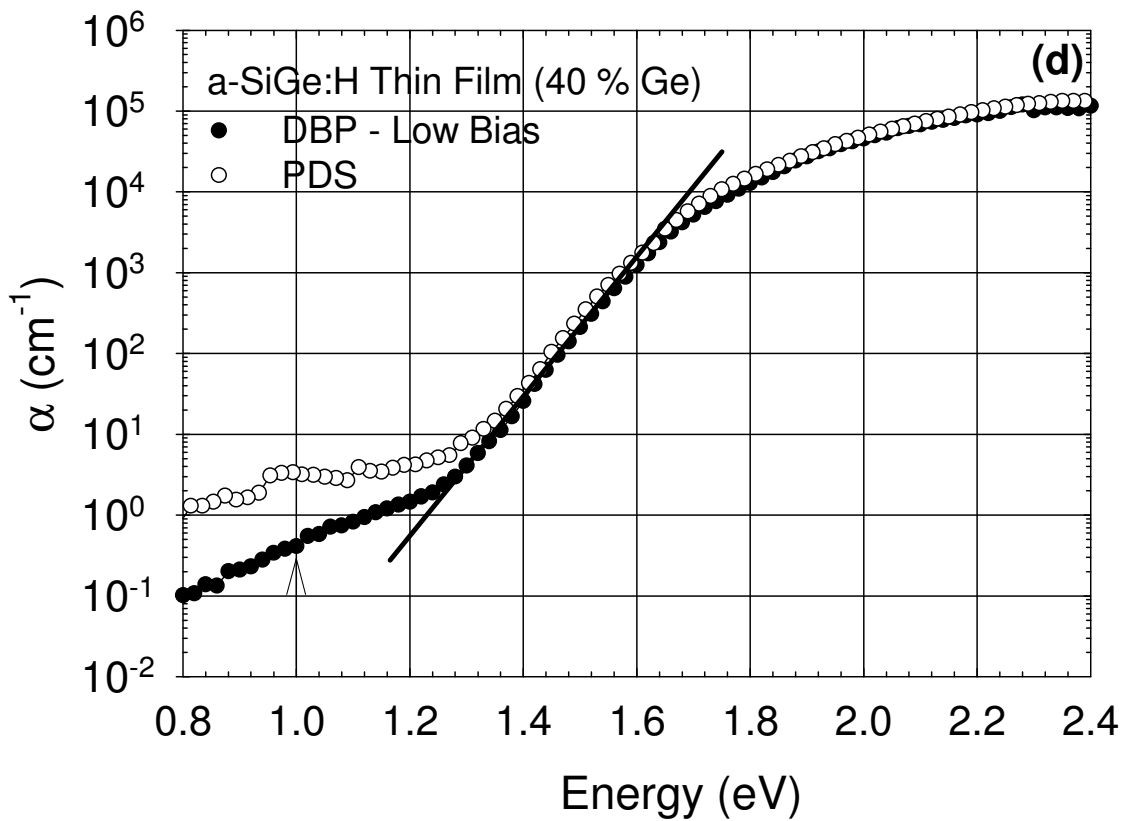
Figure 3.7 d) The calculated absolute α (hν) spectra of PDS and DBP for low bias light measurements of a-SiGe:H thin film with 40% Ge concentration.
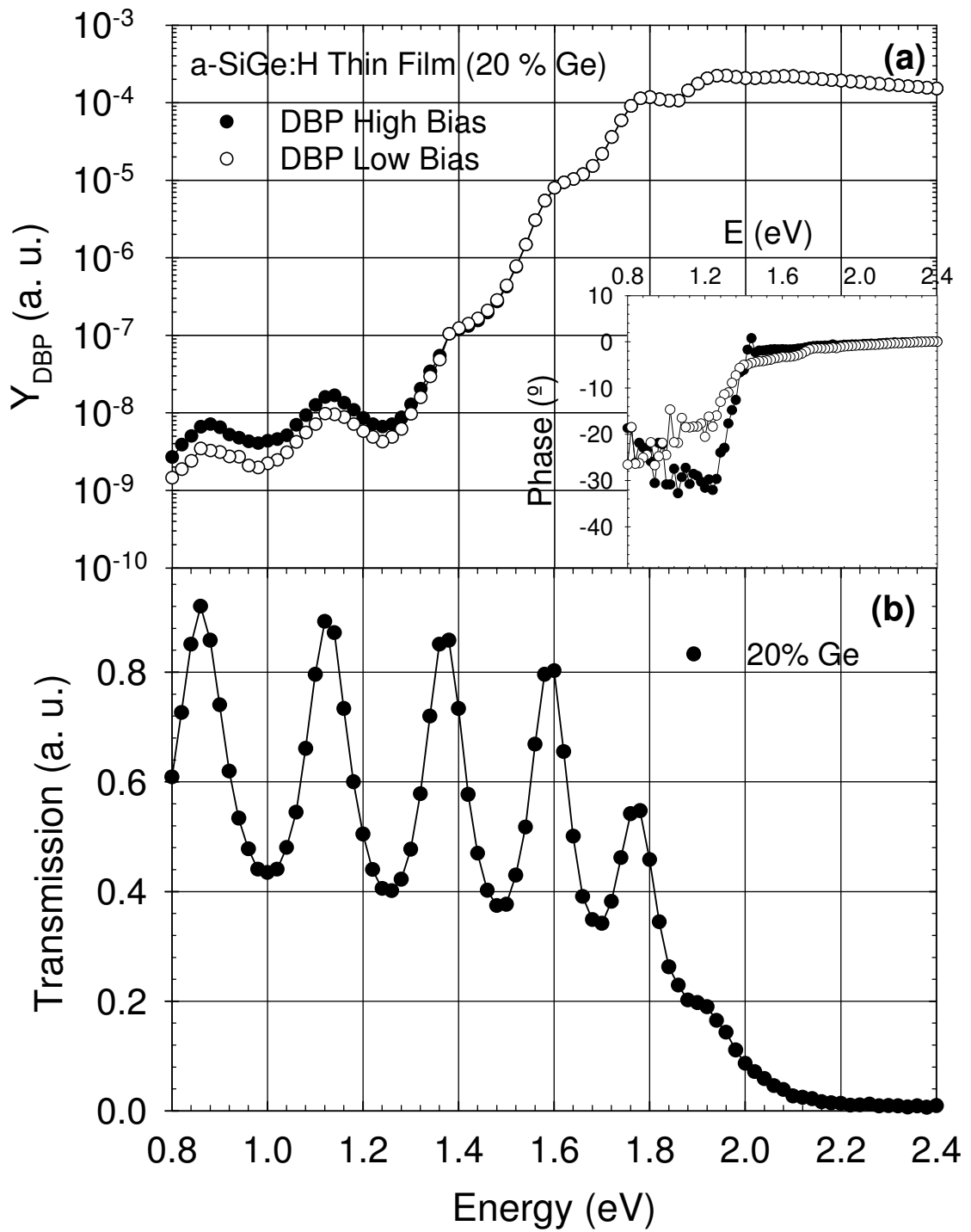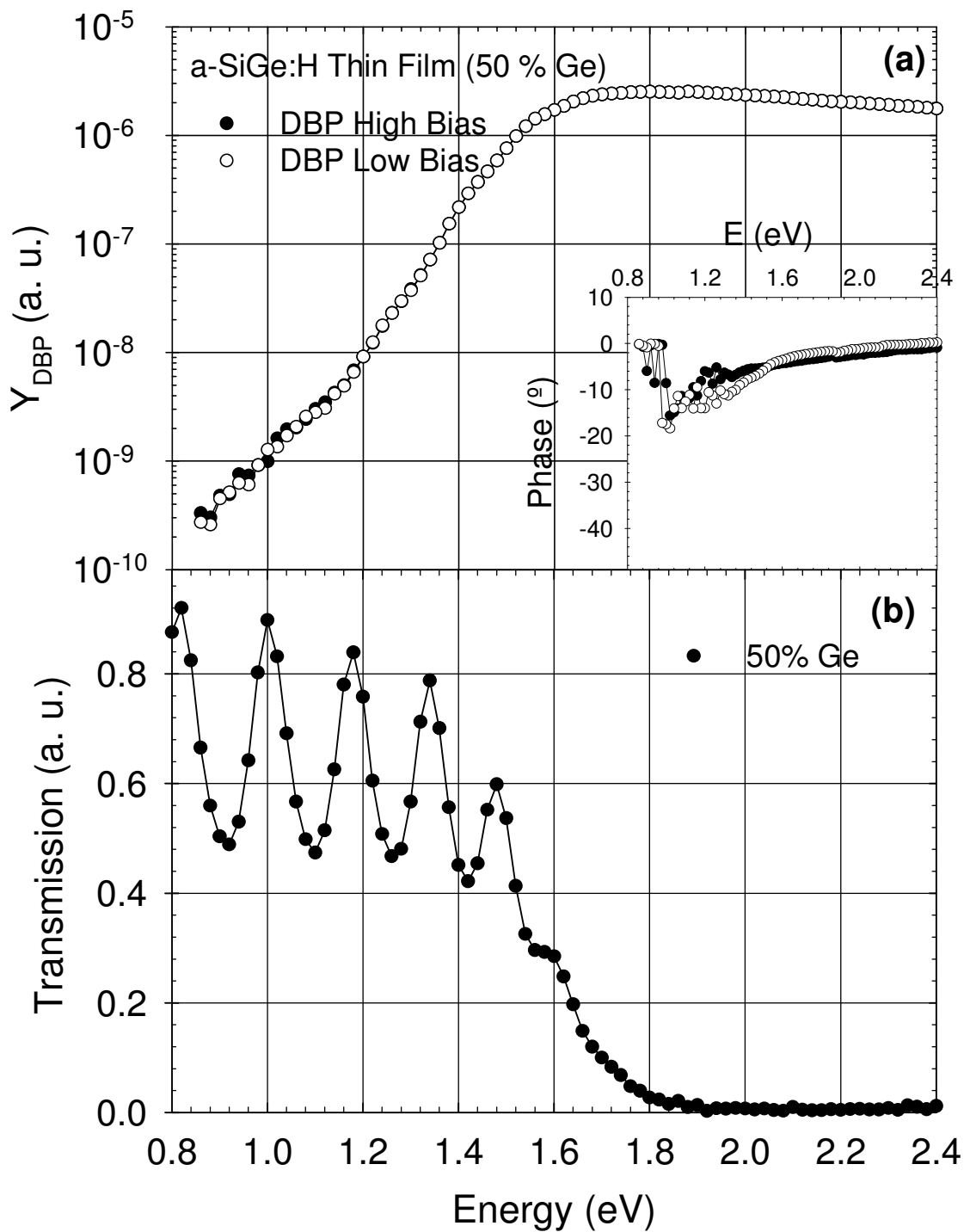
Figure 3.8 a) DBP Yield spectrum of a-SiGe:H alloy thin film of %50 Ge concentration at high and low bias light intensities in the annealed state. In the inset phase of both measurements are shown. b) Transmission spectrum of the same sample.
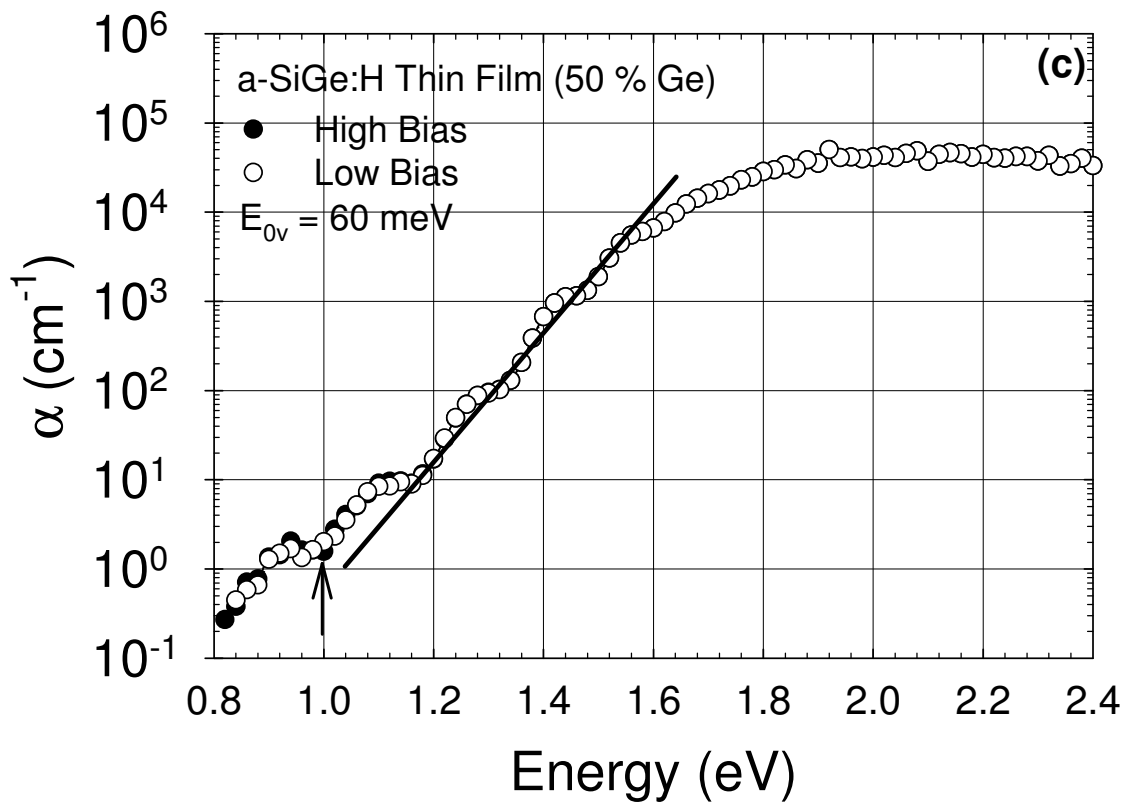
Figure 3.8 c) The calculated absolute α (hν) spectra of DBP for high and low bias light measurements of a-SiGe:H thin film with 50 % Ge concentration.
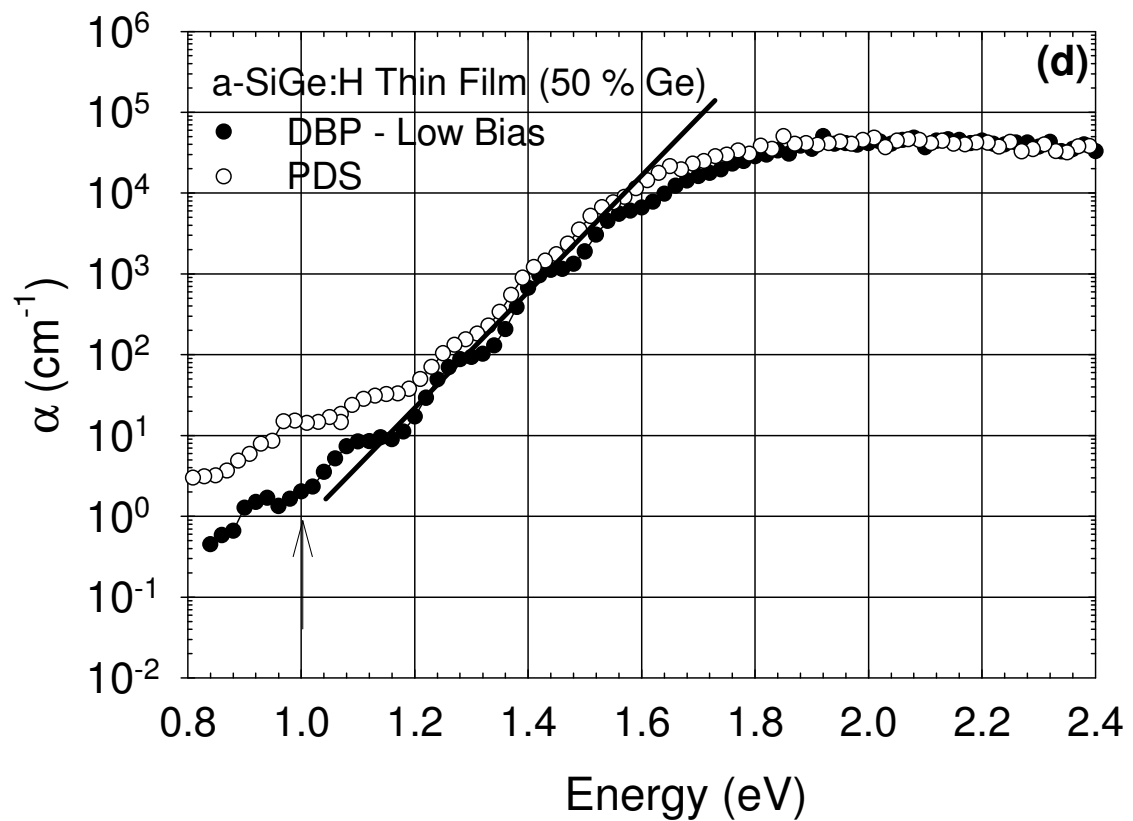
Figure 3.8 d) The calculated absolute α (hν) spectra of PDS and DBP for low bias light measurements of a-SiGe:H thin film with 50% Ge concentration.
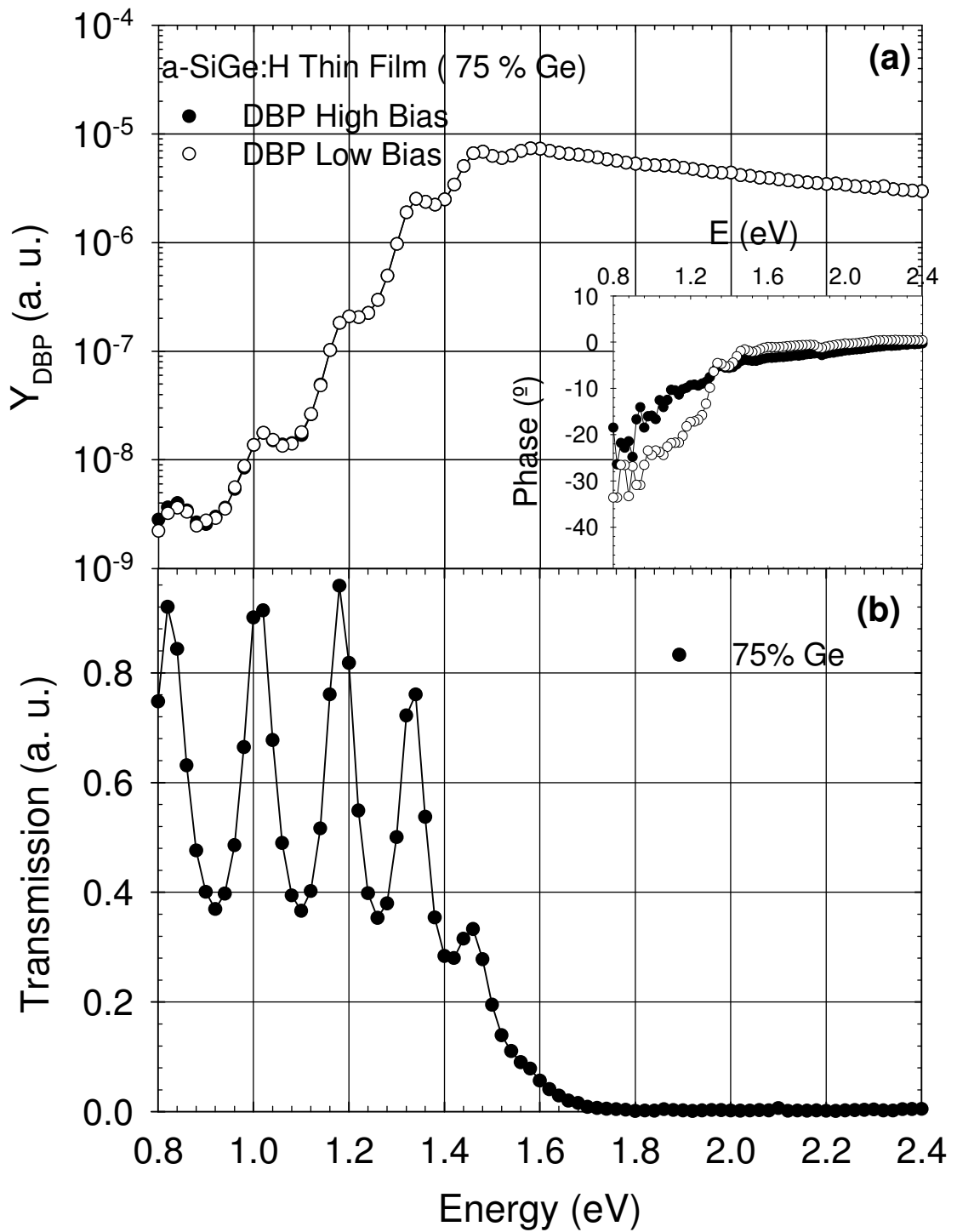
Figure 3.9 a) DBP Yield spectrum of a-SiGe:H alloy thin film of %75 Ge concentration at high and low
bias light intensities in the annealed state. In the inset phase of both measurements are shown.
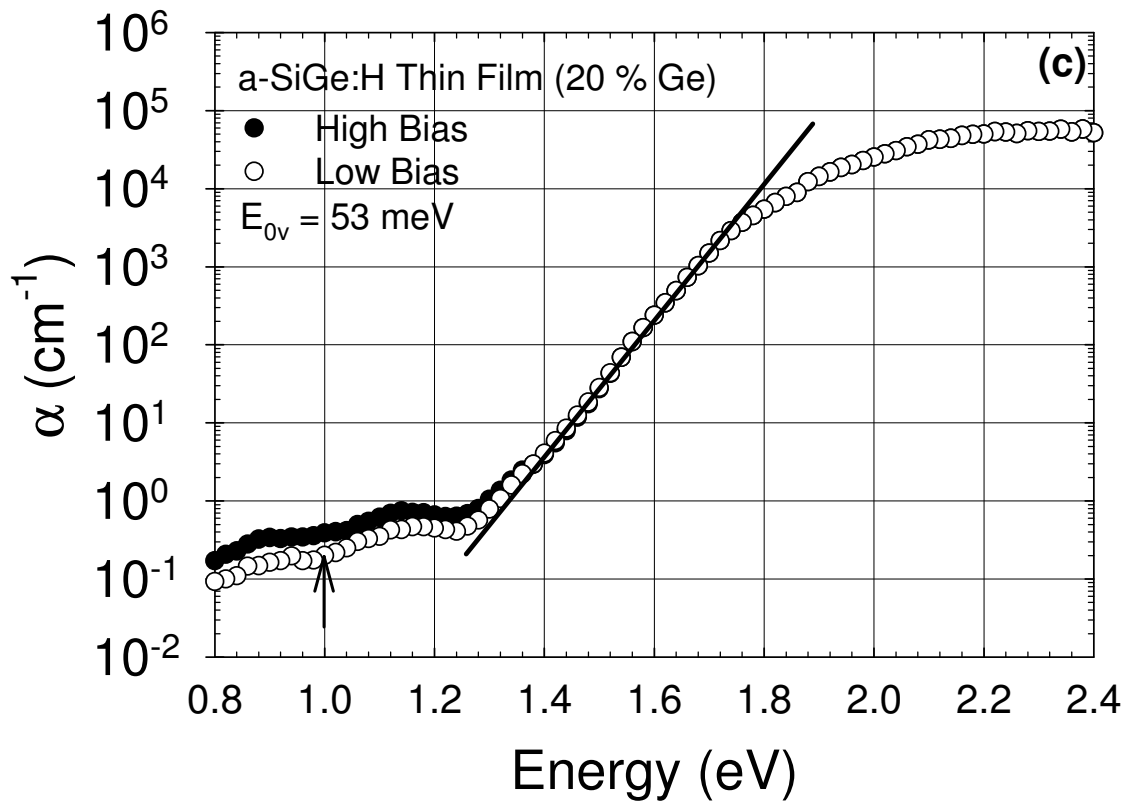b) Transmission spectrum of the same sample.
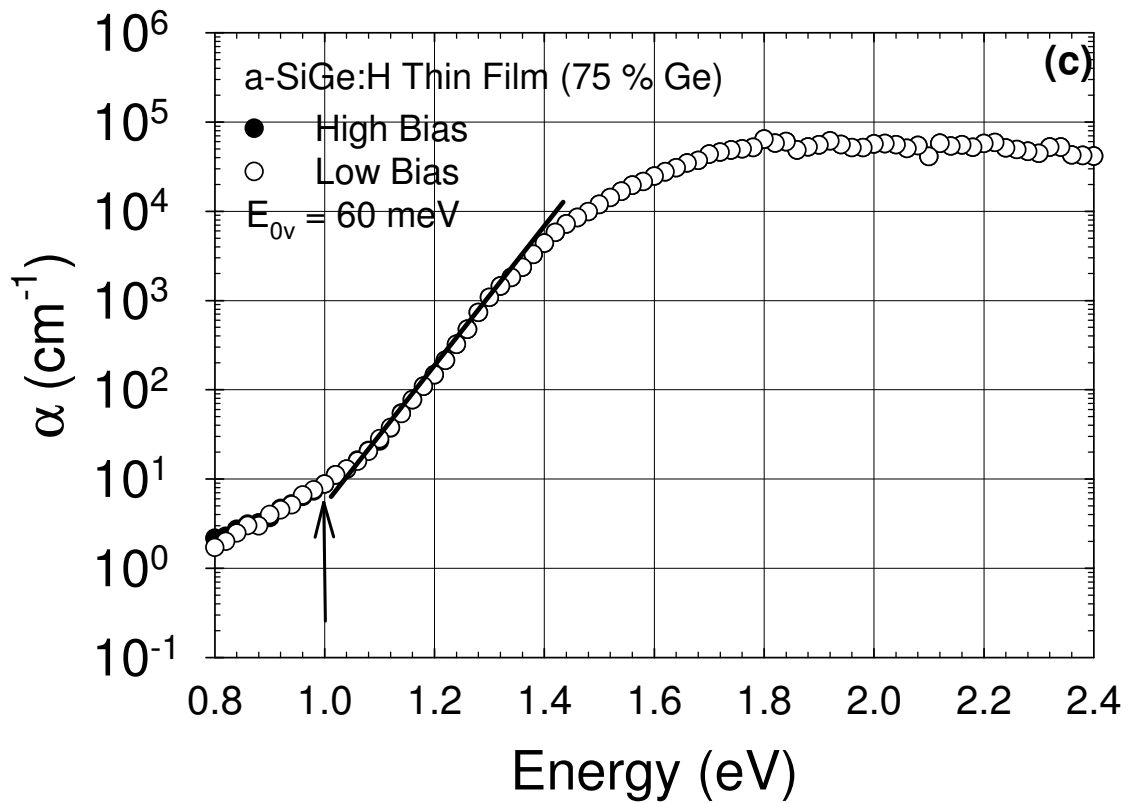
Figure 3.9 c) The calculated absolute α (hν) spectra of DBP for high and low bias light measurements of a-SiGe:H thin film with 75 % Ge concentration.
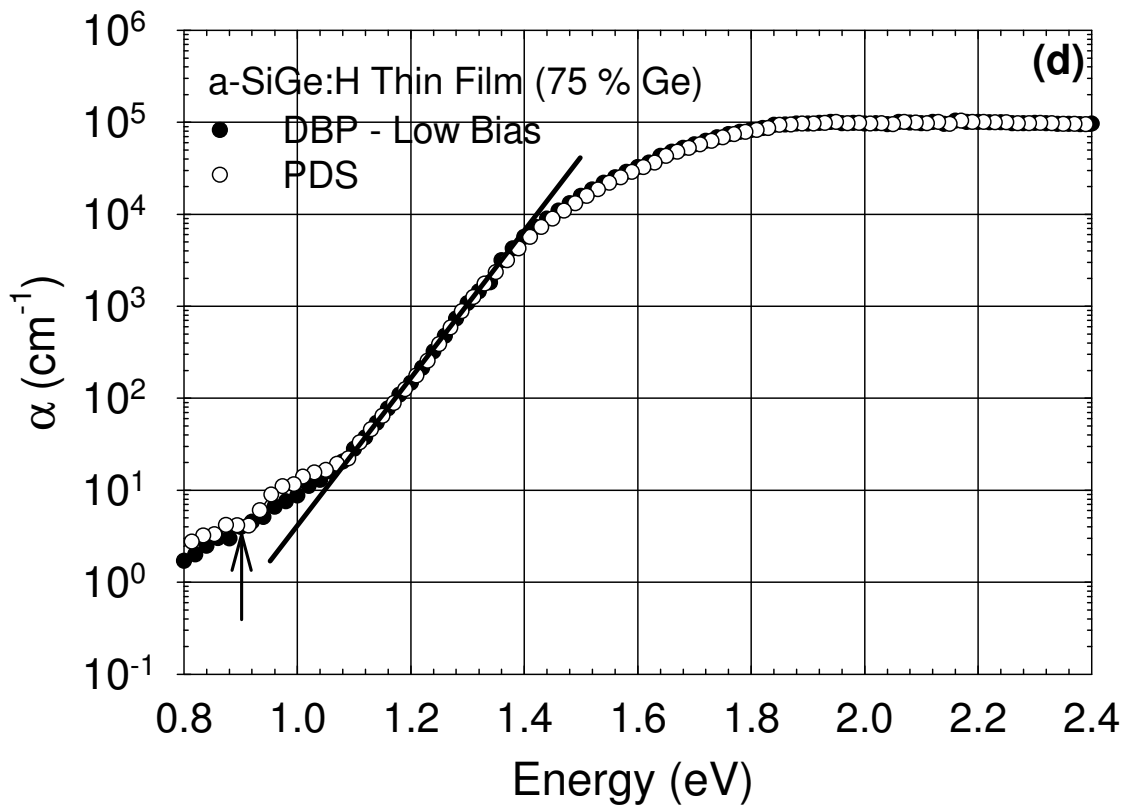
Figure 3.9 d) The calculated absolute α (hν) spectra of PDS and DBP for low bias light measurements of a-SiGe:H thin film with 75% Ge concentration.

61

As a summary of the sub-bandgap absorption results, low bias light DBP spectrum of alloy films are presented together in Figure 3.10 the effect of Ge content in amorphous silicon network clearly indicates a systematic decrease in the bandgap with increasing Ge content as the energy at $\alpha=10^4 cm^{-1}$ is taken as a reference. It decreases from 1.90eV for a-Si:H to 1.46 eV for 75% Ge alloy film. The dependence of E_{04}, and the Urbach energy, E_{0v}, are summarized in Figure 3.11a and Figure 3.11b, respectively. The E_{0v} values are almost constant around 55meV for alloying up to 40% Ge. It increases to 60 meV for 50% and 75% Ge films. Finally the changes in the defect density present in the bandgap of alloy films are inferred from the sub-bandgap absorption coefficient at low energies.

The α(1.0eV) measured by both PDS and low bias light DBP spectrum are shown in Figure 3.12. There is always a difference between PDS and low bias DBP spectra. For low Ge% alloy films, this difference is around a factor of 2 to 10. For highly defective samples, both spectra are closer together. These higher values are consistent with the nature of PDS technique. Such that it probes all the optical transitions into empty states but DBP probes only those to the conduction band. But for some samples, surface layer could be more defective and this will add up additional surface absorption in PDS measurements. This surface absorption is not detected in DBP measurements since it only probes the low defect density region in the bulk of the sample. Low bias light DBP results at 1.0 eV show a better dependence on Ge concentration. Beginning from 0% Ge a-Si:H, α(1.0eV) decreases as Ge content increases to 20% Ge and give a minimum around 0.2 cm^{-1}. It then starts increasing with increasing Ge content. The best film with lowest defect density can be prepared with alloying Ge in the range from 10% to 40% Ge. Increasing Ge content can result in lower bandgap absorber layer for infra red part of solar spectrum in multi-junction solar cells, however, it results in a substantial increase in defect density and a sharp reduction of free carrier lifetime.

Figure 3.10   The calculated absolute α (hν) spectra of DBP for low bias light measurements of a-SiGe:H alloy thin films with 0%, 10%, 20%, 30%, 40%, 50% and 75%. Ge concentrations.
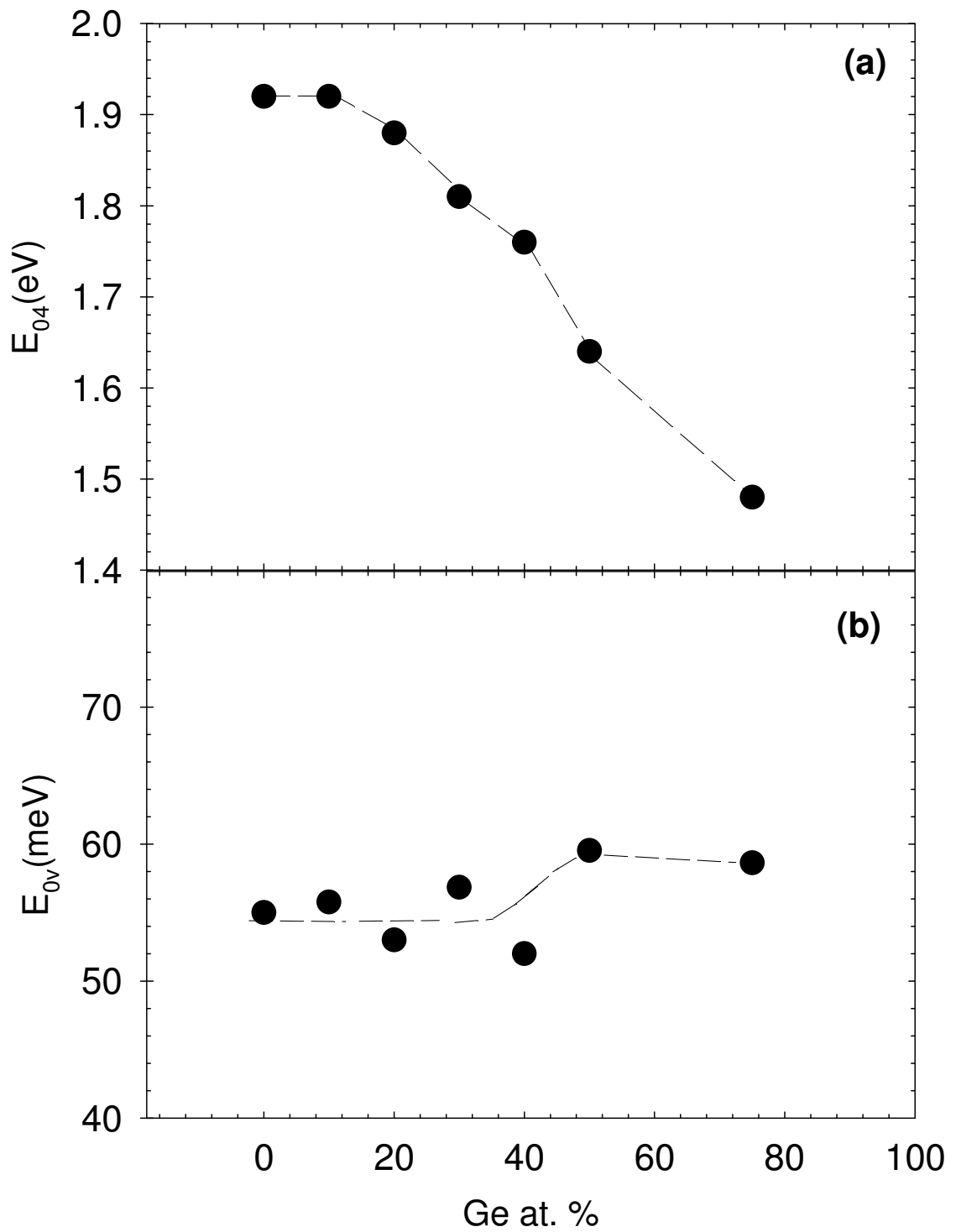
Figure 3.11 a) The bandgap at $\alpha(h\nu) = 10^4 cm^{-1}$ as a function of Ge%. b) E_{0V} as a function of Ge%. Dashed lines are guide to eye.
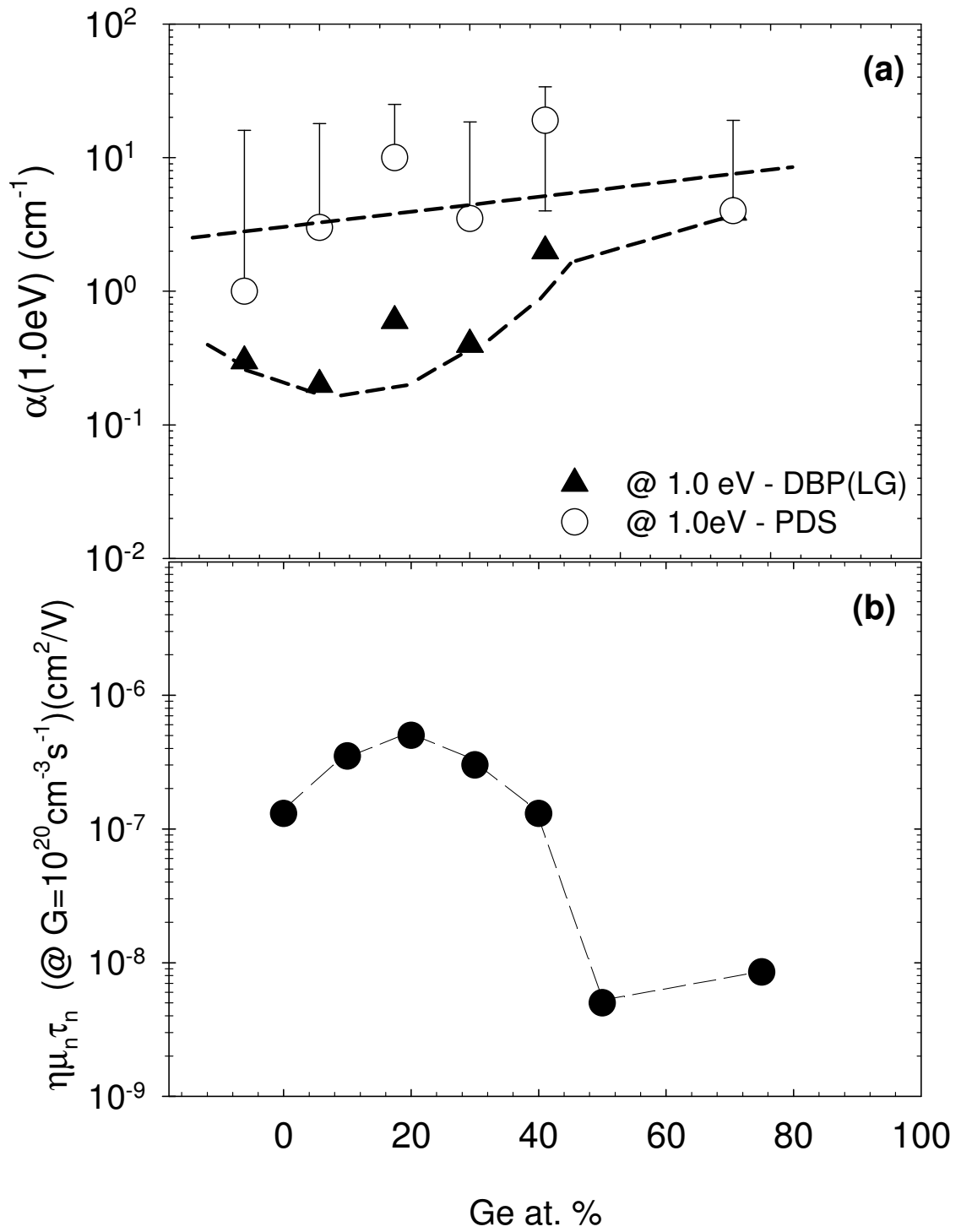
Figure 3.12 a) Absolute absorption coefficients measured by PDS and DBP at low bias light versus the Ge% for a-SiGe:H alloy thin films of 0%, 20%, 30%, 40%, 50% at 1.0eV but for 75% Ge at 0.9eV. b) $\mu\tau$ - product versus Ge concentration for a-SiGe:H alloy thin films of various Ge concentrations in the annealed state. Dashed lines are guide to eye.

CHAPTER 4

EXPERIMENTAL RESULTS IN HYDROGENATED AMORPHOUS SILICON GERMANIUM ALLOY THIN FILMS (a-SiGe:H) IN THE LIGHT SOAKED STATE

4.1 Introduction

Behavior of a-SiGe:H alloy thin films of various Ge% in the light soaked state is one of the main aspects of this thesis. It is known that illumination with intense light leads to the creation of additional metastable states in the mobility gap of a-Si:H known as the Staebler–Wronski Effect (Staebler and Wronski 1977). This effect is also observed in hydrogenated amorphous silicon germanium alloy thin films (Cohen 2003 and references therein). In this study, the Staebler-Wronski effect of intrinsic a-SiGe:H alloy thin films with different Ge concentrations were investigated using the steady-state photoconductivity and DBP techniques to understand the effect of Ge content on the kinetics of defect creation on mobility-lifetime product and low energy sub-bandgap absorption coefficients using a 15 suns of white light illumination. Since both $\mu_n\tau_n$-products and $\alpha(h\nu)$ in low energies are mainly controlled by the defect states created by light soaking, kinetics of defect creation for different germanium contents has also been compared with those present in the unalloyed hydrogenated amorphous silicon films. Results of this chapter will be discussed in two parts. The first part will be about the changes observed in photoconductivity and mobility lifetime product. And in the second part, the changes in the absolute absorption coefficient at lower energies are presented for different light soaking durations.

4.2 Steady State Photoconductivity Results

Hydrogenated amorphous silicon sample is the reference sample in these measurements. Photoconductivity and mobility-lifetime product versus generation rate plots for various light soaking durations for this sample can be seen in figure 4.1a and figure 4.1b respectively. A decrease of more than two orders of magnitude is seen in

66

photoconductivity at the generation rate of 10^{21}cm^{-3}s^{-1}. The exponent γ is around 0.90, not showing a change in light soaked state. The degradation kinetics of photoconductivity at a generation rate of 10^{21}cm^{-3}s^{-1} and 10^{17}cm^{-3}s^{-1}is shown in figure 4.1c. The relation t$^{-0.33}$ is the reported degradation behavior in literature (Stutzmann et al 1989) for a-Si:H films. However, for both generation rates, time dependence of degradation in this sample shows of t$^{-0.50}$rule. This indicate that there is no t$^{1/3}$ unique rule for degradation of photoconductivity in a-Si:H films as consistent with reported results by Gunes and Wronski 1997. For the magnitude of degradation of $\eta\mu_n\tau_n$ product at G=10^{21}cm^{-3}s^{-1}is 250 times and at G=10^{17}cm^{-3}s^{-1} is 350 times as presented in Figure 4.1c.

SSPC and $\eta\mu_n\tau_n$ product versus generation rate of 20% Ge a-SiGe:H alloy thin films are presented in Figure 4.2a and Figure 4.2b, respectively. The Staebler-Wronski effect is clearly seen in the magnitude of σ_{ph}. The exponent γ is around 0.90 for both annealed and light soaked states. The rate of degradaton in σ_{ph} at two generation rates is shown in Figure 4.2c. The slope of degradation is -0.60 for both generation rate and it is higher than pure a-Si:H sample with 0% Ge. It means that Ge added alloys degrade faster in time. Similarly the degradation experiments for different light soaking periods have been performed for other alloy thin films having different Ge contents. These results are presented in Figure 4.3, Figure 4.4, Figure 4.5 and Figure 4.6 for 30% Ge, 40% Ge, 50% Ge and 75% Ge alloy a-SiGe:H thin films, respectively. All exhibit certain degree of degradation in the magnitude of σ_{ph} and $\eta\mu_n\tau_n$ products. The exponent γ is around 0.8-0.90 in the soaked state. But for 75% Ge sample, it is lower in the annealed state. It is around 0.74 and does not change in the soaked state.
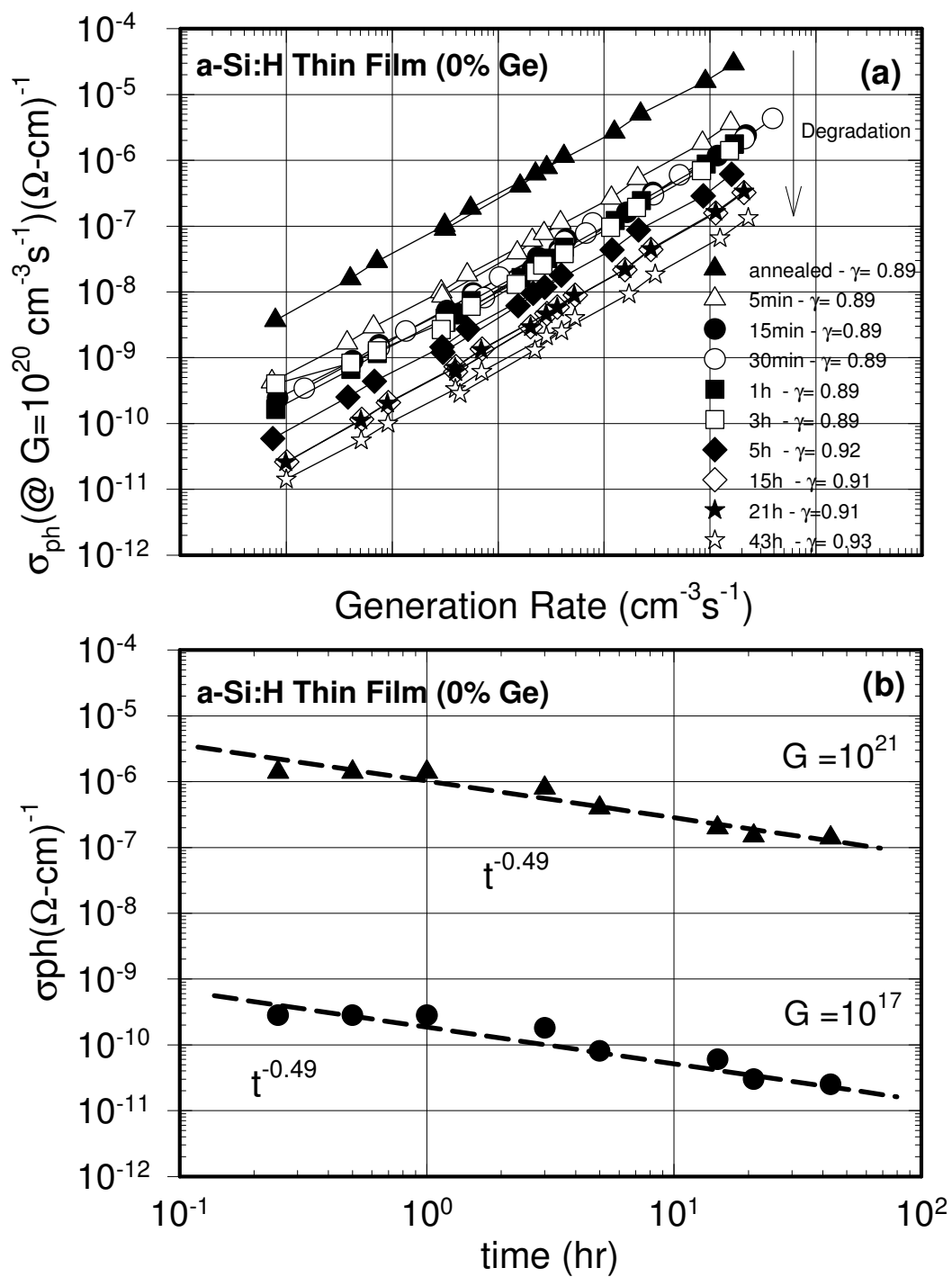
Figure 4.1 a) σ_{ph} versus generation rate for a-Si:H thin film of 0% Ge of various light soaking durations

b) Kinetics of photoconductivity degradation under 15 suns of white light illumination measured at $G=10^{17}$ cm^{-3}s^{-1} and $G=10^{21}$cm^{-3}s^{-1} as a function of illumination time for the a-Si:H thin film with 0% Ge.
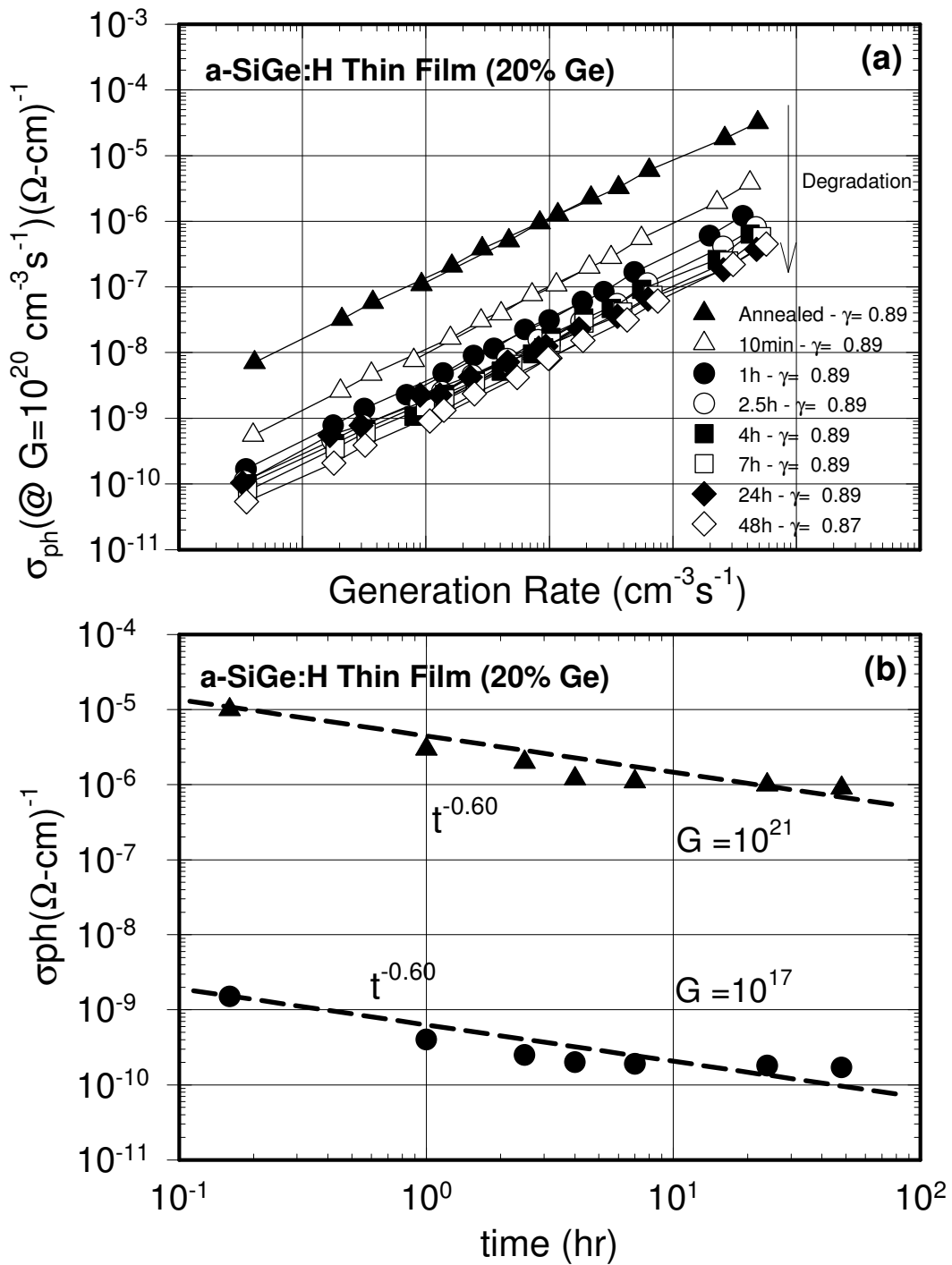
Figure 4.2 a) σ_{ph} versus generation rate for a-SiGe:H alloy thin film of 20% Ge of various light soaking durations b) Kinetics of photoconductivity degradation under 15 suns of white light illumination measured at $G=10^{17}$ cm^{-3}s^{-1} and $G=10^{21}$cm^{-3}s^{-1} as a function of illumination time for the a-SiGe:H thin film with 20% Ge.
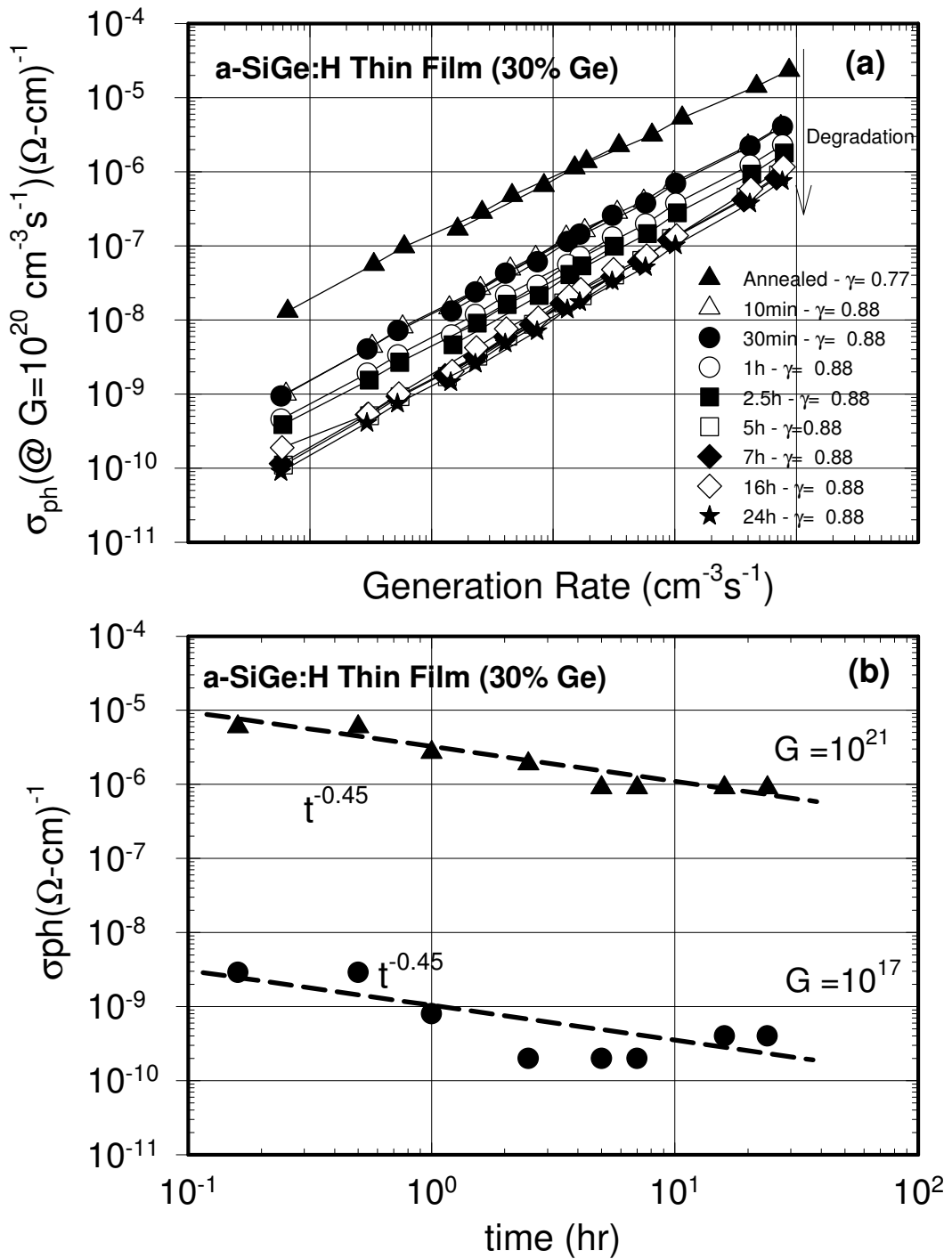
Figure 4.3 a) σ_{ph} versus generation rate for a-SiGe:H alloy thin film of 30% Ge of various light soaking durations b) Kinetics of photoconductivity degradation under 15 suns of white light illumination measured at $G=10^{17}$ cm^{-3}s^{-1} and $G=10^{21}$cm^{-3}s^{-1} as a function of illumination time for the a-SiGe:H thin film with 30% Ge.
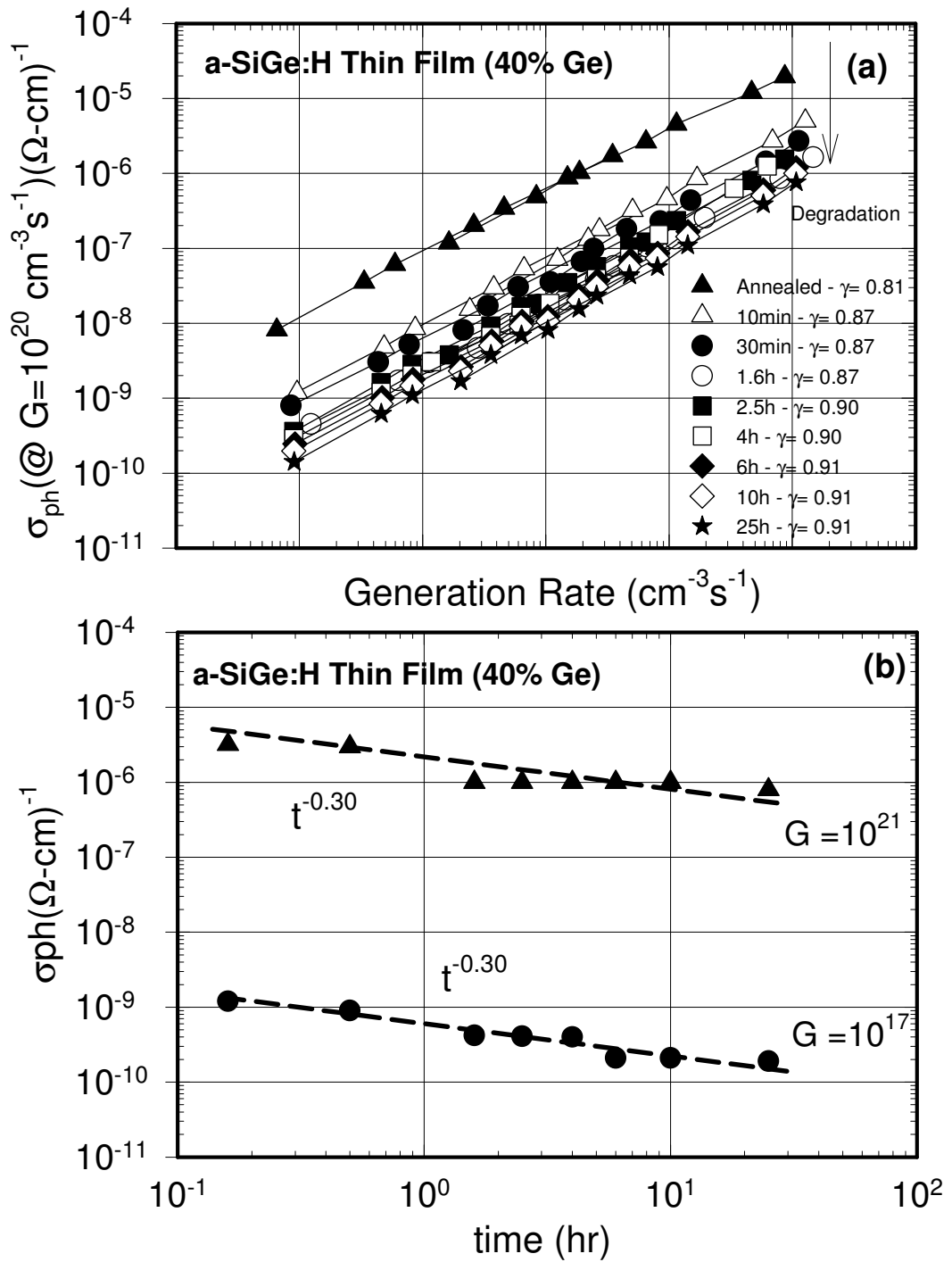
Figure 4.4 a) σ_{ph} versus generation rate for a-SiGe:H alloy thin film of 40% Ge of various light soaking durations b) Kinetics of photoconductivity degradation under 15 suns of white light illumination measured at $G=10^{17}$ cm^{-3}s^{-1} and $G=10^{21}$cm^{-3}s^{-1} as a function of illumination time for the a-SiGe:H thin film with 40% Ge.
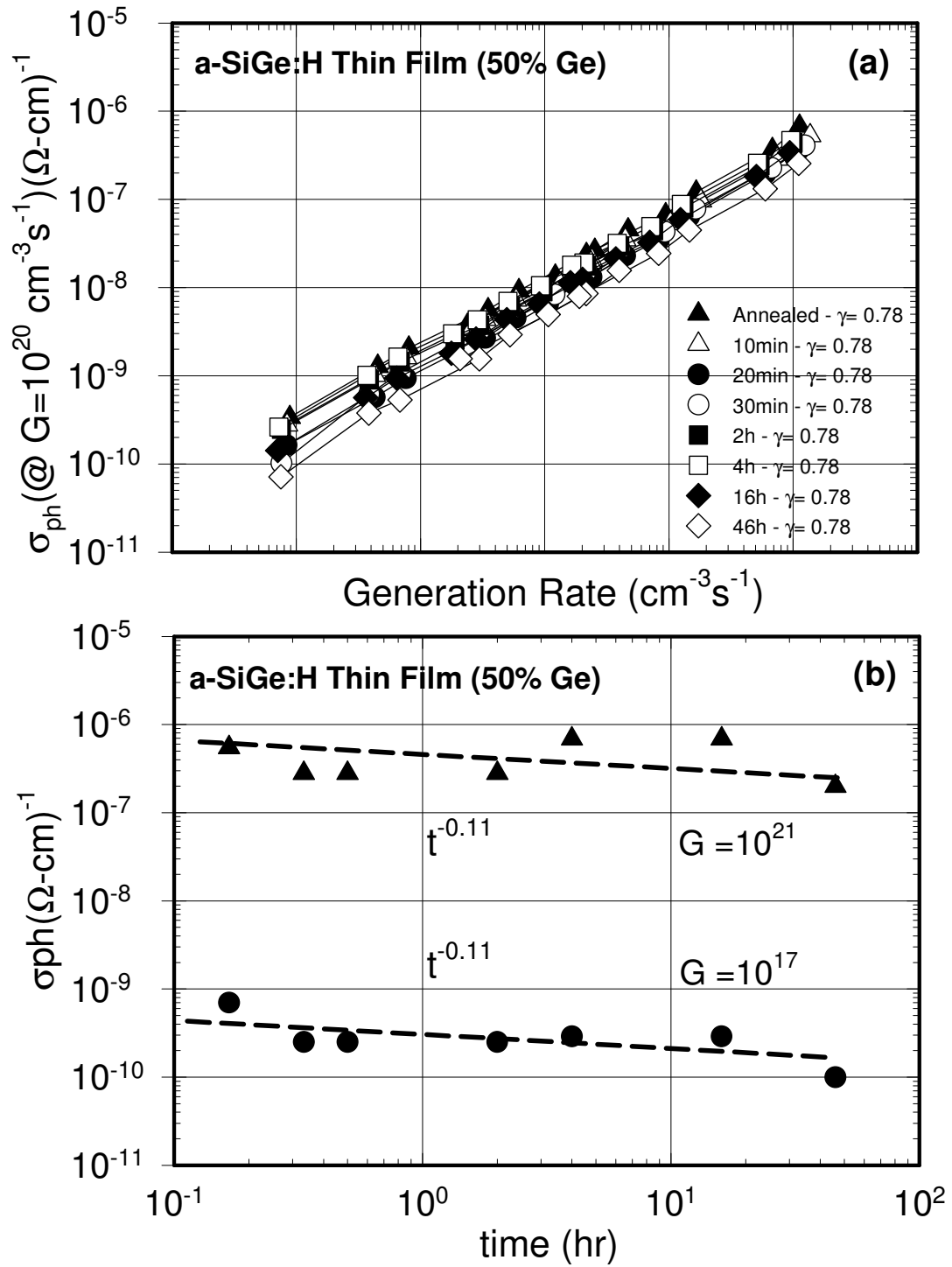
Figure 4.5 a) σ_{ph} versus generation rate for a-SiGe:H alloy thin film of 50% Ge of various light soaking durations b) Kinetics of photoconductivity degradation under 15 suns of white light illumination measured at G=10^{17} cm^{-3}s^{-1} and G=10^{21}cm^{-3}s^{-1} as a function of illumination time for the a-SiGe:H thin film with 50% Ge.
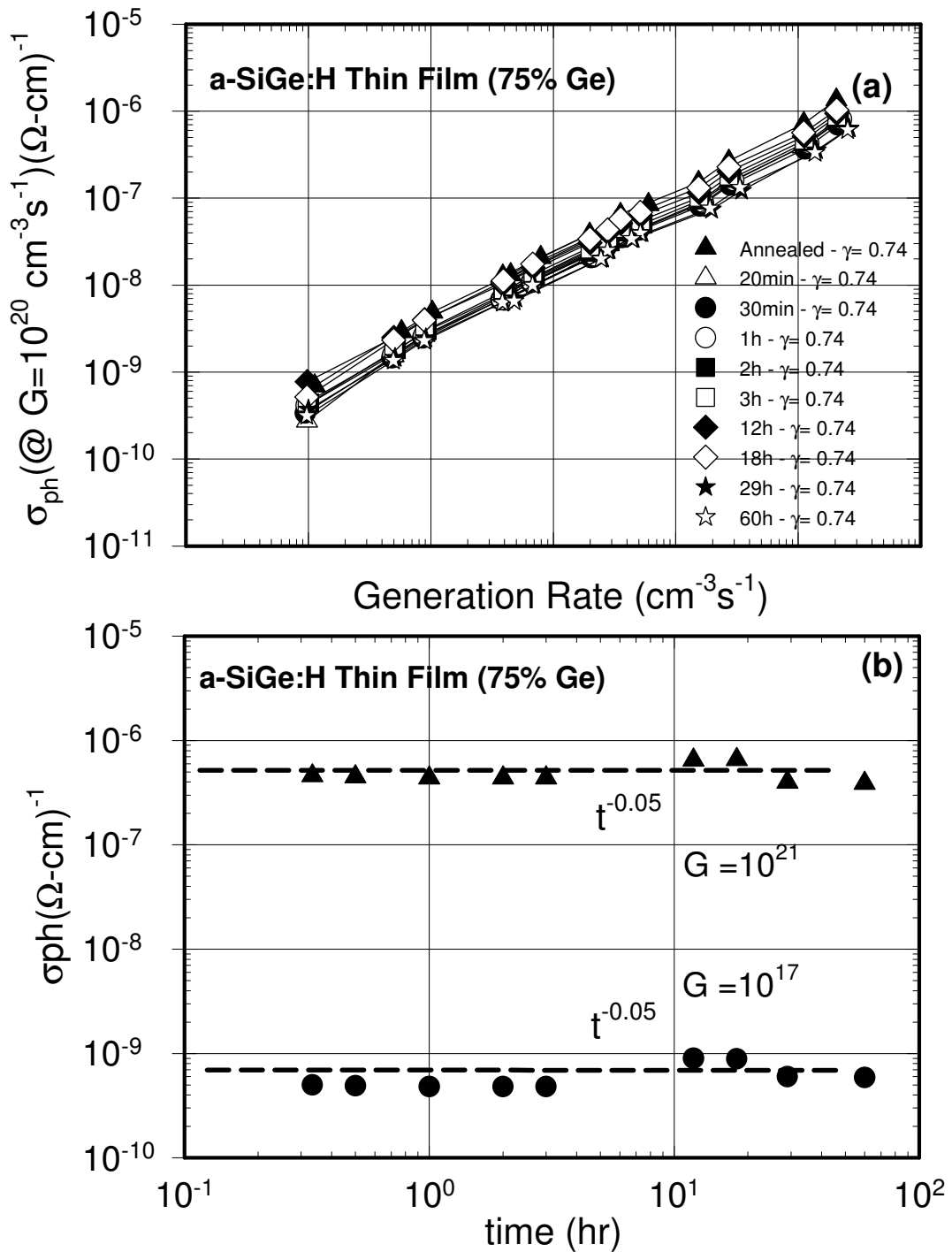
Figure 4.6 a) σ_{ph} versus generation rate for a-SiGe:H alloy thin film of 75% Ge of various light soaking durations b) Kinetics of photoconductivity degradation under 15 suns of white light illumination measured at $G=10^{17}$ cm^{-3}s^{-1} and $G=10^{21}$cm^{-3}s^{-1} as a function of illumination time for the a-SiGe:H thin film with 75% Ge.
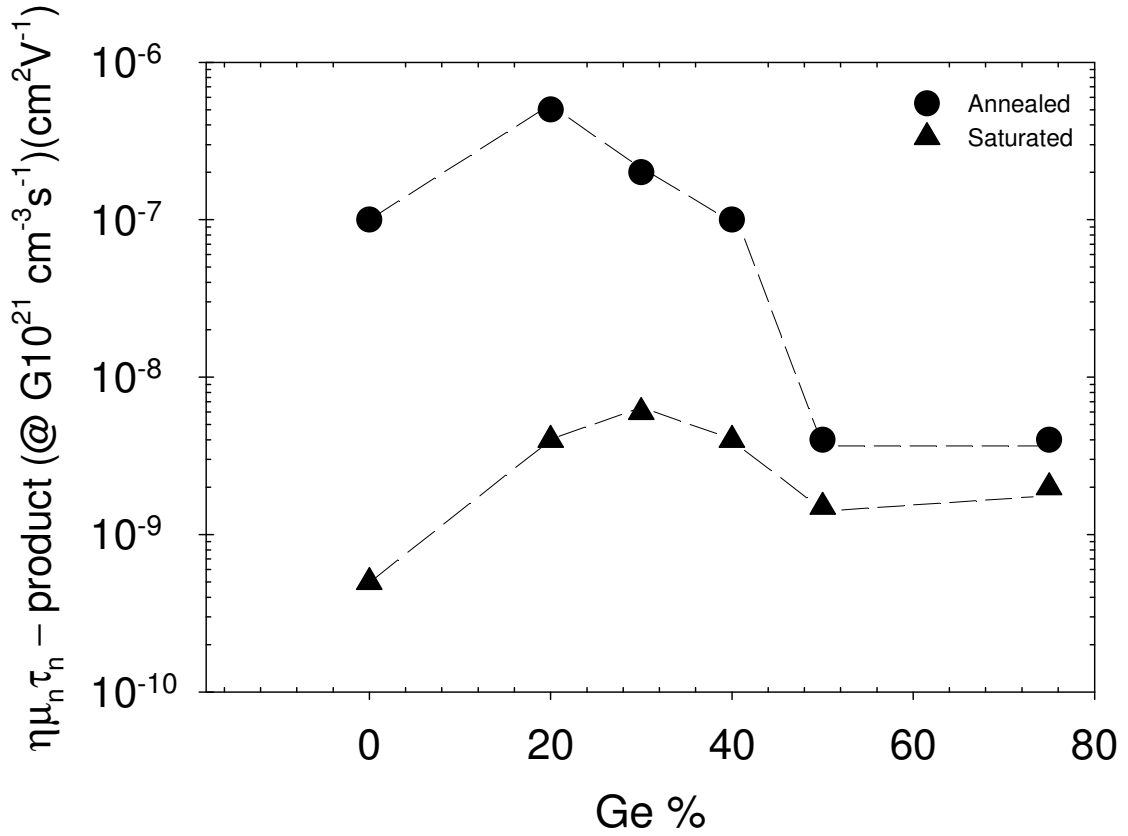
Figure 4.7   Kinetics of degradation of $\eta\mu_n\tau_n$–product under 15 suns of white light illumination measured at and $G=10^{21}cm^{-3}s^{-1}$ as a function of germanium concentration in annealed and saturated states.

The magnitude of degradation in $\eta\mu_n\tau_n$ product and slopes of degradation of σ_{ph} are summarized in Table 4.1. In addition, $\eta\mu_n\tau_n$ product measured at $G=10^{21}cm^{-3}s^{-1}$ in the annealed and light soaked state are shown in Figure 4.7 as function of Ge concentrations. Among the samples unalloyed a-Si:H film shows the highest degradation in $\eta\mu_n\tau_n$ products. As Ge content increases, the rate decreases. The alloy with 20% Ge shows the highest degradation from annealed state to the satured state by a factor of 100. The rate decreases as Ge content increases. For 50% Ge and 75% Ge, $\eta\mu_n\tau_n$ product degradation is very low by factor of 4 and 3, respectively. The rates also show the similar trend. The 20% Ge alloy degrades the fastest by the slope of -0.6. It is -0.45 and -0.3 for 30% Ge and 40% Ge alloy films. It is extremely small for 50% Ge and 75% Ge samples as can be seen from the respective figures. It can be inferred that alloying improves the $\eta\mu_n\tau_n$ product up to 40% Ge and degradation is also slower than it is for pure a-Si:H film. As the saturated values for $\eta\mu_n\tau_n$ products are compared, alloys with 20% Ge to 40% Ge are still much higher than pure a-Si:H film. This is clearly seen in Figure 4.7. Degradation of $\eta\mu_n\tau_n$ products obtained from the SSPC indicates that new

74

defects are created by light to decrease the lifetime τ_n of free carriers. However, only qualitative estimation about these defect states can be made by comparing the absolute change in $\eta\mu_n\tau_n$ products of the samples.

Table 4.1 Parameters of degradation kinetics in SSPC

Ge%	$\mu_n\tau_n$ (an)/ $\mu_n\tau_n$ (sat) (@ G=10^{17})	t^{-x} (@ G=10^{17})	$\mu_n\tau_n$ (an)/ $\mu_n\tau_n$ (sat) (@ G=10^{21})	t^{-y} (@ G=10^{21})
0	375	-0.49	250	-0.49
20	100	-0.6	100	-0.6
30	100	-0.45	33	-0.45
40	60	-0.3	25	-0.3
50	4	-0.11	4	-0.11
75	3.0	-0.05	3.0	-0.05

4.3 Sub-bandgap Absorption Results

The Staebler-Wronski effect is also directly seen in the change of sub-bandgap absorption coefficient at lower energies. The increase in the $\alpha(h\nu)$ in the lower energy part of the spectrum is direct indication of increase of defect states in the bandgap of samples, which also cause degradation of $\eta\mu_n\tau_n$ products as explained in the previous section. An example of sub-bandgap absorption spectra for annealed and 1 hour light soaked state under 15 suns of white light is shown in Figure 4.8. it is seen that only low energy part of $\alpha(h\nu)$ changes after light soaking. No change in the exponential absorption edge and higher energy part is detected. Therefore, only defects causing the recombination of free carriers are created by light. No effect is detected in the disorder. The samples were light soaked for different light soaking periods and after each period, the DBP spectra were measured and absolute absorption coefficient spectra were calculated. Summary of DBP spectra for samples 0% Ge (pure a-Si:H) is shown in Figure 4.9. The $\alpha(h\nu)$ values at lower energies increase to higher values in the arrow direction. In order to see the degradation of $\alpha(h\nu)$, the $\alpha(h\nu)$ at 1.0 eV is taken and plotted as a function of time. This is presented in Figure 4.10a. It roughly obeys to $t^{1/3}$ rule as proposed by Stuttzmann et al 1989. However the change in $1/\eta\mu_n\tau_n$ product

measured at low generation rate shows totally different time dependence as shown in Figure 4.10b. Even tough both measurements were done at similar generation rates, $\alpha(h\nu)$ degradation and $\eta\mu_n\tau_n$ product degradation are not controlled by the same distribution of defect states. This type of behavior was reported previously in detail by Gunes and Wronski 1997.
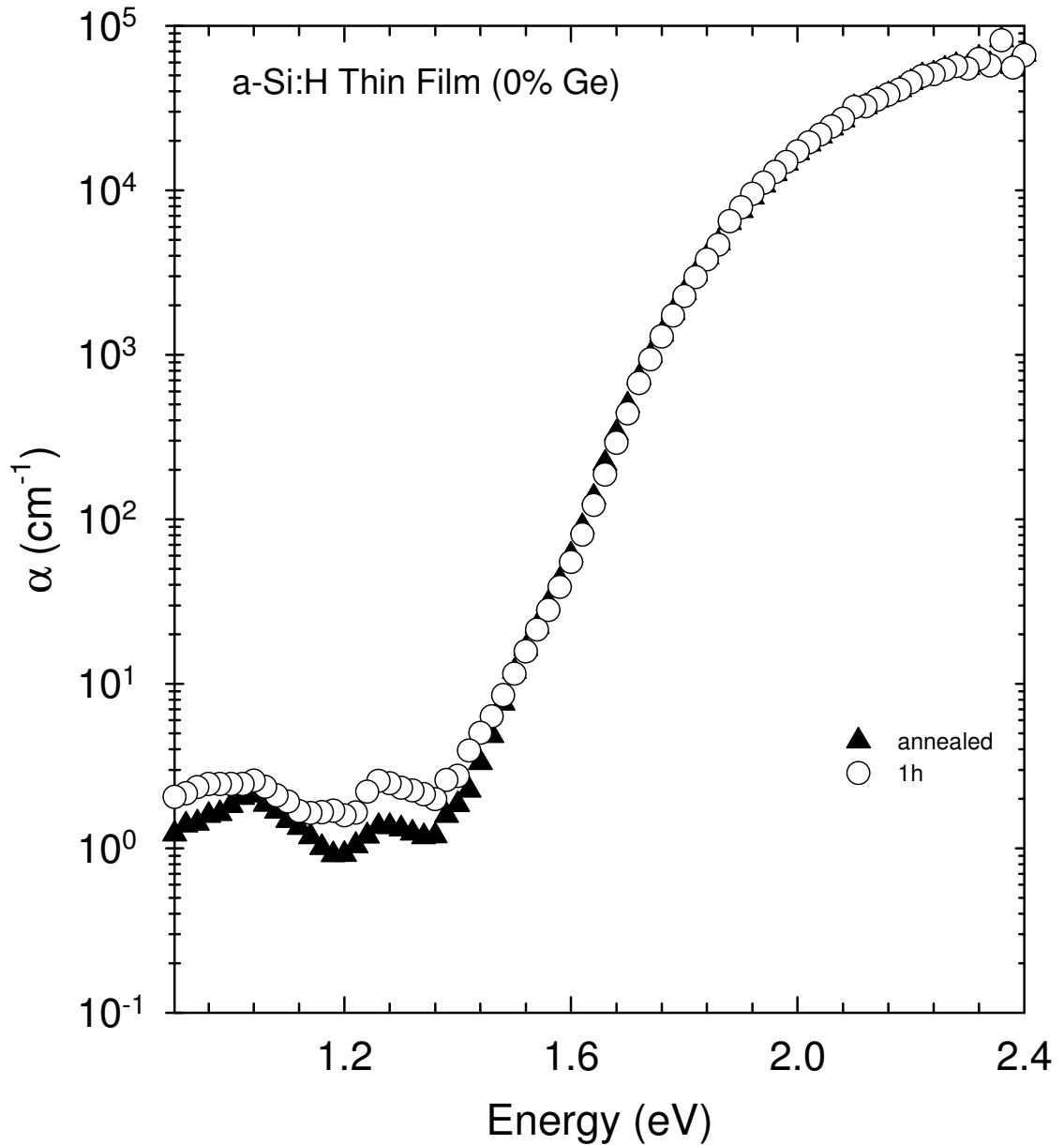
Figure 4.8 Absolute absorption spectrum of the sample with 0% Ge, for annealed and 1h light soaked states, calculated from the Y_{DBP} spectrum and simultaneously measured transmission signals.
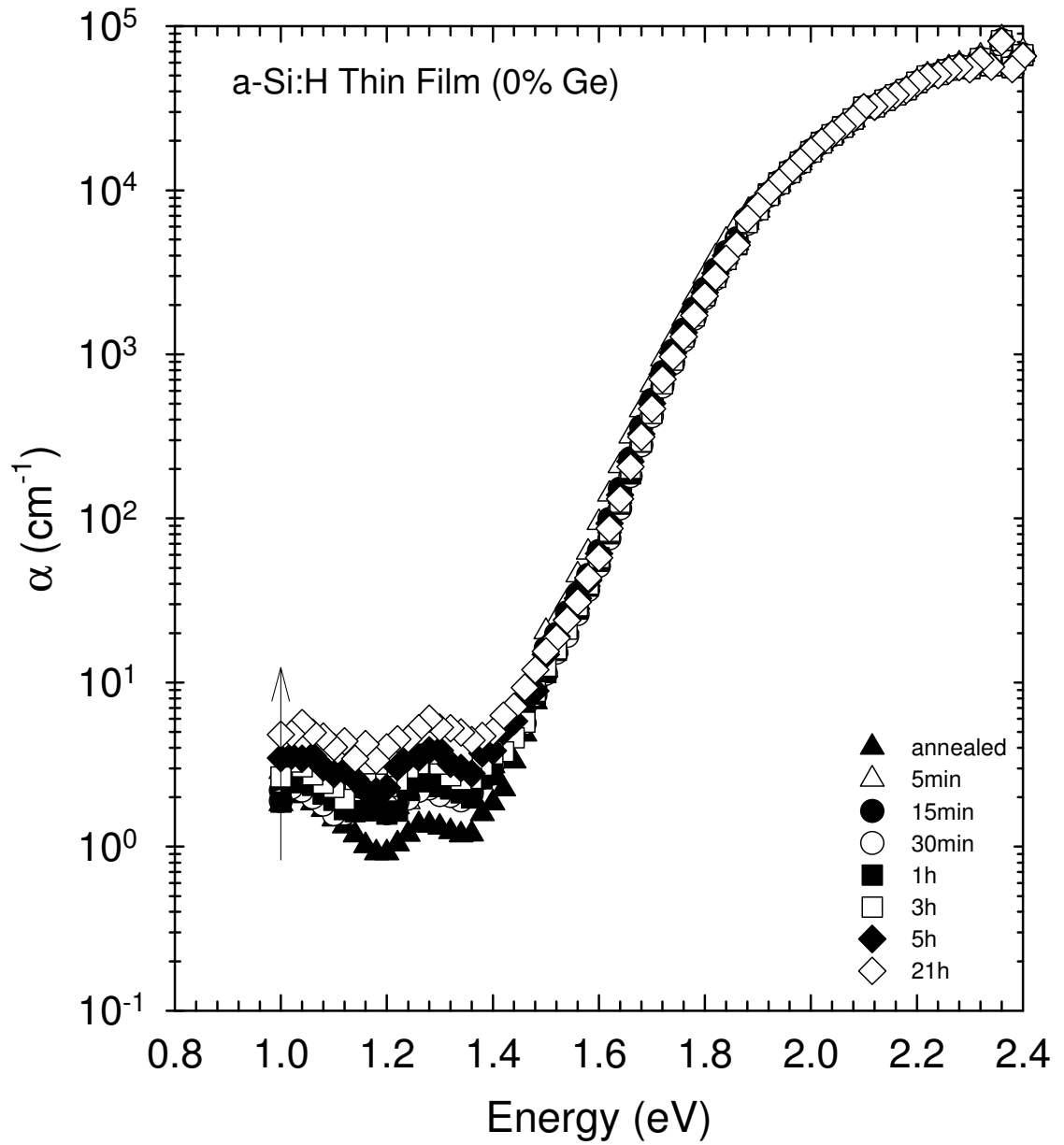
Figure 4.9 Absolute absorption spectrum of the sample with 0% Ge, for various light soaking intervals, calculated from the Y_{DBP} spectrum and simultaneously measured transmission signals.
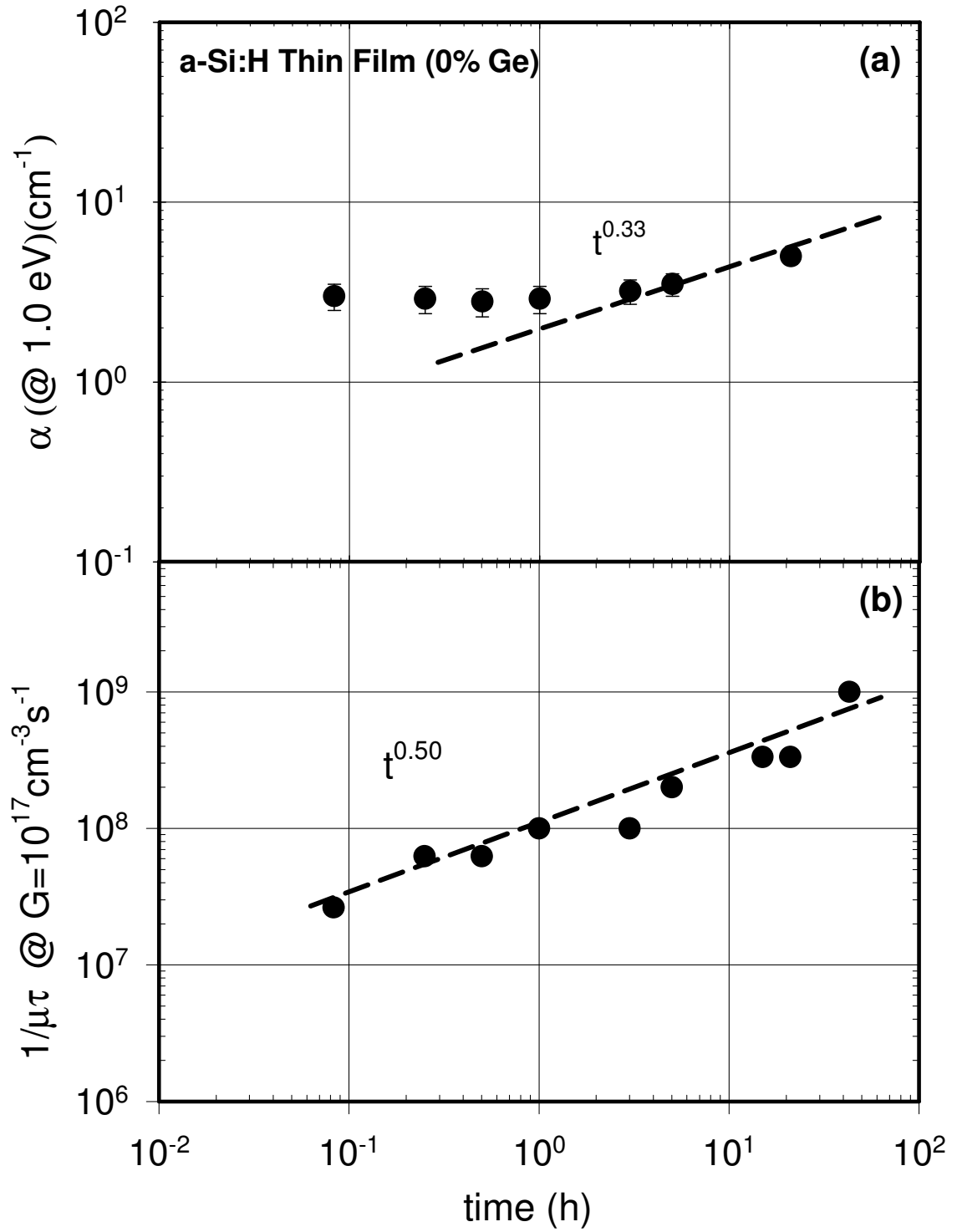
Figure 4.10 a) increase of the sub-bandgap absorption coefficient at 1.0 eV versus degradation time. b) degradation of $1/\mu\tau$ product measured at a generation rate of $10^{17}\text{cm}^{-3}\text{s}^{-1}$.

As Ge% increases, σ_{ph} degradation becomes slower in alloys. In the subgap absorption spectrum of 20% Ge alloy films, the spectra are shown in Figure 4.11. The measurement in the soaked state is sometimes dominated by noise due to loss of photoconductivity signal. Therefore, the degradation in $\alpha(h\nu)$ at 1.0 eV is presented with error bars. Its rate obeys to $t^{0.40}$ relation. It is slightly higher than that of a-Si:H film. Corresponding time dependence of $1/\eta\mu_n\tau_n$ product is 0.36 and closer to that of $\alpha(h\nu)$ degradation. Similar degradation process has been measured for other higher Ge% alloy samples. However, the rate of $\alpha(h\nu)$ at 1.0 eV decreases as Ge% increases as seen in Figure 4.13, through Figure 4.20 for alloy samples with 30% Ge, 40% Ge, 50% Ge and 75% Ge samples. The slope of $\alpha(h\nu)$ is 0.25 for 30% Ge and 40% Ge alloy films, and it is 0.1 for 50% Ge and almost 0 for 75% Ge sample. These results indicate that for higher Ge content films show almost no degradation in sub-bandgap absorption. This is also consistent with σ_{ph} degradation results presented in previous section. In degradation of $\alpha(h\nu)$, the ratio of α_{sat}/α_{an} at 1.0 eV is taken for comparison. The ratio is 2.5 for 0% Ge film. It is 15 for 20% Ge, which is the highest. It decreases to around 8 for 30% Ge and 40% Ge films, to 4 and 2 for 50% Ge and 75% Ge films, respectively.
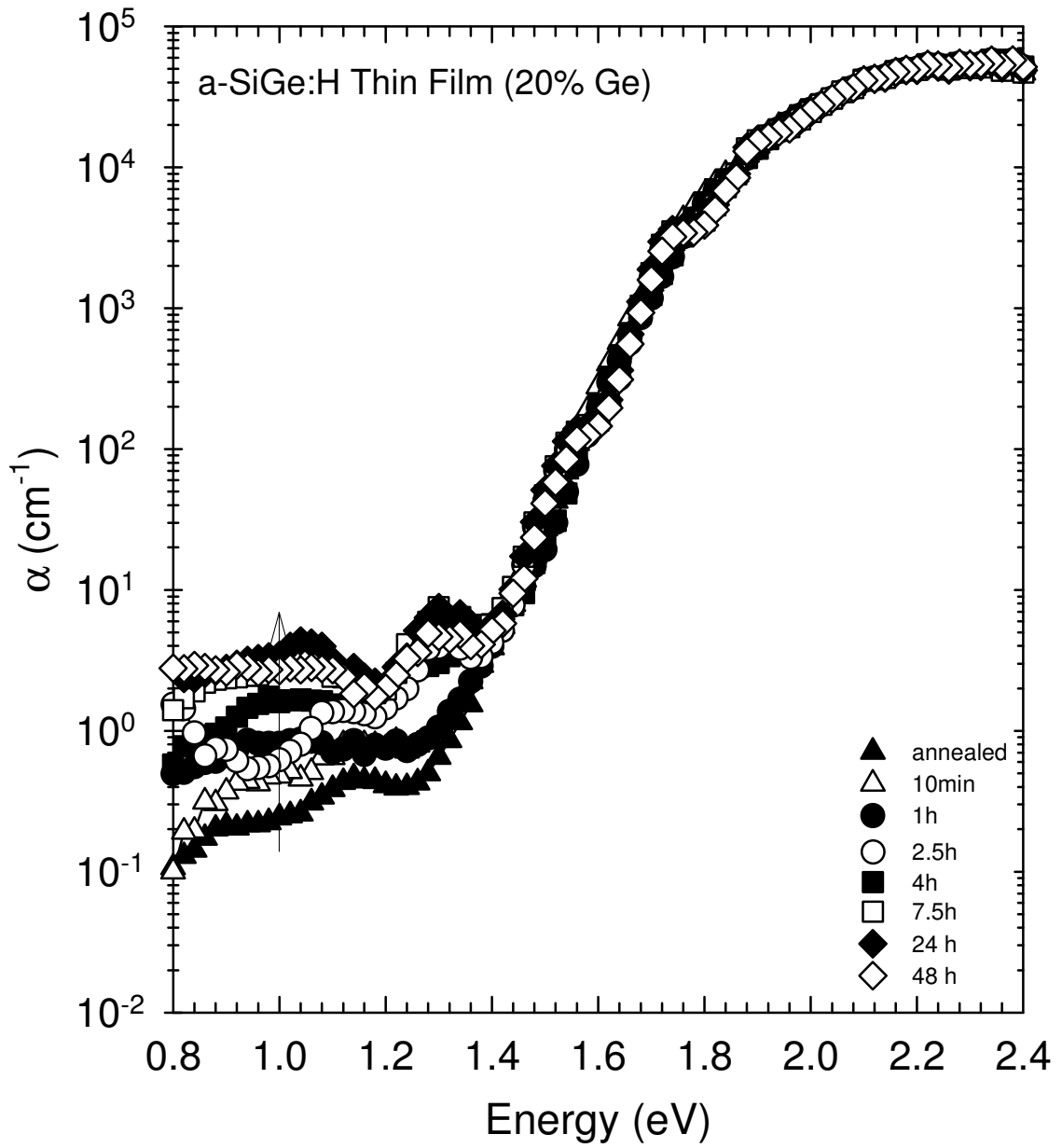
Figure 4.11 Absolute absorption spectrum of the sample with 20% Ge, for various light soaking intervals, calculated from the Y_{DBP} spectrum and simultaneously measured transmission signals.
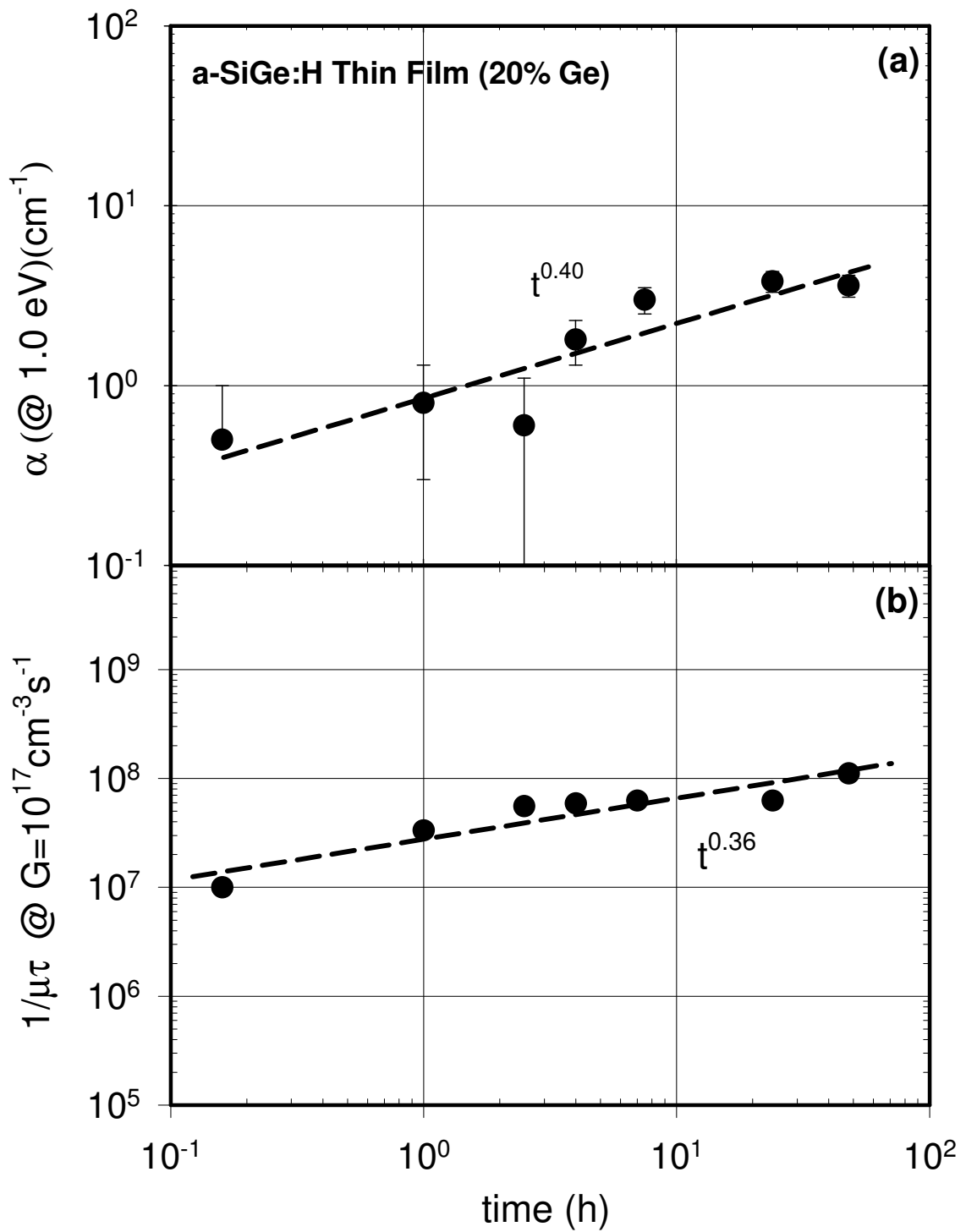
Figure 4.12 a) Increase of the sub-bandgap absorption coefficient at 1.0 eV versus degradation time. b) degradation of $1/\mu\tau$ product measured at a generation rate of $10^{17}cm^{-3}s^{-1}$.
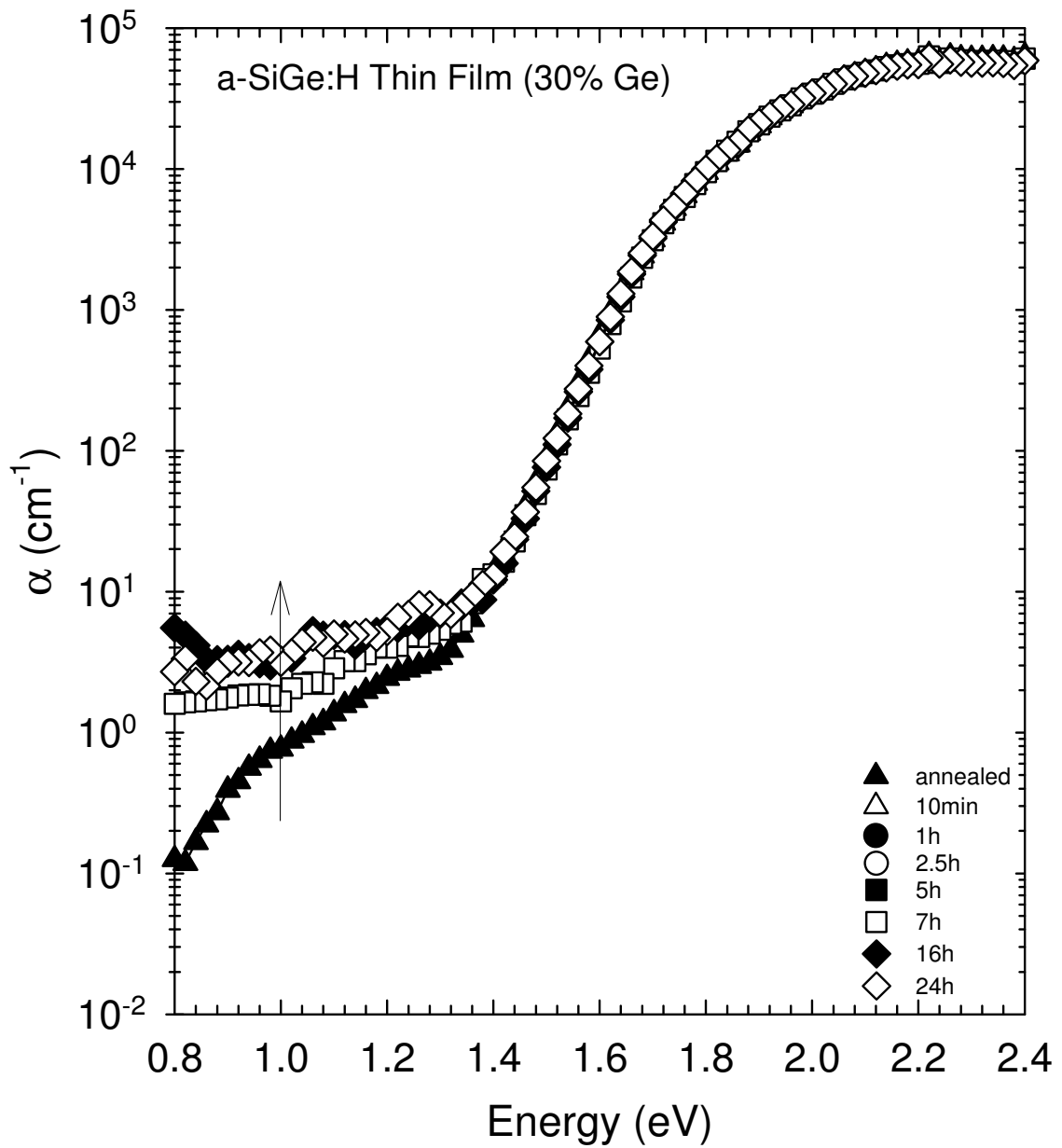
Figure 4.13 Absolute absorption spectrum of the sample with 30% Ge, for various light soaking intervals, calculated from the Y_{DBP} spectrum and simultaneously measured transmission signals.
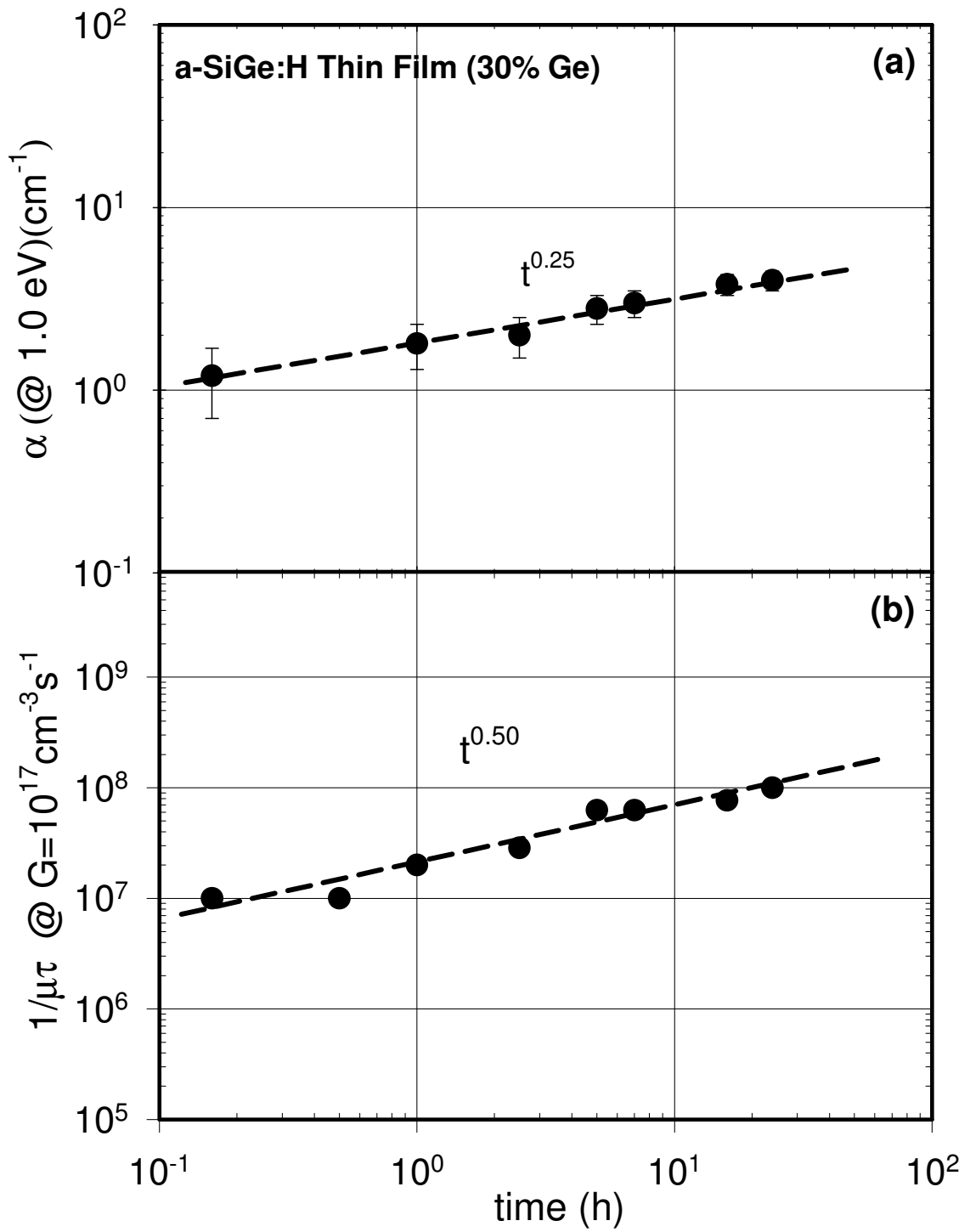
Figure 4.14 a) Increase of the sub-bandgap absorption coefficient at 1.0 eV versus degradation time. b) degradation of $1/\mu\tau$ product measured at a generation rate of $10^{17} cm^{-3} s^{-1}$.
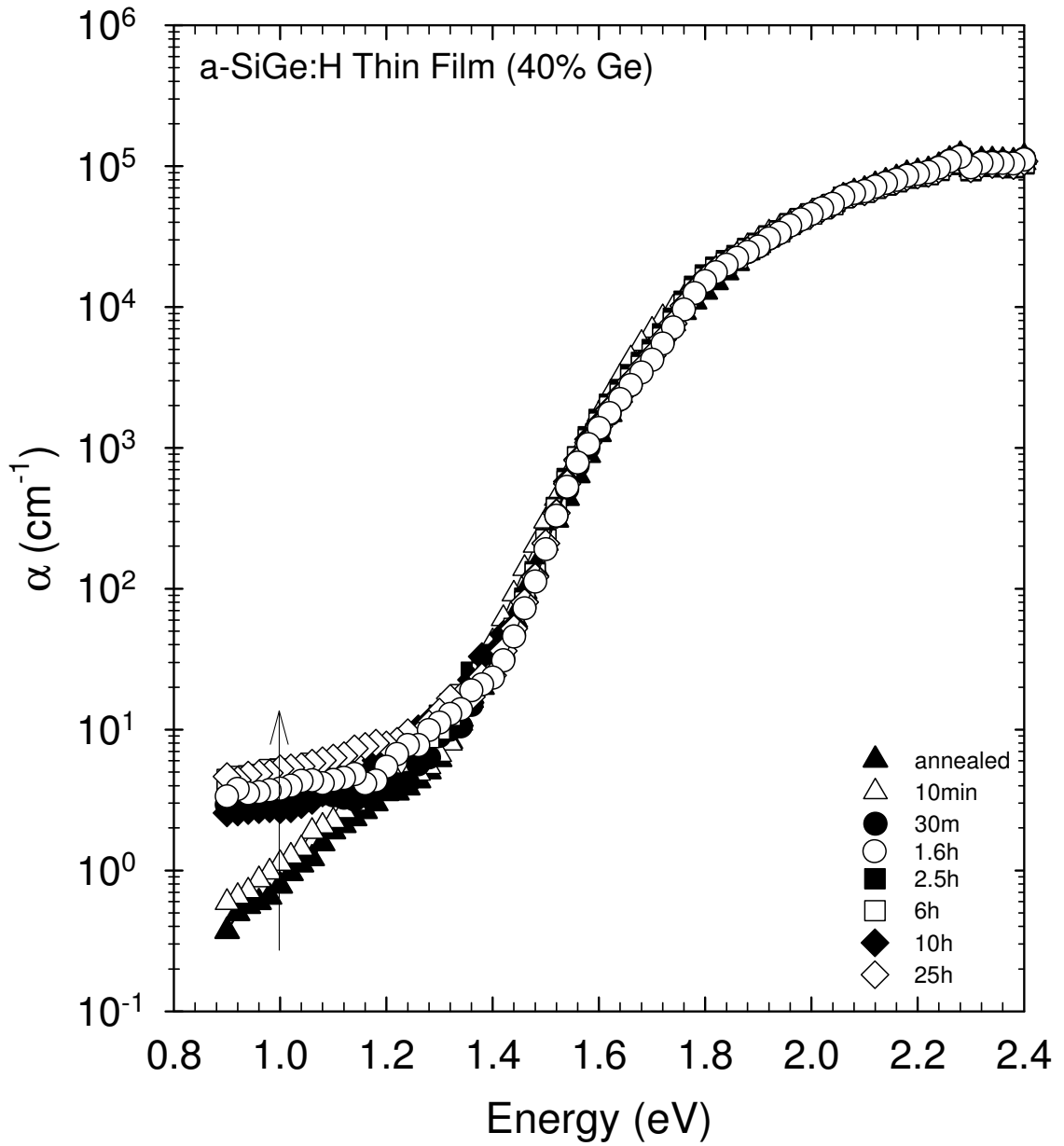
Figure 4.15 Absolute absorption spectrum of the sample with 40% Ge, for various light soaking intervals, calculated from the Y_{DBP} spectrum and simultaneously measured transmission signals.
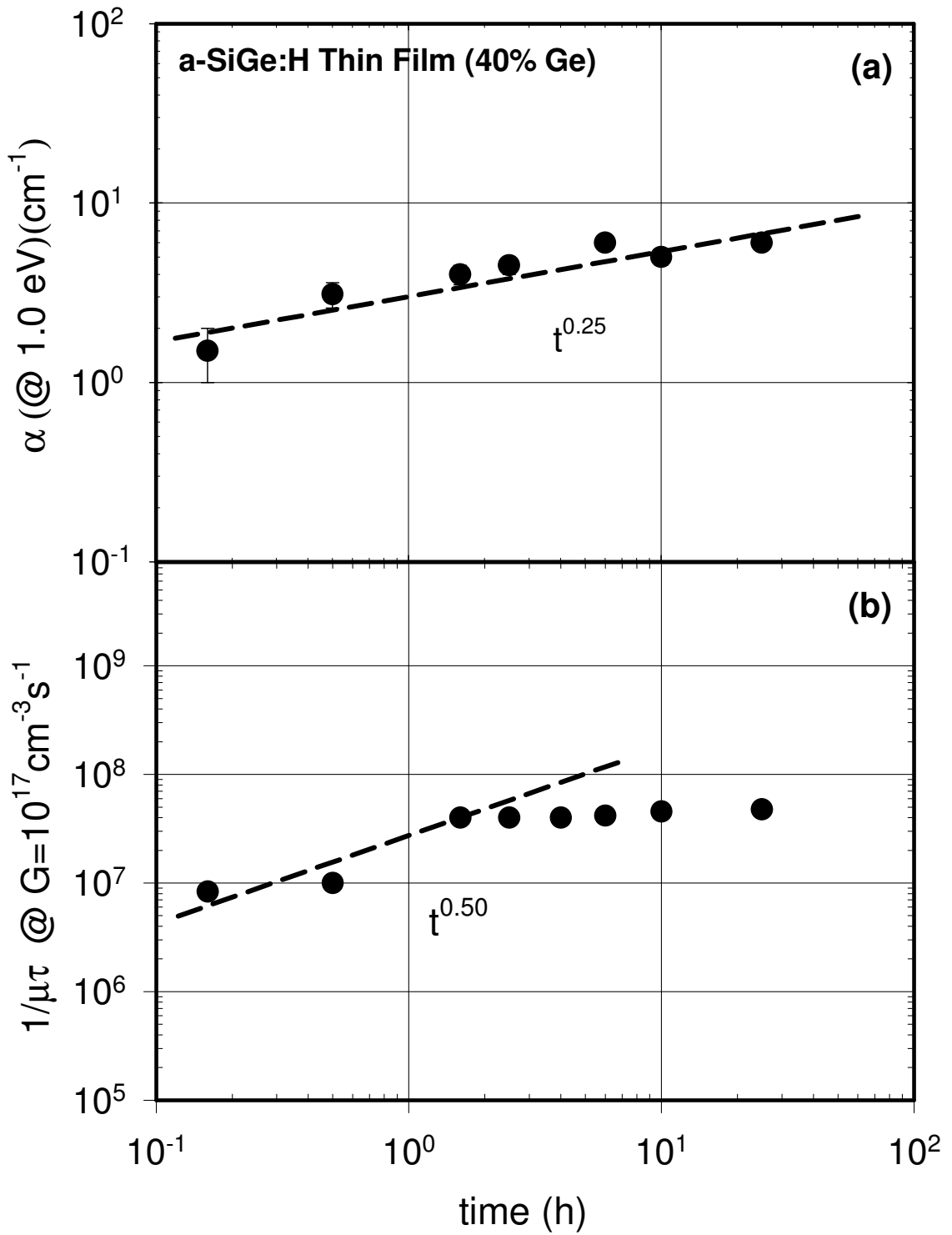
Figure 4.16 a) increase of the sub-bandgap absorption coefficient at 1.0 eV versus degradation time. b) degradation of $1/\mu\tau$ product measured at a generation rate of $10^{17}cm^{-3}s^{-1}$.
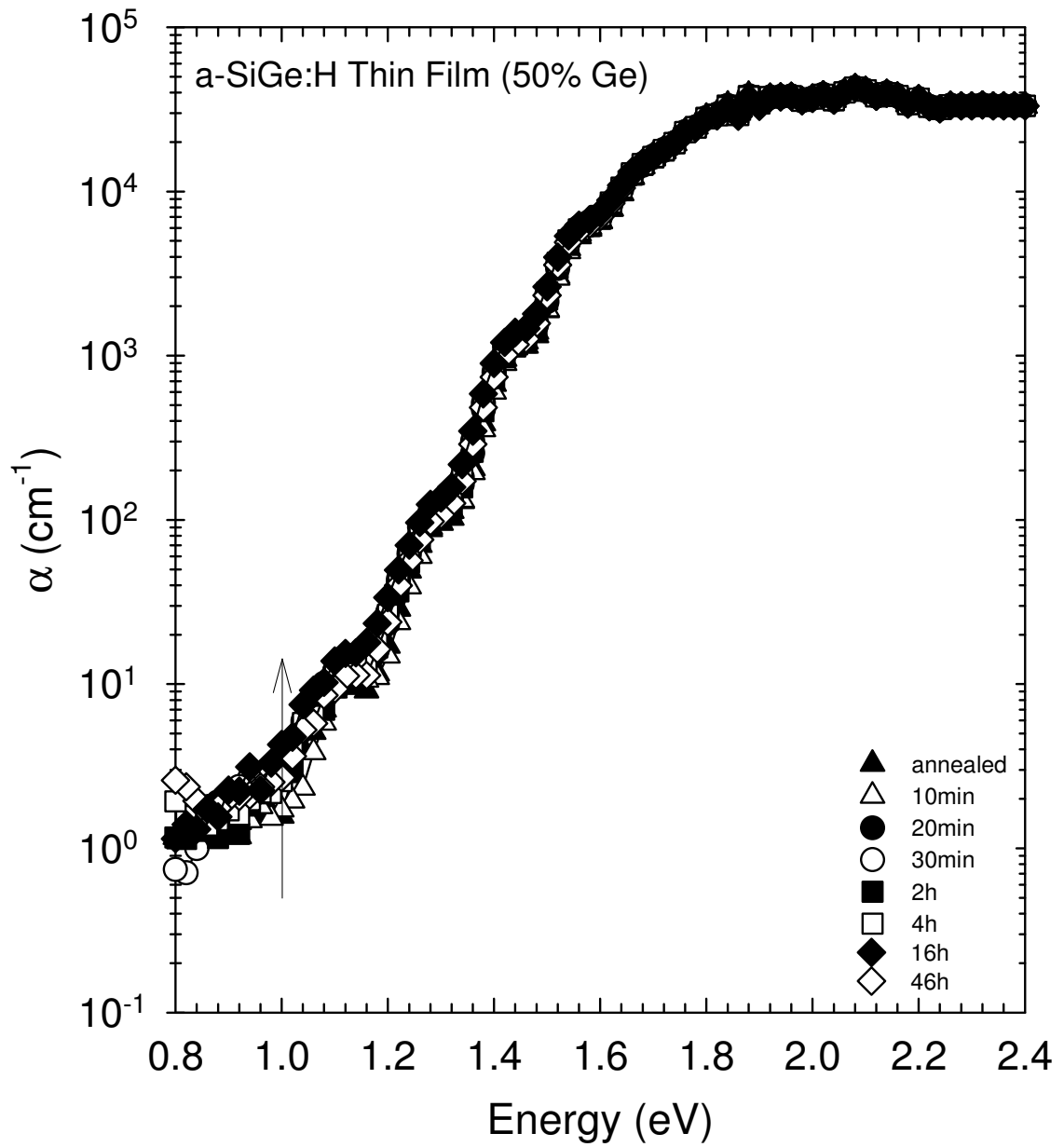
Figure 4.17 Absolute absorption spectrum of the sample with 50% Ge, for various light soaking intervals, calculated from the Y_{DBP} spectrum and simultaneously measured transmission signals.
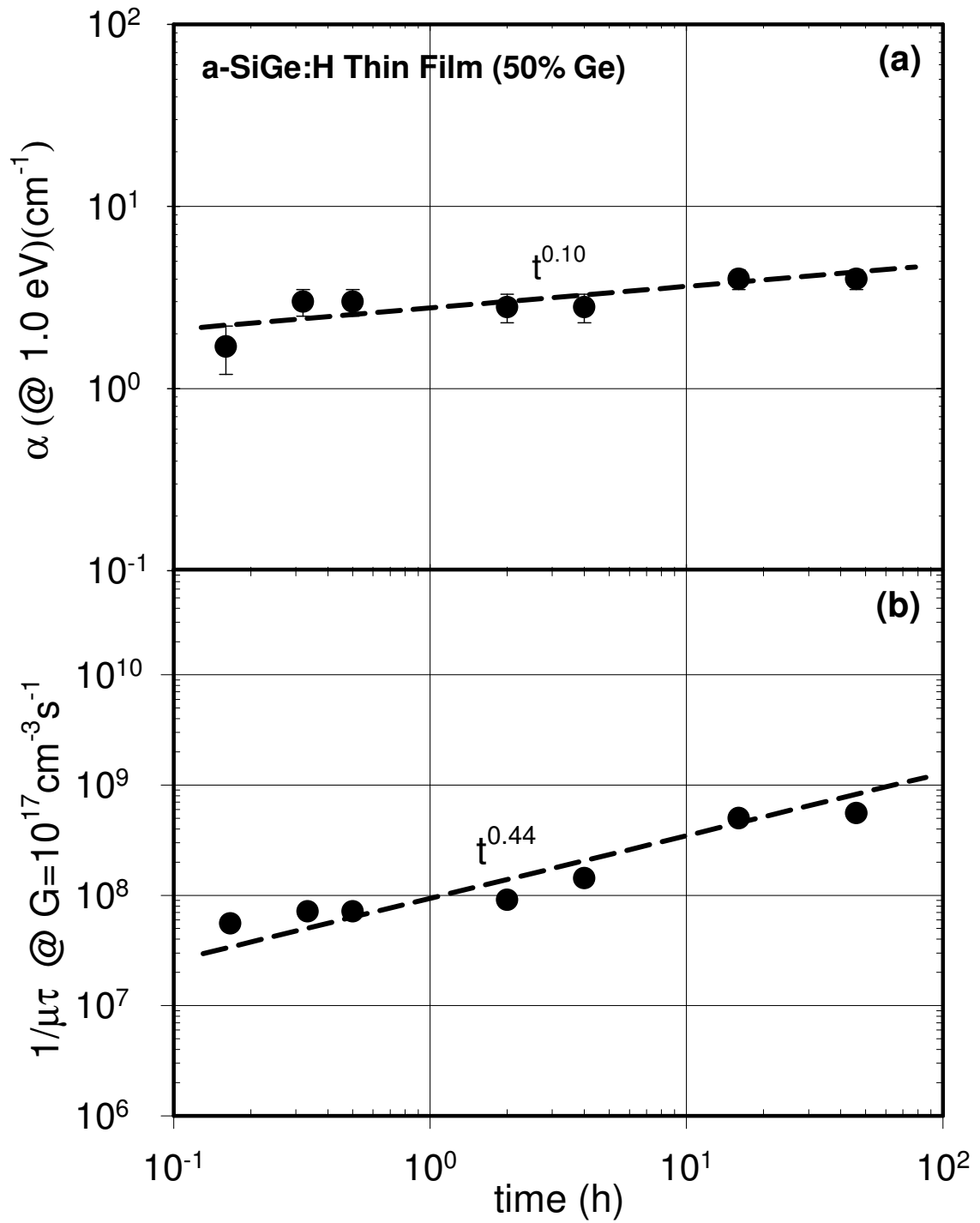
Figure 4.18 a) Increase of the sub-bandgap absorption coefficient at 1.0 eV versus degradation time.

b) degradation of $1/\mu\tau$ product measured at a generation rate of $10^{17}cm^{-3}s^{-1}$.
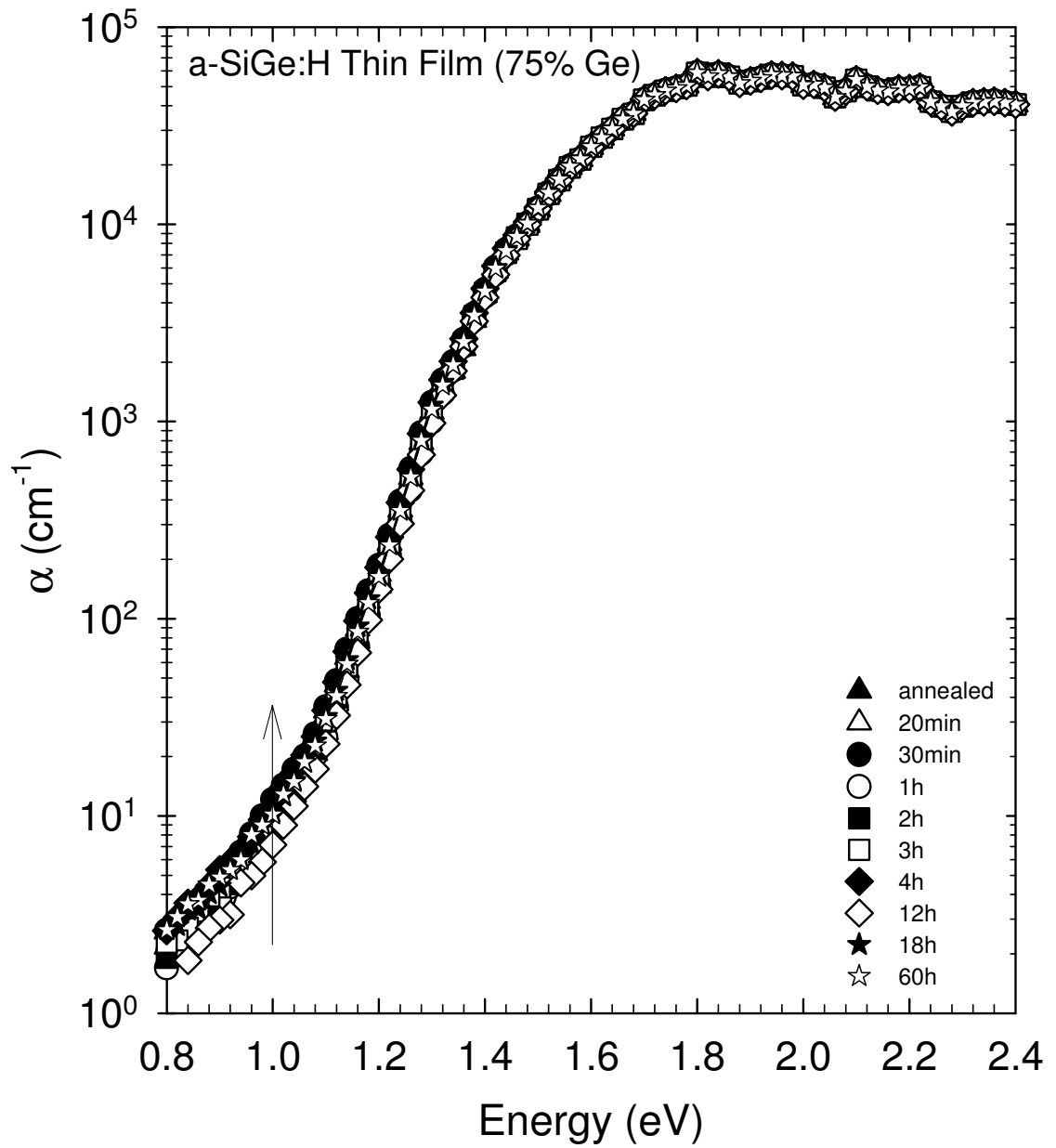
Figure 4.19 Absolute absorption spectrum of the sample with 75% Ge, for various light soaking intervals, calculated from the Y_{DBP} spectrum and simultaneously measured transmission signals.
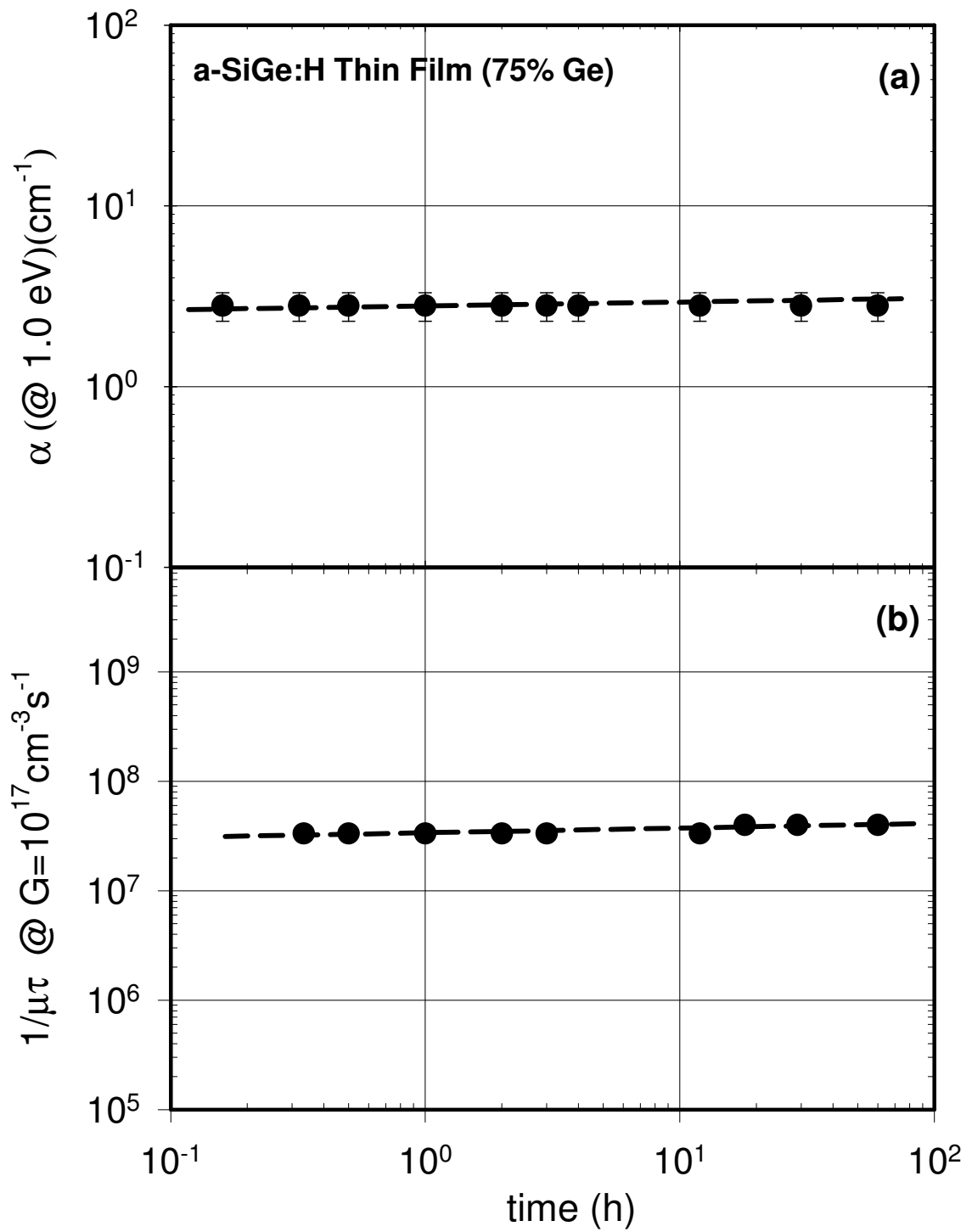
Figure 4.20 a) increase of the sub-bandgap absorption coefficient at 1.0 eV versus degradation time.
b) degradation of $1/\mu\tau$ product measured at a generation rate of $10^{17} cm^{-3} s^{-1}$.

These results together with slopes and $\eta\mu_n\tau_n$ product degradation are presented in Table 4.2. The degradation slope of $\alpha(h\nu)$ and $1/\eta\mu_n\tau_n$ product nare not same for all samples. It can be inferred that subgap absorption and photoconductivity measurements are not controlled by the same set of defects present in the bandgap. In addition, DBP measurements become almost insensitive to detect accurate change in defect density after long time light soaking. For that reason, DBP spectra contain certain degree of inaccuracy due to measurement noise present in soaked state. However, it can be roughly estimated that highest degradation in $\alpha(h\nu)$ is seen in a-Si:H (0% Ge). In alloys 20% Ge film shows the highest degradation in $\alpha(h\nu)$ and the rate decreases as Ge content increases. More careful and detailed experimentation are necessary in subgap absorption measurements in a-SiGe:H alloy films.

Table 4.2 Parameters of degradation kinetics in DBP

Ge%	$\alpha_{sat}/\alpha_{ann}$ @ (1.0eV)	Exponent of Degradation @ α=(1.0eV)	Exponent of Degradation @ $1/\mu_n\tau_n$ (@ G=10^{21})	$\mu_n\tau_{n\,an}/\mu_n\tau_{nsat}$ (@ G=10^{17})
0	2.5	0.33	0.5	375
20	15	0.4	0.36	100
30	5	0.25	0.5	140
40	8.5	0.25	0.5	67
50	4	0.1	0.44	4
75	2	0.01	0.01	3.8

CHAPTER 5

DISCUSSIONS AND CONCLUSIONS

Hydrogenated amorphous silicon germanium alloy thin films of various germanium concentrations are subjected to much interest in the development of high efficiency multi-junction photovoltaic solar cells and other optoelectronic devices where a certain bandgap is necessary. Hydrogenated amorphous silicon germanium alloys (a-SiGe:H) are prepared by alloying a-Si:H with various concentrations of germanium (Ge). By changing the alloy concentration, the electronic and optical properties of hydrogenated amorphous silicon germanium alloys can be turned to match the electronic and optical device requirements. However alloying a-Si:H with Ge introduces an increase in the defect density of the resultant material and also a-SiGe:H material suffers from the Staebler-Wronski effect, the light induced degradation, which is mainly seen in a-Si:H and also in its alloys. The aim of this thesis is to obtain reliable information about the effects of the native and light induced defect states present in a-SiGe:H alloy thin films of various germanium concentrations.

To study the effects of native defects on the opto-electronic properties of a-SiGe:H alloy thin films, samples with varying Ge concentration have been studied. SSPC, DBP and optical transmission measurements have been performed to see the effects of Ge concentration on the majority carrier $\mu_n\tau_n$-products, absolute absorption coefficient at low energies, changes in the optical gap, and the Urbach tail slope, E_{0v}. Absolute absorption coefficient spectrum has been calculated for a-SiGe:H alloy thin films from the DBP yield, Y_{DBP}, and optical transmission spectra. The calculated absolute optical absolute absorption coefficient spectrum of each sample was compared with that of independently measured by PDS .

SSPC method can be used to obtain direct quantitative information about the effect of defect states present the material. Using SSPC measurements, information about the mobility-lifetime product, $\eta\mu_n\tau_n$ – product, of majority carriers is obtained. This is called photosensitivity. It is an important parameter for photoactive semiconductor thin films. In the annealed state, the photoconductivity versus generation rate obeys the well-known non-integer power-law dependence rule, $\sigma_{ph} \propto G^{\gamma}$, for all the

samples. However, a variation occurs in the slope as a major change in the germanium concentration exists. The exponent γ has values between 0.70 – 0.90, indicating a continuous distribution of recombination centers present in films of various germanium concentrations. Majority carrier $\eta\mu_n\tau_n$–products calculated from photoconductivity vs. generation rate values show a decrease as generation rate increase with its characteristic power law, $\mu_n\tau_n \propto G^{\gamma-1}$, implying that more defect states act as recombination centers with increasing generation rate. Both σ_{ph} and $\eta\mu_n\tau_n$-products exhibit the similar functional dependence on the germanium concentration measured at a generation rate of $10^{20} \text{cm}^{-3}\text{s}^{-1}$. $\eta\mu_n\tau_n$-product has a value around 1×10^{-7} cm^2V^{-1} for the reference sample with 0% Ge, which is pure a-Si:H. As Ge% increases, $\eta\mu_n\tau_n$-product increases and peaks at 5×10^{-7} cm^2V^{-1} for 20% Ge a-SiGe:H alloy thin film. It then starts decreasing back to the value of a-Si:H thin film for 40% Ge a-SiGe:H alloy thin film. The decrease in the $\eta\mu_n\tau_n$-product indicates that the density of defect states present in the bandgap of the alloy increases with increasing germanium concentration up to 40%. A further increase of Ge concentration to 50% cause a sharp decrease in the $\eta\mu_n\tau_n$-products indicating a considerable increase in the defect states acting as recombination centers. Finally, for the highest Ge concentration film of 75%, no significant change is detected in the $\eta\mu_n\tau_n$-products. As a conclusion, these results indicate that alloy films with Ge concentration in the range of 10% to 30% have the highest $\eta\mu_n\tau_n$-products for the photogenerated free electrons, which serve as the best photoconductive absorber layer in the multijunction solar cells. For the a-SiGe:H alloys prepared with Ge% above 40% Ge indicate the high level of the recombination centers causing degradation of $\eta\mu_n\tau_n$-products more than an order of magnitude. These results are consistent with those previously reported results in the literature (Finger et al. 1987).

Optical absorption spectrum of thin films is an important parameter to characterize optical and electronic properties of absorber materials. Sub-bandgap absorption spectrum is due to absorption of photons with energies lower than the optical gap of semiconductor. For a-SiGe:H alloy thin films, there are continuous distribution of defect states below the bandgap energies. This was confirmed by the exponent γ value of σ_{ph} as explained above. These defect states consists of exponential valence band tail states originating from the disorder in amorphous network and midgap defect states due to dangling bonds and broken bonds originating from both silicon and germanium atoms. Therefore, electrons excited from these defect states into the

conduction band edge by absorption of low energy photons can be detected by measuring sub-bandgap photoconductivities. The measurements of optical absorption, α (hν), especially in the sub-bandgap region are very important since absorption in that region is related to defect states present in the materials. As the germanium concentration changes, the microstructure and defect distribution of the a-SiGe:H alloy thin films changes substantially. This affects the resulting optical and electronic properties of deposited thin films. The α(hν) spectrum of a-SiGe:H alloy thin films of different Ge concentrations, especially in the sub-bandgap region, is taken as a representation of the defects present in the material. In annealed state, absolute α (hν) spectrum was calculated from the relative DBP and optical transmission spectra and finally compared with those independently measured by PDS method.

For both high and low bias light cases, DBP yield spectrum is directly proportional to the absorbance and thus absorption coefficient. In yield DBP spectrum, there are interference fringes due to multiple reflections of the incoming light on the film and substrate interface. However, there are no interference fringes on the absolute absorption coefficient spectra. Therefore, it is necessary to obtain absorption coefficient spectrum from the Y_{DBP} spectrum without interference fringes. Usually, the fringes have been removed using fast Fourier transform method (Wiedeman et al. 1987) and resulting fringe free Y_{DBP} spectrum is normalized to absolute α(hν) values obtained from T&R or from PDS measurements (Wronski et al. 1982, Gunes and Wronski 1992a). In most cases, Fourier transform process introduces artificial errors in the spectrum for films less than 1 μm and absolute α(hν) obtained from T&R measurement is not reliable for such thin films at normalization energies. Therefore fringe free normalization of Y_{DBP} always introduces a significant degree of errors and accuracy in this process is questioned (Chen et al. 1996). For this reason in this thesis, the fringe free absolute α(hν) spectrum is directly calculated from DBP yield spectrum and transmission spectrum measured on the same sample, using a procedure based on the Ritter-Weiser formula as explained in Chapter 2.

DBP results of the reference sample with 0% Ge in the annealed state exhibits a typical α(hν) spectrum of an amorphous silicon thin film. It is made up of three different regions. The first one is the high energy region due to absorption from the parabolic extended states. The second part is the exponential valence band tail state absorption region which originates from the disorder in the amorphous network. Its

characteristic slope called as the Urbach energy, E_{0v}, shows the degree of disorder. The E_{0v} slope calculated for the a-Si:H film with 0% Ge is 55 meV, which indicates an electronic quality film. The third region in the $\alpha(h\nu)$ spectrum is called sub-bandgap absorption region due to localized defect states in the bandgap of the amorphous sample. The magnitude of $\alpha(h\nu)$ in the low energy part is an integration of all optical transitions from the defect states into the conduction band edge. Therefore, the $\alpha(h\nu)$ at 1.0 eV is taken as a representation to see the level of defect absorption. For hydrogenated amorphous silicon sample, $\alpha(h\nu)$ spectrum of low bias light DBP is around 1.0 cm^{-1}. There is a fine overlap in the absolute $\alpha(h\nu)$ spectrum obtained for both bias light DBP measurements at higher energies, down to the exponential valance band tail state. In low energy region, high bias light $\alpha(h\nu)$ spectrum gives higher values than low bias light $\alpha(h\nu)$ spectrum. There is increase only in the $\alpha(h\nu)$ spectrum at lower energies since there is no change in the occupation of states at higher energies.

As the Ge% increases to 10%, $\eta\mu_n\tau_n$-products were also found to increase. Therefore, 10% Ge a-SiGe:H alloy thin film was thought to have lower defect density than pure a-Si:H film. When subgap absorption spectrum of 10% Ge a-SiGe:H alloy thin film is compared with that of a-Si:H, it is seen that at low bias light DBP spectra, the $\alpha(h\nu)$ values at 1.0 eV has a value around 0.3 cm^{-1}, which is a factor of 3 lower than that of a-Si:H film. It indicates that 10% Ge a-SiGe:H alloy thin film has lower defect density than pure a-Si:H film. For this reason, $\eta\mu_n\tau_n$-products for 10% Ge a-SiGe:H alloy are higher than that of a-Si:H film. However, the slope of exponential valence band tail absorption and energy at $\alpha=10^4$ cm^{-1} are almost the same for a-Si:H and 10% Ge a-SiGe:H alloy thin films. Additionally, the reliability of absolute $\alpha(h\nu)$ spectrum calculated from the DBP spectra are compared with that independently measured by PDS on the same piece of the sample. These results for both PDS and low bias light DBP measurements show that both spectra overlap very well at higher energies above 1.4 eV. However, a difference exists only in the sub-bandgap energies. In this region, PDS spectrum has higher $\alpha(h\nu)$ values by almost a factor of 3. As, in the PDS spectrum, a correction for the substrate absorption has already been taken into account, the difference here is related to the detection of optical transitions from occupied defect states into empty states. In DBP, only transitions to the conduction band are detected. However, PDS detects all transitions to empty states; conduction band, conduction band tail states, and defect states above the midgap. For this reason PDS spectrum results in

higher $\alpha(h\nu)$ values in subgap region. DBP spectrum is more representation of the occupied defect states below the dark Fermi level. As a conclusion, both techniques probe the same distribution of defect states at higher energies and absolute $\alpha(h\nu)$ spectrum of DBP can be reliably used to compare films with different Ge concentrations.

As Ge concentration increases to 20%, $\eta\mu_n\tau_n$-products show the highest values. The slope of the exponential valence band tail absorption is 53 meV indicating good quality film and energy at $\alpha=10^4 cm^{-1}$ decrease from 1.90 to 1.86 eV. Absolute $\alpha(h\nu)$ at 1.0 eV for the low bias light DBP spectrum is around 0.2 cm^{-1}, lower than that of 10% Ge a-SiGe:H alloy. It means that 20% Ge alloy has lower defect density than 10% Ge alloy film. The $\alpha(h\nu)$ spectra calculated from DBP results are similarly compared with that obtained from the PDS measurements. A perfect overlap of two spectra at higher energies can be seen at higher energy part of spectrum similar to that found in 10% Ge sample. A similar difference is found in the low energy part of spectrum. In this case, PDS is a factor of 10 higher than 10% Ge film. This could be due to higher surface defects that PDS is very sensitive to in 20% Ge film.

A further decrease in Ge% starts to degrade $\eta\mu_n\tau_n$-products. The slope of exponential tail absorption are 55meV and 53meV for 30% Ge and 40% Ge alloy film, which are similar to previous samples. The energy at $\alpha=10^4 cm^{-1}$ decreases to 1.80eV for 30% Ge and to 1.75eV for 40% Ge, showing the effect of Ge, which decrease the bandgap of the alloy. Corresponding effect on defect states is monitored on the $\alpha(h\nu)$ at 1.0 eV. It increases from 0.2 cm^{-1} to 0.5cm^{-1} as Ge increase from 20% to 30% and it is around 0.6 cm^{-1} for 40% Ge alloy. This slight increase in the $\alpha(1.0eV)$ indicate an increase in defect density as Ge concentration increases from 20% to 40% and these results are consistent with slight decrease found in $\eta\mu_n\tau_n$-products of same samples. In addition, for both samples, PDS measurements show a perfect agreement with that of DBP as previous samples.

Increasing Ge concentration above 40% causes a decrease in $\eta\mu_n\tau_n$-products drastically. The alloys prepared at 50% Ge and 75% Ge have been characterized in a similar way using the same measurements. The energy gap at $\alpha=10^4 cm^{-1}$ decrease to 1.64eV for 50% Ge and to 1.46eV for 75% Ge sample. The characteristic Urbach energy, E_{0v}, also increases to 60meV for both samples, indicating higher disorder in these highly Ge content samples. The defect absorption at 1.0 eV increases substantially

to 2 cm^{-1} for 50% Ge film. For 75% Ge film, the $\alpha(h\nu)$ at 0.9 eV is taken to be away from the exponential absorption edge since bandgap decreased substantially for 75% Ge film. The $\alpha(0.9eV)$ is around 6 cm^{-1}, which is the highest among other films. It indicates that high Ge content films have higher defect states in the bandgap, which cause a sharp degradation in electron lifetime τ_n, as measured from photoconductivity measurements.

As a summary of the sub-bandgap absorption results, low bias light DBP spectrum of alloy films with different Ge content indicates a systematic decrease in the bandgap with increasing Ge content as the energy at $\alpha=10^4$cm^{-1} is taken as a reference. It decreases from 1.90eV for a-Si:H to 1.46 eV for 75% Ge alloy film. The E_{0v} values are almost constant around 55meV for alloying up to 40% Ge. It increases to 60 meV for 50% and 75% Ge films. Finally the changes in the defect density present in the bandgap of alloy films are inferred from the sub-bandgap absorption coefficient at low energies.

The $\alpha(1.0eV)$ measured by both PDS and low bias light DBP spectrum show a difference between PDS and low bias DBP spectra. For low Ge% alloy films, this difference is around a factor of 2 to 10. For highly defective samples, both spectra are closer together. These higher values are consistent with the nature of PDS technique. Such that it probes all the optical transitions into empty states but DBP probes only those to the conduction band. But for some samples, surface layer could be more defective and this will add up additional surface absorption in PDS measurements. This surface absorption is not detected in DBP measurements since it only probes the low defect density region in the bulk of the sample. Low bias light DBP results at 1.0 eV show a better dependence on Ge concentration. Beginning from 0% Ge a-Si:H, $\alpha(1.0eV)$ decreases as Ge content increases to 20% Ge and give a minimum around 0.2 cm^{-1}. It then starts increasing with increasing Ge content. The best film with lowest defect density can be prepared with alloying Ge in the range from 10% to 40% Ge. Increasing Ge content can result in lower bandgap absorber layer for infra red part of solar spectrum in multi-junction solar cells; however, it results in a substantial increase in defect density and a sharp reduction of free carrier lifetime.

Another aspect of this study has been to investigate the kinetics of Staebler Wronski Effect (SWE) on various a-SiGe:H alloys with different Ge content. The effects of different intervals of white light illumination on the SWE has been investigated by looking at degradation in SSPC and increase in the sub-band gap

absorption coefficient obtained from DBP measurements. Kinetics of defect creation for different germanium contents has also been compared with those present in unalloyed hydrogenated amorphous silicon films (a-Si: H). It is known that illumination with intense light leads to the creation of additional metastable states in the mobility gap of a-Si:H known as the Staebler–Wronski Effect (Staebler and Wronski 1977) This effect is also observed in hydrogenated amorphous silicon germanium alloy thin films (Cohen 2003 and references therein). In this study, the Staebler-Wronski effect of intrinsic a-SiGe:H alloy thin films with different Ge concentrations were investigated using the steady-state photoconductivity and DBP techniques to understand the effect of Ge content on the kinetics of defect creation on mobility-lifetime product and low energy sub-bandgap absorption coefficients using a 15 suns of white light illumination.

Hydrogenated amorphous silicon sample is the reference sample in these measurements. Photoconductivity and mobility-lifetime product versus generation rate plots have been measured for various light soaking durations for this sample. A decrease of more than two orders of magnitude is seen in photoconductivity at the generation rate of 10^{21}cm^{-3}s^{-1}. The exponent γ is around 0.90, not showing a change in light soaked state. The relation $t^{-0.33}$ is the reported degradation behavior in literature (Stutzmann et al 1989) for a-Si:H films. However, for generation rates of 10^{21}cm^{-3}s^{-1} and 10^{17}cm^{-3}s^{-1} time dependence of degradation in this sample shows of $t^{-0.50}$ rule. This indicate that there is no $t^{1/3}$ unique rule for degradation of photoconductivity in a-Si:H films as consistent with reported results by Gunes and Wronski (Gunes and Wronski 1997). The magnitude of degradation of $\eta\mu_n\tau_n$ product at G=10^{21}cm^{-3}s^{-1} is 250 times and at G=10^{17}cm^{-3}s^{-1} is 350 times.

As the Ge% increases to 20%, the Staebler-Wronski effect is clearly seen in the magnitude of σ_{ph}. The exponent γ is around 0.90 for both annealed and light soaked states. The slope of degradation is -0.60 for both generation rates of G=10^{21}cm^{-3}s^{-1} and G=10^{17}cm^{-3}s^{-1} and it is higher than pure a-Si:H sample with 0% Ge. It means that Ge added alloys degrade faster in time. Similarly the degradation experiments for different light soaking periods have been performed for other alloy thin films having different Ge contents such as 30% Ge, 40% Ge, 50% Ge and 75% Ge. All exhibit certain degree of degradation in the magnitude of σ_{ph} and $\eta\mu_n\tau_n$ products. The exponent γ is around 0.8-0.90 in the soaked state. But for 75% Ge sample, it is lower in the annealed state. It is around 0.74 and does not change in the soaked state. Among, the samples unalloyed a-

Si:H film shows the highest degradation in $\eta\mu_n\tau_n$ products. As Ge content increases, the rate decreases. The alloy with 20% Ge shows the highest degradation from annealed state to the saturated state by a factor of 100. The rate decreases as Ge content increases. For 50% Ge and 75% Ge, $\eta\mu_n\tau_n$ product degradation is very low by factor of 4 and 3, respectively. The rates also show the similar trend. The 20% Ge alloy degrades the fastest by the slope of -0.6. It is -0.45 and -0.3 for 30% Ge and 40% Ge alloy films and extremely small for 50% Ge and 75% Ge samples. It can be inferred that alloying improves the $\eta\mu_n\tau_n$ product up to 40% Ge and degradation is also slower than it is for pure a-Si:H film. As the saturated values for $\eta\mu_n\tau_n$ products are compared, alloys with 20% Ge to 40% Ge are still much higher than pure a-Si:H film. Degradation of $\eta\mu_n\tau_n$ products obtained from the SSPC indicates that new defects are created by light to decrease the lifetime τ_n of free carriers. However, only qualitative estimation about these defect states can be made by comparing the absolute change in $\eta\mu_n\tau_n$ products of the samples.

The Staebler-Wronski effect is also directly seen in the change of sub-badgap absorption coefficient at lower energies. The increase in the $\alpha(h\nu)$ in the lower energy part of the spectrum is direct indication of increase of defect states in the bandgap of samples, which also cause degradation of $\eta\mu_n\tau_n$ products. It is seen that only low energy part of $\alpha(h\nu)$ changes after light soaking. No change in the exponential absorption edge and higher energy part is detected. Therefore, only defects causing the recombination of free carriers are created by light. No effect is detected in the disorder. The samples were light soaked for different light soaking periods and after each period, the DBP spectra were measured and absolute absorption coefficient spectra were calculated. In order to see the degradation of $\alpha(h\nu)$, the $\alpha(h\nu)$ at 1.0 eV is taken and plotted as a function of time. DBP spectra for the sample with 0% Ge (pure a-Si:H).roughly obeys to $t^{1/3}$ rule as proposed by Stuttzmann et al (Stuttzmann et al 1989). However the change in $1/\eta\mu_n\tau_n$ product measured at low generation rate shows totally different time dependence. Even tough both measurements were done at similar generation rates, $\alpha(h\nu)$ degradation and $\eta\mu_n\tau_n$ product degradation are not controlled by the same distribution of defect states. This type of behavior was reported previously in detail by Gunes and Wronski (Gunes and Wronski 1997).

As Ge% increases, σ_{ph} degradation becomes slower in alloys. In the subgap absorption spectrum of 20% Ge alloy films, the degradation in $\alpha(h\nu)$ at 1.0 eV obeys to

$t^{0.40}$ relation. It is slightly higher than that of a-Si:H film. Corresponding time dependence of $1/\eta\mu_n\tau_n$ product is 0.36 and closer to that of $\alpha(h\nu)$ degradation. Similar degradation process has been measured for other higher Ge% alloy samples. However, the rate of $\alpha(h\nu)$ at 1.0 eV decreases as Ge% increases for alloy samples with 30% Ge, 40% Ge, 50% Ge and 75% Ge. The slope of $\alpha(h\nu)$ is 0.25 for 30% Ge and 40% Ge alloy films, and it is 0.1 for 50% Ge and almost 0 for 75% Ge sample. These results indicate that higher Ge content films show almost no degradation in sub-bandgap absorption. This is also consistent with σ_{ph} degradation results presented above. In degradation of $\alpha(h\nu)$, the ratio of α_{sat}/α_{an} at 1.0 eV is taken for comparison. The ratio is 2.5 for 0% Ge film. It is 15 for 20% Ge, which is the highest. It decreases to around 8 for 30% Ge and 40% Ge films, to 4 and 2 for 50% Ge and 75% Ge films, respectively.

The degradation slope of $\alpha(h\nu)$ and $1/\eta\mu_n\tau_n$ product are not same for all samples. It can be inferred that subgap absorption and photoconductivity measurements are not controlled by the same set of defects present in the bandgap. In addition, DBP measurements become almost insensitive to detect accurate change in defect density after long time light soaking. For that reason, DBP spectra contain certain degree of inaccuracy due to measurement noise present in soaked state. However, it can be roughly estimated that highest degradation in $\alpha(h\nu)$ is seen in a-Si:H (0% Ge). In alloys 20% Ge film shows the highest degradation in $\alpha(h\nu)$ and the rate decresaes as Ge content increases. More careful and detailed experimentations are necessary in subgap absorption measurements in a-SiGe:H alloy films.

5.1 Future Proposed Research

In this thesis a-SiGe:H alloy thin films of various Ge% have been investigated in both annealed and light soaked states by using SSPC, DBP, transmission spectroscopy and PDS methods. However, in the light soaked state experiments, DBP measurements become almost insensitive to detect accurate change in defect density after long time light soaking. Consequently, because in light soaked state there is noise present in the measurement, DBP spectra contain certain degree of inaccuracy. Therefore more in depth experimentations are necessary in subgap absorption measurements in a-SiGe:H alloy films.

REFERENCES

Aljishi, S., Smith, Z.E. and Wagner, S. 1989. Amorphous Silicon and Related Materials edited by Fritzsche H. p. 887.

Amer, N.M., Skumanich, A. and Jackson, W.B. 1983. Physica 117&118B, p. 897.

Bullot, J., Galin, M., Gauthier, M., Bourdon, B. 1983. "Electronic Properties of Hydrogenated Amorphous Silicon-Germanium Alloys", Journal de Physique. Vol. 44, No. 6, p. 713.

Carius, R., Stiebig, H., Siebke, F., Fölsch, J. 1998. "Defect Distributions in a-SixGe1-x:H", Journal of Non-Crystalline Solids. Vol. 227, p.432.

Chapman, B.D., Han, S.W., Seidler, G.T., Stern, E.A., Cohen, J.D., Guha, S., Yang, J. 2002. "Short Range Compositional Randomness of Hydrogenated Amorphous Silicon–Germanium Films", Journal of Applied Physics. Vol. 92, No. 2, p. 801.

Chen, L., Tauc. J., Lee, J. K., Schiff, E. A. 1991. "Defects in Hydrogenated Amorphous Silicon Germanium Alloys Studied by Photomodulation Spectroscopy", Physical Review B. Vol. 43, No. 34.

Chen, I.S., Jiao, L., Collins, R.W. and Wronski, C.R. 1996. "A Novel Approach to the Analysis of Sub-bandgap Absorption in a-Si:H Based Materials", J.Non.Cryst. Solids. Vol. 198-200, p. 391.

Cody, G.D. edited by Pankove J.I. 1984. Semiconductors and Semimetals. Vol. 21B, p. 11.

Cody, G.D., Wronski, C.R., Abeles, B., Stephens, R. and Brooks, B. 1980. Solar Cells. Vol. 2, p. 227.

Cohen, J. D. 2003."Light-induced Defects in Hydrogenated Amorphous Silicon Germanium Alloys, "Solar Energy Materials & Solar Cells. Vol. 78, p. 399.

Cohen, J.D. in T. Searle (Ed.), "Properties of Amorphous Silicon and its Alloys", EMIS Datareview Series No. 19, INSPEC, London, 1998, pp. 180.

Cohen, J.D. 1998. "Identifying Electronic Properties Relevant to Improving Stability in a-Si:H-Based Cells and Overall Performance in a-Si,Ge:H-Based Cells", NREL/SR-520-25802.

Cohen, J.D. 2002. "Identifying Electronic Properties Relevant to Improving the Performance and Stability of Amorphous Silicon Based Mid-Gap and Low-Gap Cells", NREL/SR-520-32535.

Dersch, H., Stuke, J., Beichler, J. 1981. "Light-induced Dangling Bonds in Hydrogenated Amorphous Silicon", Applied Physics Letters. Vol. 38, No. 6, p. 456.

Finger, F. and Beyer, W. 1997. "Growth of a-Si:Ge:H Alloys by PECVD - Gas Sources, Conditions in the Plasma and at the Interface in Properties of Amorphous Silicon and its Alloys", emis Datareview Series 19, ed. T. Searle p. 20.

Finger, F. and Beyer, W. 1997. "Growth of a-Si:Ge:H Alloys by PECVD - Optimisation of Growth Parameters, Growth Rates, Microstructure and Material Quality in Properties of Amorphous Silicon and its Alloys", emis Datareview Series 19, ed. T. Searle p. 30.

Finger, F., Fuhs, W., Beck, G., Carius, R. 1987. "Defect States in a-Si1−xGex:H Studied by Electron Spin Resonance", Journal of Non-Crystalline Solids. Vol. 97, p. 1015.

Fritzsche, H., Stradins, P., Belomoin, G. 1996. "Temperature Dependence of the Photoconductivity and the Near Absence of Light-Induced Defects in a-Si$_x$Ge$_{1-x}$:H", Amorphous Silicon Technology; Materials Research Society Symposium Proceedings. Vol. 420, pp. 563.

Fuhs, W. and Finger, F. 1989. "Defects and Recombination in a-Si:1−xGex:H", Journal of Non-Crystalline Solids. Vol. 114, Part 2, p. 387.

Goodman, N.B. 1982. "Effect of Annealing and Light Exposure on the Field-Effect Density of States in Glow-Discharge Hydrogenated Amorphous Silicon", Philos. Mag. B. Vol. 45, p. 407.

Grunewald, M., Weber, K., Funs, W. and Thomas, P. 1981. Journal Phys.Colloq. Vol. 42, C4-523.

Guha, S., Payson, J.S., Argawal, S.C. and Ovshinsky, S.R. 1987. "Fluorinated Amorphous Silicon-Germanium Alloys Deposited from Disilane-Germane Mixture", Journal of Non-Crystalline Solids. Vol. 97-98, p. 1455.

Guha, S., Yang, J., Jones, S.J., Yan Chen, Williamson, D.L. 1992. "Effect of Microvoids on Initial and Light-Degraded Efficiencies of Hydrogenated Amorphous Silicon Alloy Solar Cells", Applied Physics Letters. Vol. 61, No. 12, p. 1444.

Gunes, M. and Wronski, C.R. 1992. "Differences between light induced and native midgap states in intrinsic hydrogenated amorphous silicon obtained from detailed modeling of photoconductivities and subband-gap apsorption", Appl. Phys. Lett.Vol. 61, p. 678.

Gunes, M. and Wronski C.1997. "Differences in the Densities of Charged Defect States and Kinetics of Staebler-Wronski Effect in Undoped (Nonintrinsic) Hydrogenated Amorphous Silicon Thin Films", J. Appl. Phys. Vol.81, p. 8.

Hirabayashi, I., Morigaki, K., Nitta, S. 1980. Jpn. Journal of Applied Physics. Vol 19, L357.

Jackson, W.B. and Amer, N.M. 1982. "Direct Measurement of Gap-State Absorption in Hydrogenated Amorphous Silicon by Photothermal Deflection Spectroscopy", Phys. Rev. B. Vol. 25, p. 5559.

Kolodzey, J., Aljishi, S., Smith, Z.E., Chu, V., Schwarz, R., Wagner, S. 1986. "Measurements of Light-Induced Degradation in a-Si,Ge:H,F Alloys", Materials Issues in Amorphous-Semiconductor Technology Symposium. p. 237.

Kroesen, G.M.W., Oehrlein., G.S., de Frésart., E., Scilla., G.J., 1992. "Refractive Index Determination of SiGe Using Reactive Ion Etching/Ellipsometry: Application for the Depth Profiling of the Ge Concentration", Applied Physics Letters.Vol. 60, p. 1351.

Lang, D.V., Cohen, J.D., Harbison, J.P., Sergent, A.M. 1982. "Observation of Photoinduced Changes in the Bulk Density of Gap States in Hydrogenated Amorphous Silicon", Applied Physics Letters. Vol. 40, No. 6, p. 474.

Lee, S., Kumar, S., Wronski, C.R. and Maley, N.M. 1989. J. Non Cryst. Solids. Vol. 114, p. 316.

Mackenzie, K.D., Eggert, J.R. , Leopold D.J., Li, Y.M., Lin, S., William, P. 1984. "Structural, Electrical, and Optical Properties of a-Si1-xGex:H and an Inferred Electronic Band Structure", Physical Review B. Vol. 31, p. 2198.

Matsuda, A., Yagii, K., Koyama, M., Toyama, M., Imanishi, Y., Ikuchi, N. and Tanka, K. 1985. "Preparation of Highly Photosensitive Hydrogenated Amorphous Si-Ge Alloys Using a Triode Plasma Reactor", Applied Physics Letters. Vol. 47, No. 10, p. 1061.

Michelson, C.E., Gelatos, A.V., Cohen, J.D. 1985. "Drive-Level Capacitance Profiling: Its Application to Determining Gap State Densities in Hydrogenated Amorphous Silicon Films," Applied Physics Letters. Vol. 4, No. 4, p. 412.

Morin, P.A., Wang, N.W., Wagner, S. 1992. "Optimization of the Deposition Conditions for High-Gap a-Si,Ge:H,F Alloys", Amorphous Silicon Technology Symposium. pp. 577.

Nakamara, G., Sato, K., Yukimoto, Y., 1983. Solar Cells. Vol. 9, p. 75

Nebel, C.E., Weller, H.C., Bauer, G.H. 1988. "Extended State Mobility and Tail State Distribution of a-Si1-xGex:H Alloys", Amorphous Silicon Technology Symposium. p. 507.

Pankove, J.I. and Berkeyheiser, J.E. 1980. "Light-induced Radiative Recombination Centers in Hydrogenated Amorphous Silicon", Applied Physics Letters. Vol. 37, No. 8, p. 705.

Paula, W., Chenb, J.H., Liua, E.Z., Wetsela A.E., Wickboldta, P. 1993. "The Mott Lecture. Structural and Electronic Properties of Amorphous SiGe:H Alloys", Journal of Non-Crystalline Solids. Vol. 164, p. 1

Ranganathan, R., Gal, M., Viner, J.M., Taylor, P.C. 1987. "Photoluminescence in a-Si1-xGex:H Alloys", Physical Review B. Vol. 35, p. 9222.

Ritter, D. and Weiser, K. 1986. Opt. Commun. Vol. 57, p. 336.

Schumm, G., Abel, C.D., Bauer, G.H. 1992. "Defect Kinetics and Saturation in Amorphous Silicon-Germanium Alloys", Amorphous Silicon Technology Symposium. 1992, pp. 505

Sheng, S.R., Braunstein, R., Dalal, V.L. 2001. "Electrical and Optical Properties of High Quality Low Bandgap Amorphous (Ge,Si) Alloys", Material Research Society Symposium Proceeding. 664, pp. A8.4.

Staebler, D.L. and Wronski, C.R. 1977. "Reversible Conductivity Charge in Discharge-Produced Amorphous Si", Applied Physics Letters.Vol. 31, No. 2, p. 292.

Street, R.A., Tsai, C.C., Stutzmann, M., Kakalios, J. 1987. "The Role of Dangling Bonds in the Transport and Recombination of a-Si:Ge:H Alloys", Philosophical Magazine B. Vol. 56, No.3, pp. 289.

Stutzmann, M., R.J. Nemanich, Stuke, J. 1984. "Electron-Spin-Resonance Study of Boron-Doped Amorphous SixGe1-x: H Alloys", Physical Review B. Vol. 30, p. 3595.

Stutzmann, M., Street, R.A., Tsai, C.C., Boyce, J.B., Ready, S.E. 1989. "Structural, Optical, and Spin Properties of Hydrogenated Amorphous Silicon-Germanium Alloys", Journal of Applied Physics. Vol. 66, No. 2, p. 569.

Swanepoel, R. 1983. J. Phys. Vol. E 16, p. 1214.

Unold, T. 1994. "The Role of the Band Gap in the Light-Induced Degradation of Amorphous Silicon Alloys", Amorphous Silicon Technology Symposium 1994. pp. 287.

Unold, T., Cohen, J.D., Fortmann, C.M. 1994. "Electronic Mobility Gap Structure and Deep Defects in Amorphous Silicon-Germanium Alloys", Applied Physics Letters. Vol. 64, No. 13 , p. 1714.

Vanecek, M., Kocka, J., Poruba, A. and Fejfar, A. 1995. J. Appl. Phys. Vol.78, p. 6203.

Wagner, S., Xu, X., Li, X.R., Shen, D.S., Isomura, M., Bennett, M., Delahoy, A.E., Li, X., Arch, J.K., Nicque, J.L. and Fonash, S.J. IEEE Photovoltaic Specialists Conference. p.1307.

Wang, N.W., Morin, P.A., Chu, V., Wagner, S. 1992. "Defect Saturation in a-SiGe:H(F) Alloys", Amorphous Silicon Technology Symposium. pp 589.

Web_1, 2003. Coating Theory website, 21 November 2005. http://www.mellesgriot.com/products/optics/oc_2_2.htm

Wickboldt, P., Pang, D., Paul, W., Chen, J.H., Fan Zhong, Chih-Chiang Chen, Cohen, J.D., Williamson, D.L. 1997. "High Performance Glow Discharge a-Si1-xGex:H of Large x", Journal of Applied Physics. Vol. 81, No. 9, p. 6252.

Wiedeman, S., Bennett, M.S. and Newton, J.L. 1987. Mat. Res. Soc. Symp. Proc.Vol. 95, p. 145.

Wronski, C.R., Abeles, B., Tiedje, T. and Cody, G.D. 1982. "Recombination Centers in Phosphorous Doped Hydrogenated Amorphous Silicon", Solid State Communications. Vol. 44, No. 10, p. 1423.

Wronski, C.R., Smith, Z.E., Aljishi, S., Chu, V., Shepard, K., Shen, D.S., Schwarz, R., Slobodin, D., Wagner, S. 1987. AIP Conf. Proc. Vol.157, p. 70.

Yang, J., Banerjee, A., Guha, S., 1997. "Triple-Junction Amorphous Silicon Alloy Solar Cell with 14.6% Initial and 13.0% Stable Conversion Efficiencies", Applied Physics Letters. Vol. 70, No. 22, p. 2975.

APPENDIX A

Computer Program for
Sub-bandgap Absorption Measurement

```
start:
graphcomment$="Comments about the graph "
sensflag=0
timeflag=0.3
oldflag=0.3
E3msec=1.4
E1sec=1.2
E3sec=1.1
E10sec=1.0
E30sec=0.9
dim par(5)
dim standdev(50)
dim angldev(50)
dir$="D:\data2004\elif\"
input "sample name",sampname$
filecomment$=sampname$

rem ********************************
input "data file name",dbs$
format #1,energy["energy=","eV"],average["average
current=","A"],avgdevia["angle=",""],ratio["dc/ac=",""],absorp["absorp. coeff.=",""]
format #2,energy["energy=","eV"],curr[" current=","a"],avgdevia["angle=",""]
rem logaritmik graph file
format #3,energy["energy=","eV"],Logaverage["average
current=","A"],avgdevia["angle=",""],Logratio["dc/ac=",""],Logabsorp["absorp.
coeff.=",""]
open #1, file= dir$+dbs$+".dat",desc$,overwrite
rem open #1, file= dbs$+".dat",desc$,overwrite
open #2, file= "v"+dbs$+".dat",desc$,overwrite
open #3, file= "graph_f.dat",desc$,overwrite
open #3, graph= "dualbeam",overwrite
open #3, screen
rem ********************************
input "first value of energy",start
input "step value for energy",step
input "input number of measurements for each energy",n
input "enter dc current dueto bias light(format 1e-5 )",dcac
input "enter time constant(sec)[0.3 recommended]",tc
rem -----------------------------
rem ---------------------------
rem ****************************************
rem flux file is to be read into y variable **
rem ****************************************
```

```
gosub fluxRead
rem include"fx070502"
rem*****************************************
gpibwrite(8,"OUTX 1,OVRM 1")
gpibwrite(8,"*RST")
gpibwrite(8,"*CLS")
gpibwrite(8,"FMOD 0")
gpibwrite(8,"DDEF 1,1,0")
gpibwrite(8,"DDEF 2,1,0")
gpibwrite(8,"ICPL 0")
gpibwrite(8,"ISRC 2")
gpibwrite(8,"OFSL 3")
gpibwrite(8,"IGND 1")
rem gpibwrite(8,"SENS 23")
gpibwrite(8,"SYNC 1")
gpibwrite(8,"OFLT 9")
gpibwrite(8,"AGAN")
gosub delay4

gosub delay4
gpibwrite(8,"ARSV")
gosub delay4
gosub delay4
gpibwrite(8,"APHS")
gosub delay4
gosub delay4
gosub delay4
gpibwrite(8,"RMOD 1")
gosub delay4
gosub delay4
gosub delay4
rem
energy=start
wl=6200/energy

fark=(2.5-start)
fark=fark/(0.02)
bbb$=str$(fark)
z=val(mid$(bbb$,1,2))

loop:
sum=0
dvsum=0
r=0
z=z+1
rem *******************************


loopa:
r=r+1
```

```
gpibwrite(8,"OUTR? 1")
a$=gpibread$(8)
gpibwrite(8,"OUTR? 2")
j$=gpibread$(8)
curr=val(mid$(a$,1))
standdev(r)=curr
? "current=",curr," A"
devia=val(mid$(j$,1))
angldev(r)=devia
? devia
sum=sum+curr
dvsum=dvsum+devia


rem *************
rem **veri dat****
write #2
rem loopb:
rem sd1=(curr-average)**2
rem sd1=sd1+(curr-average)**2
rem sd=sqrt(sd1/n)
rem ? "Standart deviation=",sd
rem absorp=average/y(z)
rem ? y(z)
rem write #1



if timeflag=0.3 then gosub delay3msec
if timeflag=1 then gosub delay1sec
if timeflag=3 then gosub delay3sec
if timeflag=10 then gosub delay10sec
if timeflag=30 then gosub delay30sec
rem if energy<=1 and energy>=0.8 then gosub measnum
rem if energy<0.8 then gosub measnum1

rem ***********************

if r<n then goto loopa

average=sum/n
avgdevia=dvsum/n
rem ***********************************

b$=str$(wl)
wv=val(mid$(b$,1,5))
realw=2*wv
rem ? avgdevia
rem ? wv
rem ? z
rem ? "Average for",energy," eV(",realw,"A)=",average," A"
ratio=dcac/average
```

```
absorp=average/y(z)
Logabsorp=0.43429489*log(absorp)
Logaverage=0.43429489*log(average)
Logratio=0.43429489*log(ratio)
rem ? "Current/flux for",energy," eV=",absorp

write #1
write#3
if z=94 then goto bitti
rem   gosub kontrol

energy=energy-step
wl=6200/energy
rem ------------------------------------
c$=str$(wl)
wk=val(mid$(c$,1,5))
filterw=2*wk
kf=wk-wv
d$=str$(kf)
rem ------------------------------------
kw=0.5*kf
f$=str$(kw)
wt=val(mid$(f$,1,3))
i$=str$(wt)
rem ----------------------
kg=0.3*kf
g$=str$(kg)
wy=val(mid$(g$,1,3))
rem ? wy
h$=str$(wy)
rem ------------------------------
 if energy=1.86 then gosub ttl
 if energy=1.36 then gosub ttl
 if energy=1.0 then gosub ttl
gosub delay2


gpibwrite(14,"C")
gpibwrite(14,"E")
if energy>=0.9 then gosub shortw
if energy<0.9 and energy>0.8 then gosub midw
if energy<=0.8 then gosub longw
gosub delay
rem *******************

rem ******************************
```

```
rem **************************************
rem **********sensitivity ayari ******************
rem ****************************

if timeflag=0.3 then gosub delay1sec
gosub bosoku
if timeflag=0.3 then gosub delay1sec

if timeflag=1 then gosub delay1sec
gosub bosoku
if timeflag=1 then gosub delay1sec
if timeflag=1 then gosub delay1sec


if timeflag=3 then gosub delay3sec
gosub bosoku
if timeflag=3 then gosub delay3sec
if timeflag=3 then gosub delay3sec
if timeflag=3 then gosub delay3sec

if timeflag=10 then gosub delay10sec
gosub bosoku
if timeflag=10 then gosub delay10sec
if timeflag=10 then gosub delay10sec
if timeflag=10 then gosub delay10sec
if timeflag=10 then gosub delay10sec

if timeflag=30 then gosub delay30sec
gosub bosoku
if timeflag=30 then gosub delay30sec
if timeflag=30 then gosub delay30sec
if timeflag=30 then gosub delay30sec
if timeflag=30 then gosub delay30sec

xxx=1
lopsens:

gpibwrite(8,"OUTR? 1")
a$=gpibread$(8)
gpibwrite(8,"OUTR? 2")
j$=gpibread$(8)
curr=val(mid$(a$,1))
? "current=",curr," A"
devia=val(mid$(j$,1))
average=average+curr
xxx=xxx+1
if xxx<6 goto lopsens
average=average/5
rem ? "Current/flux for",energy," eV=",absorp
```

```
gosub delay
gosub delay
? "varege",average
if 4.9e-7<=average and average<1e-6 then gosub sensita
if 1.9e-7<=average and average<4.9e-7 then gosub sensitb
if 9e-8<=average and average<1.9e-7 then gosub sensitc
if 4.5e-8<=average and average<9e-8 then gosub sensitd
if 1.5e-8<=average and average<4.5e-8 then gosub sensite
if 8e-9<=average and average<1.5e-8 then gosub sensitf
if 4e-9<=average and average<8e-9 then gosub sensith
if 1.5e-9<=average and average<4e-9 then gosub sensitk
if 7.5e-10<=average and average<1.5e-9 then gosub sensitl
if 3.5e-10<=average and average<7.5e-10 then gosub sensitm
if 1.5e-10<=average and average<3.5e-10 then gosub sensitn
if 7.5e-11<=average and average<1.5e-10 then gosub sensito
if 3.5e-11<=average and average<7.5e-11 then gosub sensitp
if 1.5e-11<=average and average<3.5e-11 then gosub sensitr
if 7.5e-12<=average and average<1.5e-11 then gosub sensits
if 3.5e-12<=average and average<7.5e-12 then gosub sensitt
if 1.5e-12<=average and average<3.5e-12 then gosub sensitab
if 6.5e-13<=average and average<1.5e-12 then gosub sensitac
if 2.5e-13<=average and average<6.5e-13 then gosub sensitad
if 8e-14<=average and average<2.5e-13 then gosub sensitae
if 1e-14<=average and average<8e-14 then gosub sensitaf
if  average<=1e-14 then gosub sensitag
? "sensflag",sensflag

if sensflag>=15  then gosub tflag300msec
if sensflag=14 then gosub tflag1sec
if sensflag=13 then gosub tflag3sec
if sensflag<13 and sensflag=>10  then gosub tflag10sec
if sensflag<10   then gosub tflag30sec

? "oldflag",oldflag
? "newflag",timeflag

if sensflag>=15  and oldflag<>timeflag then gosub tcons300msec
if sensflag=14 and oldflag<>timeflag then gosub tcons1sec
if sensflag=13 and oldflag<>timeflag then gosub tcons3sec
if sensflag=12 and oldflag<>timeflag then gosub tcons10sec
if sensflag=11 and oldflag<>timeflag then gosub tcons10sec
if sensflag=10 and oldflag<>timeflag then gosub tcons10sec
if sensflag<10  and oldflag<>timeflag then gosub tcons30sec

rem ****************************
rem ***********************
if timeflag=0.3 then gosub delay1sec
if timeflag=0.3 then gosub delay1sec

if timeflag=1 then gosub delay1sec
```

```
if timeflag=1 then gosub delay1sec
if timeflag=1 then gosub delay1sec
if timeflag=1 then gosub delay1sec
if timeflag=1 then gosub delay1sec

if timeflag=3 then gosub delay3sec
if timeflag=3 then gosub delay3sec
if timeflag=3 then gosub delay3sec
if timeflag=3 then gosub delay3sec
if timeflag=3 then gosub delay3sec
if timeflag=3 then gosub delay3sec

if timeflag=10 then gosub delay10sec
if timeflag=10 then gosub delay10sec
if timeflag=10 then gosub delay10sec
if timeflag=10 then gosub delay10sec
if timeflag=10 then gosub delay10sec
if timeflag=10 then gosub delay10sec

if timeflag=30 then gosub delay30sec
if timeflag=30 then gosub delay30sec
if timeflag=30 then gosub delay30sec
if timeflag=30 then gosub delay30sec
if timeflag=30 then gosub delay30sec
if timeflag=30 then gosub delay30sec
if timeflag=30 then gosub delay30sec

if z<=93 then goto loop
bitti:
gosub delay
? "Wait 30 seconds to finish the experiment"

gosub delay
gosub back
rem ********************************
 close #1
close #3
stop
rem---------------
read dbs$+".dat",d
print d.time$
rem -----------------------------
if not yesnobox("Okey?") then goto start
stop
bosoku:
gpibwrite(8,"OUTR? 1")
abc$=gpibread$(8)
gpibwrite(8,"OUTR? 2")
jbc$=gpibread$(8)
return
```

```
ttl:
gpibwrite(8,"AUXV 1,1.4")
gpibwrite(8,"AUXV 1,0.8")
 ? "filitrenin degisip degismedigini kontrol  edýp enterleyin"
 input "fýlýtreyý degýstýrýp enterleyýn",turn
? "Filter at",filterw," A is ready"
return
measnum:
n=20
return
measnum1:
n=20
return


sensita:
gpibwrite(8,"SENS 26")
sensflag=26
return
sensitb:
gpibwrite(8,"SENS 25")
sensflag=25
return
sensitc:
gpibwrite(8,"SENS 24")
sensflag=24
return
sensitd:
gpibwrite(8,"SENS 23")
sensflag=23
return
sensite:
gpibwrite(8,"SENS 22")
sensflag=22
return
sensitf:
gpibwrite(8,"SENS 21")
sensflag=21
return
sensith:
gpibwrite(8,"SENS 20")
sensflag=20
return
sensitk:
gpibwrite(8,"SENS 19")
sensflag=19
return
sensitl:
gpibwrite(8,"SENS 18")
sensflag=18
return
```

```
sensitm:
gpibwrite(8,"SENS 17")
sensflag=17
return
sensitn:
gpibwrite(8,"SENS 16")
sensflag=16
return
sensito:
gpibwrite(8,"SENS 15")
sensflag=15
return
sensitp:
gpibwrite(8,"SENS 14")
sensflag=14
return
sensitr:
gpibwrite(8,"SENS 13")
sensflag=13
return
sensits:
gpibwrite(8,"SENS 12")
sensflag=12
return
sensitt:
gpibwrite(8,"SENS 11")
sensflag=11
return
sensitab:
gpibwrite(8,"SENS 10")
sensflag=10
return
sensitac:
gpibwrite(8,"SENS 9")
sensflag=9
return
sensitad:
gpibwrite(8,"SENS 8")
sensflag=8
return
sensitae:
gpibwrite(8,"SENS 7")
sensflag=7
return
sensitaf:
gpibwrite(8,"SENS 6")
sensflag=6
return
sensitag:
gpibwrite(8,"SENS 5")
```

```
sensflag=5
return

shortw:
gpibwrite(14,"V100,S")
gosub delay
gpibwrite(14,"G+"+d$+",S")
return
midw:
gpibwrite(14,"V100,S")
gpibwrite(14,"G+"+d$+",S")
return
longw:
gpibwrite(14,"V100,S")
gpibwrite(14,"G+"+d$+",S")
return
rem *******************************

tflag300msec:
timeflag=0.3
? "newflag",timeflag
return

tflag1sec:

timeflag=1
return

tflag3sec:
timeflag=3
return

tflag10sec:
timeflag=10
? "10da"
return

tflag30sec:
timeflag=30
return

tcons300msec:
gpibwrite(8,"OFLT 9")
? "time constant changed to 300 msec"
return

tcons1sec:
oldflag=timeflag
gpibwrite(8,"OFLT 10")
? "time constant changed to 1 sec"
```

```
return
tcons3sec:
oldflag=timeflag
gpibwrite(8,"OFLT 11")
? "time constant changed to 3 sec"
return
tcons10sec:
oldflag=timeflag
gpibwrite(8,"OFLT 12")
? "time constant changed to 10 sec"
return
tcons30sec:
oldflag=timeflag
gpibwrite(8,"OFLT 13")
? "time constant changed to 30 sec"
return
back:
gpibwrite(14,"V120,S")
gpibwrite(14,"G-7208,S")
return
rem -------------------------------
delay0:
t=time
delay01:if time-t<500 then goto delay01
      return
delay:
t=time
delay0a1:if time-t<1000 then goto delay0a1
      return
rem -------------------------------------
delay3msec:
t=time
delay111:if time-t<1000 then goto delay111
      return

delay1sec:
t=time
delay1sa:if time-t<1000 then goto delay1sa
      return
rem -------------------------------------

delay3sec:
t=time
delay1:if time-t<3000 then goto delay1
      return
rem -------------------------------------
delay10sec:
t=time
delay133:if time-t<10000 then goto delay133
      return
```

```
rem -------------------------------------
delay30sec:
t=time
delay1a1:if time-t<30000 then goto delay1a1
        return
rem -------------------------------------

rem -------------------------------------
delay4:
t=time
delay5:if time-t<6000 then goto delay5
        return
delay2:
t=time
delay5ed:if time-t<3 then goto delay5ed
        return
rem -------------------------------------
delayshort:
t=time
delayshrt:if time-t<10000 then goto delayshrt
        return
rem -------------------------------------
delaymidle:
t=time
delaymid:if time-t<60000 then goto delaymid
        return

delaylong:
t=time
delayl:if time-t<150000 then goto delayl
        return
arabek:
t=time
delayl123:if time-t<6000 then goto delayl123
        return

rem ---------------------------
delay6:
t=time
delay7:if time-t<10000 then goto delay7
        return
delay8:
t=time
delay9:if time-t<10000 then goto delay9
        return
fluxRead:
rem flux file is to be read into y variable
dim y(94)
m=0
? "okunuyor"
```

```
read "D:\data2004\fx\Fx_12jul.dat",oku
k=0
okut:
k=k+1
y(k)=oku(k,3)
rem print "y(",k,")",y(k)
if k<94 then goto okut
return
rotar:
t=time
rotarr: if time-t<15000 then goto rotarr
return
kontrol:
k=0
kontr:
k=k+1
toplam=toplam+standev(k)
toplamang=toplamang+angldev(k)
if k<=n goto kontr

return
rem -------------------------------------
                stop
rem ----------------------------
```